Chemistry of Vanadium and Zinc Antiviral Tetra-*aza* Macrocycles

A Thesis Submitted for the Degree

of

Doctor of Philosophy

at

The University of Edinburgh

by

Allison Ross B.Sc.(Hons.)

Department of Chemistry

University of Edinburgh

September 2008

Declaration

I hereby declare that except where specific reference is made to other sources, the work contained in this thesis is the original work of the author. It has been composed by myself and has not been submitted, in whole or in part of, for any other degree, diploma or other qualification.

Allison Ross

September 2008

Acknowledgements

I would like to thank my supervisor, Professor Peter J Sadler, FRS, for his support, advice and encouragement throughout the project and for always being available when needed. It has been a most enjoyable three years and I am privileged to have worked for him.

My sincere thanks go to the Sadler research group for members past and present, both in Edinburgh and Warwick, for their continued support and friendship. In particular, special thanks are due to Dr Ana Pizarro and Dr Abraha Habtemariam for invaluable assistance and discussions on many occasions. I would also like to thank Dr Neil Robertson for acting as my second supervisor in Edinburgh when Professor Sadler moved to Warwick University.

Thanks are also due to Professor Simon Parsons and his research group, and the EPSRC National Crystallographic Service at the University of Southampton for the crystallography work in this thesis. I also thank Mr Juraj Bella for assistance with NMR experiments. I am very grateful to Dr Daniel Stone, National EPR Service, University of Manchester for all his help with EPR data simulations and Miss Danielle Covelli, University of British Columbia, for her assistance with the EXAFS/XANES data.

A very special thank you is due to Dr Peter J Kirsop of the University of Edinburgh for many invaluable discussions, and for his support, patience and understanding throughout the project.

Finally, I would like to say a big thank you to my parents, family and friends for their much appreciated support and encouragement throughout the last three years. Also remembering Jim & Mary, and Pat & Barbara who would have been very proud.

Abstract

Some bicyclam compounds are highly active as HIV inhibitor agents with high selectivity for the CXCR4 coreceptor, an important protein receptor for the human immunodeficiency virus. One particular bicyclam, AMD3100 (1,1'-(1,4-phenylenebismethylene)-bis-1,4,8,11-tetra*aza*cyclotetradecane, known as xylyl-bicyclam) reached Phase II clinical trials in 2001. More recently, it has been relaunched commercially as *Mozobil*, a stem cell mobiliser. The activity of this macrocycle and configurationally restricted analogues as antivirals against HIV, have been shown to increase on complexation with zinc. A range of metals has been studied with varying degrees of activity seen, but none show activity comparable with the zinc complexes.

In order to investigate the chemistry of macrocycles in their role as anti-HIV agents, the syntheses of vanadium-cyclam, vanadium-bicyclam and zinc constrained cyclam complexes have been carried out. Of the many oxovanadium(IV) cyclam complexes synthesised, those with a sulfate or chloride axial ligand *trans*- to the V=O group were chosen for comparison purposes with oxovanadium(IV) bicyclam analogues for both solid state and solution analyses. X-ray crystallography showed that the oxovanadium(IV) cyclam complexes crystallised in the thermodynamically stable *trans*-III configuration. Aqueous solution studies using EPR spectroscopy revealed a different behaviour for the oxovanadium(IV) cyclam and bicyclam complexes studied. Results suggested that the 6th axial ligand *trans*- to the V=O group could undergo facile exchange in solution for the cyclam complexes but may be retained in the bicyclam complexes. Antiviral test

results for oxovanadium(IV) cyclam complexes revealed these to be completely inactive against HIV.

Xylyl-bicyclam was synthesised and complexed with vanadium, as oxovanadium(IV) sulfate and chloride structures. EPR spectroscopy results suggested that for the bicyclam chloride complex some displacement of the 6th axial ligand may occur, but the bicyclam sulfate appeared to retain both axial ligands. More importantly, these ligands also appear to have a significant effect on the hyperfine coupling constant, A.

Antiviral test results for oxovanadium(IV) bicyclam sulfate and chloride complexes revealed these to be highly active against HIV, with the chloride structure showing similar activity to AMD3100.

Possible interactions between the V=O group and the protein backbone of CXCR4 were studied using molecular modelling techniques, incorporating the X-ray crystal structure obtained for the oxovanadium(IV) cyclam sulfate complex. This revealed the possibility of a weak interaction between the oxygen of the V=O group and the proton of the alpha-carbon of a tryptophan residue, Trp195. No metal-carboxylate interaction was seen between the vanadium centre and aspartate residue Asp171 in the binding site investigated, possibly due to the distance between them being unfavourable for formation of a coordination bond (3.4 Å). Possible hydrogen bonding was seen between the carboxylate oxygens of Asp171 and the NH protons of the *trans*-III configured ring. These studies may demonstrate how oxo-metals interfere with the protein backbone in such a way as to distort the molecule from an optimum binding geometry. It may also indicate the importance of a second binding site known to support a

cis-V configuration of the macrocycle, bearing in mind that vanadium bicyclam complexes do show activity as antivirals against HIV. It is possible that one ring of the vanadium bicyclam complexes interacts with the binding site for the *trans*-III configuration in a similar fashion to the cyclam complexes and the antiviral activity may result, in this case, from interactions formed through binding of the second ring. The aromatic linker is also thought to be important.

Cyclams can be constrained by adding bulky substituents and/or additional rings to the structure and this has the effect of stabilising one configuration. NMR studies show how a zinc constrained cyclam retains the *trans*-III configuration in solution and also shows high activity against HIV, comparable with the vanadium bicyclam sulfate complex. This emphasises how the oxo-vanadium cyclams must be in an unfavourable position and unable to form crucial interactions known to be important for antiviral activity. A 4-coordinate zinc constrained macrocycle showed unusual binding to three ring nitrogens and may reveal an intermediate species in the uptake and release of metals by cyclams. Further complexation by exchange of the axial ligand revealed a 5-coordinate zinc bound to all four nitrogens on the ring.

This thesis provides the first investigation into the role of oxo-vanadium complexes as antiviral agents against HIV looking at possible interactions of the oxo-metal group with the protein backbone of the CXCR4 receptor. An investigation into configurational change in solution for zinc constrained cyclams is also described.

Abbreviations

AA	Amino acid
AIDS	Acquired immune deficiency syndrome
Asp	Aspartic acid
AZT	Zidovudine
BFC	Bifunctional chelator
bpy	2,2′-bipyridine
Calc.	calculated
cbdca	1,1-cyclobutanedicarboxylic acid
CC	Cysteine cysteine
CCBP2	Cysteine cysteine binding protein 2
CCR5	Cysteine cysteine receptor 5
CC_{50}	50% cytotoxic concentration
CD4	Cluster of differentiation 4
CHR	C-terminal heptad repeat
COSY	Correlation spectroscopy
CSD	Cambridge structural database
CXCR4	Cysteine (AA residue) cysteine receptor 4

Cys	Cysteine
DMSO	Dimethyl sulfoxide
DPPH	2,2′-Diphenyl-1-picrylhydrazyl
DSC	Differential scanning calorimetry
EC_{50}	50% effective concentration
EPR	Electron paramagnetic spectroscopy
ESI-MS	Electrospray ionisation mass spectrometry
equiv.	Equivalents
EtOAc	Ethyl acetate
EXAFS	Extended X-ray absorption fine structure
Glu	Glutamic acid
Gly	Glycine
gp	Glycoprotein
GPCR	G-protein coupled receptor
HIV	Human immunodeficiency virus
HMC	Hexyl-Me_2-cyclam
HSQC	Heteronuclear single quantum correlation
Hz	Hertz

IR	Infrared spectroscopy
J	symbol for NMR spectroscopy coupling constant
M	Molecular ion
m/*z*	mass to charge ratio
Me	Methyl
min	Minutes
NHMC	Naphthyl-hexyl-Me_2-cyclam
NHR	N-terminal heptad repeat
NMR	Nuclear magnetic spectroscopy
NARTI	Nucleoside analogue reverse transcriptase inhibitor
NtARTI	Nucleotide analogue reverse transcriptase inhibitor
NNRTI	Non-nucleoside reverse transcriptase inhibitor
PCR	Polymerase chain reaction
PDB	Protein database
Ph	Phenyl
RTIs	Reverse transcriptase inhibitors
SDF-1	Stromal-cell derived factor 1
t	Time

TLC	Thin layer chromatography
TM	Trans-membrane
TOCSY	Total correlation spectroscopy
Trp	Tryptophan
UV	Ultraviolet
vis	Visible
VOTPP	Oxovanadium(IV) triphenyl porphyrin
XANES	X-ray absorption near-edge spectroscopy
XRD	X-ray diffraction
ZDV	Zidovudine

APPENDIX 1: EPR simulation data for all complexes are attached as .pdf files in the enclosed CD.

APPENDIX 2: EXAFS k-space data for oxovanadium(IV) cyclam sulfate **21** and chloride **22**, and oxovanadium(IV) bicyclam sulfate **30** and chloride **31** are attached as .pdf files in the enclosed CD.

APPENDIX 3: All crystallographic .cif files are attached in the enclosed CD.

1. INTRODUCTION

1.1. Bioactivity of macrocycles

The biochemistry of organic macrocycles has long been utilised by Nature to enable some of the most important processes essential for the continuation of life. Prime examples include i) the transport and storage of oxygen in mammalian and other respiratory systems and ii) the mechanism of photosynthesis.[1] In these examples structurally related organic macrocycles are found as metal complexes. Iron-porphyrin complexes involved in the majority of dioxygen binding processes are associated with haem proteins and this porphyrin family of natural macrocycles provides a chemical ring system upon which many biologically important molecules are based. Much research has been done concerning the synthesis of compounds that mimic biological species involved in processes such as dioxygen activation and electron transfer.

The latter process is associated with photosynthesis, another important biochemical mechanism. The chlorophylls form part of the structurally related family of chlorin macrocycles that function as magnesium complexes in the conversion of light energy to chemical energy in green plants. In chlorins, the porphyrin structure is altered by the addition of another 5-membered ring and a long hydrocarbon chain for orientation of the molecules during the photosynthetic process. The same tetrapyrrolic structure of porphyrin and chlorin is again employed by Nature to produce another important family of macrocycles known as the corrins that include vitamin B12. The corrins are a partially reduced form of porphyrin where a *meso* carbon atom is replaced by a direct C-C bond. This

ring system is found within the group of vitamin B12 cobalt complexes. The cobalt ion is axially bonded to both a heterocyclic nitrogen donor and a cyanide ligand, a result of the particular purification process adopted.[2] Figure 1.1 shows the structures of the Fe(II) complex haem, **1** and the chlorophyll *a* molecule, **2**.

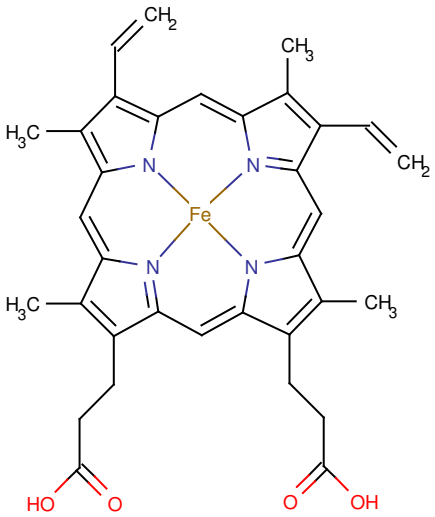

Fe(II)Protoporphyrin 9, **1**

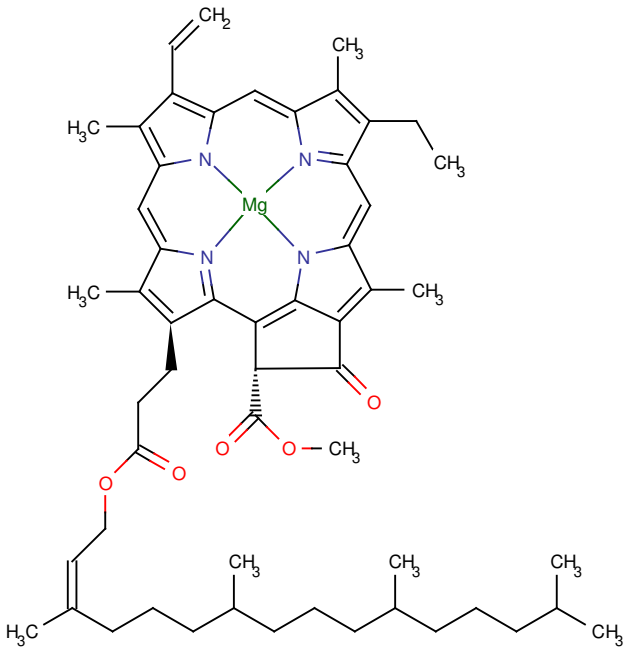

Chlorophyll *a*, **2**

Figure 1.1 A metal complexed porphyrin structure – haem 1, and the modified but structurally related chlorin structure - a chlorophyll, 2

It is believed that these ligands are important in Nature because of their enhanced kinetic and thermodynamic stabilities arising from the firmly held metal ion within the cyclic cavities. In addition, the planar delocalised electronic structure is a key characteristic. As Nature has chosen to use macrocyclic structures for such fundamental processes, it would seem reasonable to apply synthetic derivatives for medicinal application in a physiological frame.[1]

1.1.1. Synthetic Macrocycles

A large number of macrocyclic compounds with complexed metal ions have been prepared and investigated. Cyclic polyamines in particular bind to a wide range of metals and in many cases show configurational changes during binding.[3] For the coordination chemist, macrocyclic ligands are usually defined as having at least 3 donor atoms and a minimum of 9 atoms forming the ring. The donor atoms can either be integrated within or alternatively (although much less common), attached to a cyclic backbone. Much of the coordination chemistry is defined by steric and electronic considerations associated with the macrocyclic cavity, the size of which plays a large part in influencing the properties of resultant metal complexes. The actual hole-size of a cyclic ligand is dependent upon the number of atoms in the macrocyclic ring; the nature of the donor atoms possibly playing a role in affecting the cavity size.[1] Many variations of both organic backbone and donor atom combinations exist, some of which have proved active in a medicinal capacity while others are successful in applications as diverse as microelectronic devices and sensors.[4, 5]

The chemistry of macrocyclic ligand complexes has important implications for many areas of biochemistry with commercial application as

contrast agents for magnetic resonance imaging (MRI), radionuclide-directing agents within the field of radiopharmaceuticals and more recent application as anti-viral compounds and stem cell mobilising agents. In addition, high intensity γ-ray emitters such as ^{99m}Tc, ^{67}Ga and β emitters such as ^{89}Sr and ^{153}Sm are used in diagnostic imaging and therapy respectively.[6, 7] A highly successful commercial example in the field of magnetic resonance imaging (MRI) is a chelated non-radioactive metal ion complex known as Gd-DOTA, a Gd(III) complexed 12-membered ring 1,4,7,10-tetra*aza*cyclododecane (cyclen) shown in Figure 1.2. For MRI procedures the required dose of paramagnetic ion is very high in order to obtain a clear image, resulting in high toxicity levels. Chelation by macrocycles not only reduces the acute toxicity but also helps to increase the rate of elimination from the body. As a result, this reduces long-term toxic effects and is why macrocyclic complexes have been so successful in this field. Gd(III) is paramagnetic and 8-coordinated to the macrocycle donor atoms (4 nitrogen and 4 carboxylate groups) with a 9th inner sphere coordination to a water molecule providing the chemical mechanism of the MRI process.[8]

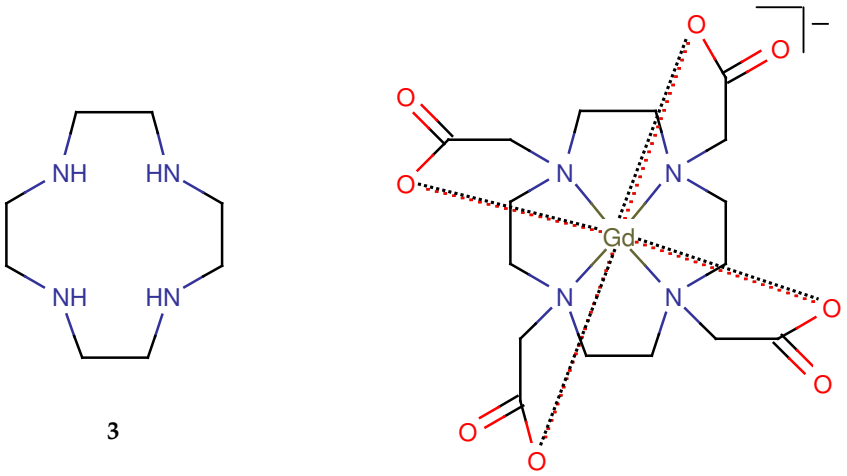

Figure 1.2 1,4,7,10-tetraazacyclododecane (cyclen) 3, and a tetra-carboxylate gadolinium (III) complex (Gd-DOTA), 4

In radiopharmaceutical agents, a macrocycle is often used to bind the radionuclide used to kill the cancer cells found in tumours. A target-specific metalloradiopharmaceutical consists of a targeting biomolecule, a linker, a BFC (bifunctional chelator) and a metallic radionuclide. The BFC is an intentionally designed polydentate chelator that binds strongly to the radionuclide through complexation and through covalent attachment of the targeting molecule to its backbone. This interaction can be through a linker molecule, often used to modify the pharmacokinetic properties of the radiopharmaceutical, such as a hydrocarbon chain to increase lipophilicity (Figure 1.3).

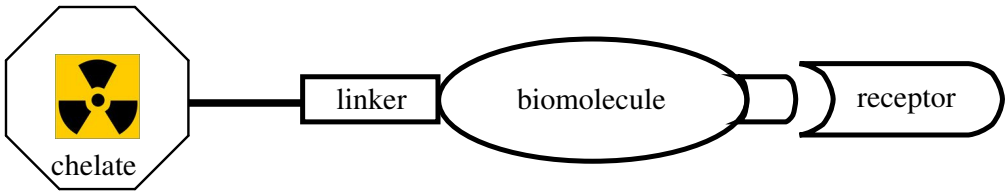

Figure 1.3 ***Schematic representation of a metalloradiopharmaceutical and tumour receptor***

It is crucial that the BFC forms a stable metal chelate and is kinetically inert at physiological pH. A slow rate of dissociation in solution is essential to avoid accumulation of radioactivity in non-targeted organs. Isotopes such as ^{67}Cu and a number of radiolanthanides possess the required therapeutic properties while others are more suitable for diagnostic imaging.[9]

Cyclic polyethers (crown ethers) form another large family of ligands with varying numbers of donor atoms and subsequent ring sizes. These show similar coordination chemistry to that of natural antibiotics like nonactin. These macrocycles can also be structurally altered and numerous derivatives with varying degrees of substituent functionality are known.[2] Mixed donor atoms within macrocyclic ligands are also widely used, having selectivity for metal ion binding and different bonding preferences. Combinations include N,O-donor compounds representing a mixture of *aza*macrocycles and crown ethers while others include softer donor atoms such as phosphorus, selenium and sulfur. The latter has been shown to have rich coordination chemistry in the form of thiacrown ethers.[2]

1.2. HIV and AIDS

Acquired Immunodeficiency Syndrome (AIDS) has killed more than 25 million people since the effect of the Human Immunodeficiency Virus was first reported in 1981, making it one of the most destructive epidemics in recorded history.[10] The 2007 AIDS epidemic update by UNAIDS (Joint United Nations Program on HIV/AIDS) reports that global estimates for 2007 are:[10]

Total number of people living with HIV in 2007: [30.6 - 36.1 million]	***33.2 million***
Adults living with HIV in 2007: [28.2 – 33.6 million]	***30.8 million***
Women living with HIV in 2007: [13.9 – 16.6 million]	***15.4 million***
Children under 15 years living with HIV in 2007: [1.9 - 2.4 million]	***2.1 million***

The disease is caused by the Human Immunodeficiency Virus (HIV) - a retrovirus that attacks the immune system. Retroviruses contain an RNA genome that relies on the reverse transcriptase enzyme in order to replicate *via* the host cell DNA. HIV is classified as belonging to a subgroup of retroviruses called lentiviruses, characterised by their long incubation period. Other lentiviruses include SIV (Simian Immunodeficiency Virus) and FIV (Feline Immunodeficiency Virus). Infection of a cell requires particular surface proteins that act as receptors for specific envelope proteins of the retrovirus.

1.2.1. Polyoxometallates

The first polyoxometallate that proved active against HIV (HPA-23 [$(NH_4)_{17}Na(NaSb_9W_{21}O_{86}).14H_2O$]) was produced by Rozenbaum *et al*. in 1985.[11] This led to a search for similar compounds with the ability to suppress HIV replication without being cytotoxic to the host cells and the process of examining hundreds of polyoxometallates began in earnest. This work resulted in examples such as JM1493, **5** and JM2820, **6** in the 1990s (Figure 1.4) illustrating the proposed structures of potential anti-HIV agents at that time.[11] These polyoxometallates are seen as globular or spherical polyanionic structures with anionic charge arising from peripheral oxygen atoms.

In the course of treatment of HIV and AIDS a potential anti-viral agent may require to be administered over a prolonged period of time. The outcome of such treatment would probably result in deposition of the compound in the body, thought to be mainly in the liver. This led to the recommendation that incorporation of metals in an organic macrocycle, not dissimilar to those used in nature for fundamental biochemical processes, seemed a logical alternative.

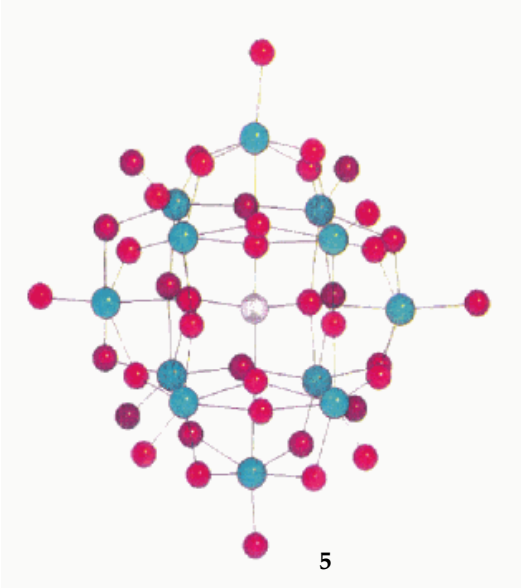

5

JM1493 $H_4SiW_{12}O_{40}$, 5

(Si - white, W – cyan)

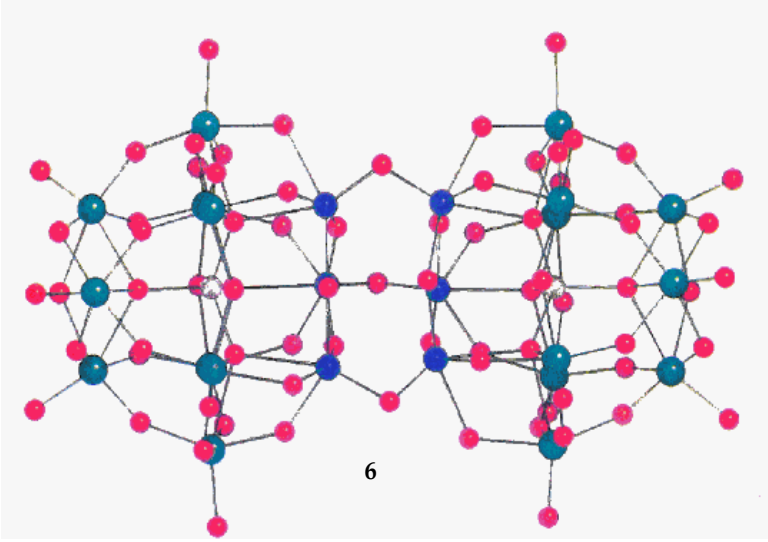

6

JM2820 $[Me_3NH]_8[Si_2W_{18}Nb_6O_{77}]$, 6

(Si – white, W – cyan, Nb – dark blue)

Figure 1.4 *JM1493, 5 and JM2820, 6*

1.3. Existing Drug Treatments

The drug treatments used today in the treatment against HIV infection and associated AIDS disease are primarily associated with post-infection and are classified as follows.

1.3.1. Reverse Transcriptase Inhibitors (RTIs)

These antiretroviral drugs inhibit the enzyme reverse transcriptase, essential for successful replication of HIV. There are three known types of RTI; Nucleoside Analogue Reverse Transcriptase Inhibitors (NARTIs or NRTIs), Nucleotide Analogue Reverse Transcriptase Inhibitors (NtARTIs or NtRTIs) and Non-Nucleoside Reverse Transcriptase Inhibitors (NNRTIs). Both NRTIs and NtRTIs act in a similar way (*via* phosphorylation steps) and their mechanism of action is through chain termination of viral DNA.[12] Three examples are shown in Figure 1.5: Zidovudine is also known as AZT, ZDV and azidothymidine, trading commercially as Retrovir. Didanosine has trade names Videx and Videx EC. Alcabar, also known as ABC, has the trade name Ziagen and is an analogue of guanosine (a nucleoside).

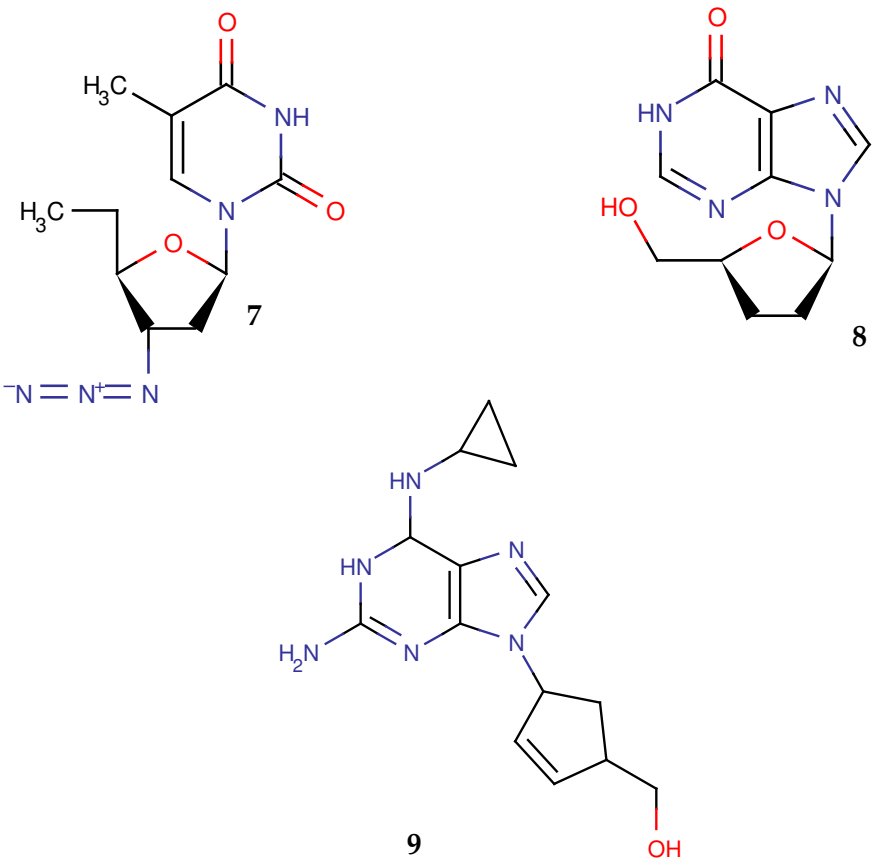

Figure 1.5 *Zidovudine, 7; Didanosine, 8; Abacavir, 9*

In contrast, NNRTIs mode of action occurs by blocking the movement of protein domains of reverse transcriptase essential for carrying out DNA synthesis. NNRTIs are bound in a hydrophilic pocket close to the catalytic site of reverse transcriptase in HIV-1. The major problem with these antivirals is the continual ability of HIV-1 to form resistant strains *in vitro* and *in vivo*.[13] These drugs are not incorporated into the viral DNA unlike NRTIs. Figure 1.6 shows some current examples from this class of antiretroviral drugs.

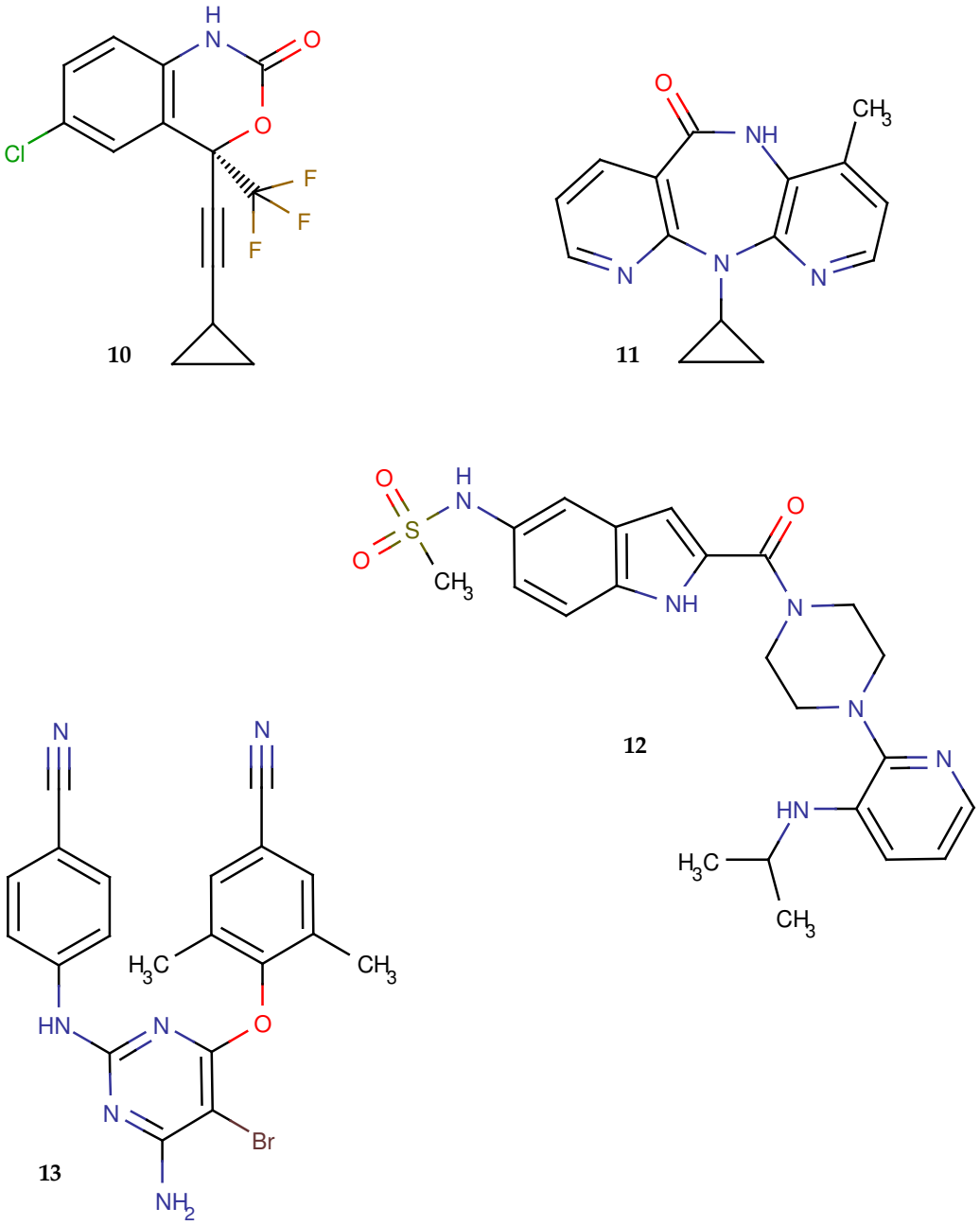

Figure 1.6 *Efavirenz, 10 Nevirapine, 11 Delavirdine, 12 Etravirine, 13*

1.3.2. Protease inhibitors (pharmacology)

It is important to distinguish between natural protease inhibitors and protease inhibitors associated with antiviral activity. Natural protease inhibitors inhibit the function of peptidases by digesting long protein chains into short fragments and are associated with physiological processes. Protease inhibitors (pharmacology) are a class of antiretroviral drugs that inhibit the function of HIV-1 protease. HIV-1 protease is an enzyme essential to the life-cycle of the virus used to cleave newly synthesised polyproteins. Without effective HIV-1 protease new virions remain non-infectious, resulting in new virions that are unable to infect new cells.

Structural analysis revealed that inhibitor drugs like Darunivir, **15** interact closely with Asp29 and Asp30 in the active site and these carboxylate interactions are critical to its activity.[14, 15]

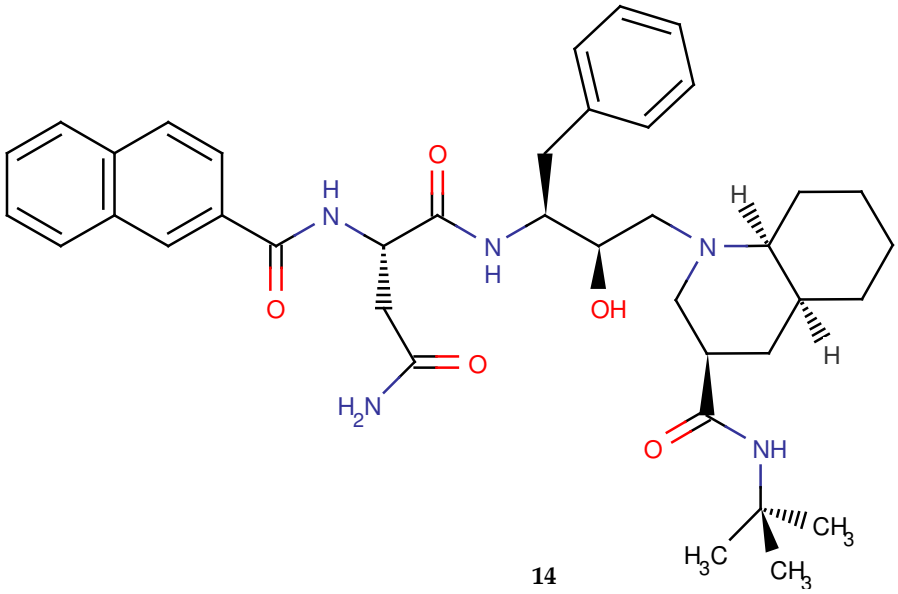

14

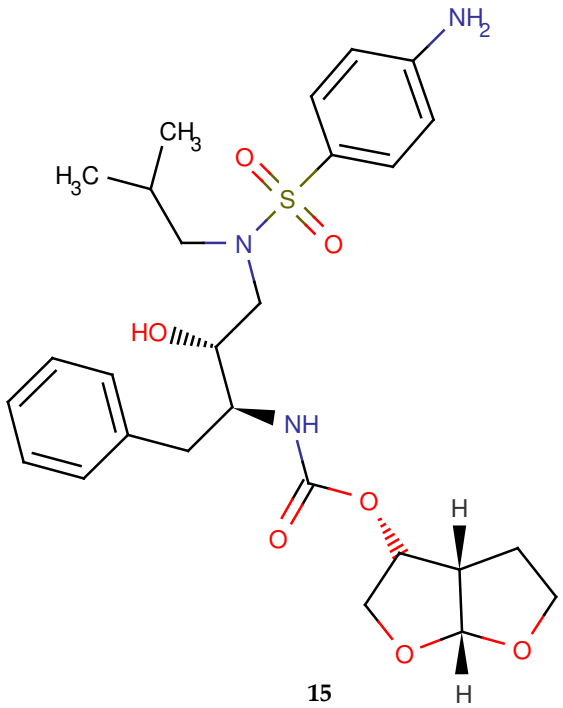

15

Figure 1.7 *Saquinavir, 14; Darunavir, 15*

1.3.3. Entry inhibitors

The biological target of entry inhibitor drugs is specific protein receptors expressed on the surface of Helper T-cells (a type of white blood cell or leukocyte) found in the immune system. CD4 (cluster of differentiation 4) is a glycoprotein receptor and the primary receptor used by HIV-1 to gain entry to host cells.[16-18] Binding of the virus to CD4 occurs through attachment of the viral envelope glycoprotein, gp120 and through this association the virus gains access to a very important receptor, CXCR4. The interaction with CXCR4 enables the virus to fuse with the cell membrane, gaining entry to the cell where it effectively discharges the viral RNA, leading to replication and the onset of infection.[12] CXCR4 is associated with HIV infection at later stages of AIDS disease when the immune system deteriorates rapidly. Another cell surface protein used by the virus is CCR5 (CC chemokine Receptor 5), found on Helper T-cells and macrophages and is associated with the transfer of HIV through body fluids. Nomenclature and classification of these chemokine receptors is based on the arrangement of four conserved N-terminal cysteine residues that are important in determining the protein tertiary structure.[19] The abbreviation CC refers to the proximity of two cysteine residues. CCR5 has adjacent cysteines whereas in CXCR4 they are separated by one amino acid.

1.3.3.1. Fuzeon

T-20 (Enfuvirtide, *Fuzeon*) was the first of a new class of anti-HIV drugs known as entry (or fusion) inhibitors, named for their ability to prevent the virus binding to and entering the cell. T-20 is an approved anti-HIV peptide developed by Trimeris Pharmaceuticals and Roche in 2003. The viral entry process of Human Immunodeficiency Virus type 1 (HIV-1) into

target cells is assisted by envelope glycoprotein gp41.[20] Envelope glycoproteins gp120 and gp41 of HIV-1 are both involved in viral entry into target cells. GP120 interacts with the cell surface protein receptor CD4 and coreceptor CXCR4, after which gp41 enables the fusion of viral and cellular membranes.[21] It is believed that formation of a six-helical bundle structure consisting of a gp41 N-terminal heptad repeat (NHR) and C-terminal heptad repeat (CHR) facilitates this interaction.[22] The mechanism of action of T-20 is thought to be through binding to gp41, preventing fusion with important cell surface receptors on Helper T-cells.

1.3.3.2. Maraviroc

Maraviroc is an entry inhibitor that specifically targets the chemokine receptor, CCR5. Importantly, Pfizer's Celsentri® (maraviroc), is the first new oral class of HIV treatment and was licensed by the European Agency for the Evaluation of Medicinal Products (EMEA) in September 2007. Maraviroc works by blocking entry of the virus into human immune (CD4) cells, preventing HIV from entering and replicating. It is licensed for treatment of patients infected with only CCR5-tropic HIV-1 (in combination with other antiretroviral drugs) Currently, all other available oral HIV medicines target HIV only after it has entered the immune cells.[23]

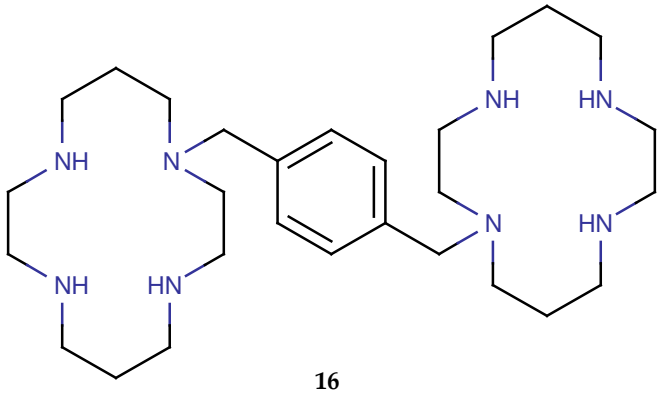

16

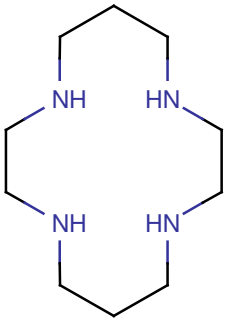

17

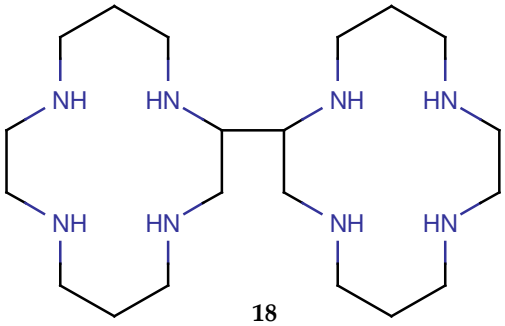

18

Figure 1.8 *Xylyl-bicyclam (AMD3100), 16; Cyclam, 17; JM1657 18*

1.3.3.3. AMD3100

The small molecular CXCR4 antagonist xylyl-bicyclam, Figure 1.8, **16** (AMD3100) was the first CXCR4 antagonist to enter clinical trials for treatment of HIV infection.[24] A chance discovery in a contaminated batch of cyclam (1,4,8,11-tetra*aza*tetradecane) Figure 1.8, **17** showed distinct anti-HIV activity at an EC_{50} value of ~10 μg per mL. Typically, polyoxometallates showed an EC_{50} value of ~ 1 μg per mL. The impurity was identified through HPLC analysis as the bicyclam JM1657 Figure 1.8, **18** - a cyclam dimer with macrocyclic rings connected through a C-C bond. Development of a linker molecule that would effectively hold the two cyclam rings together resulted in AMD3100. By changing the C-C bond (which proved difficult to replicate) to an aromatic bridge, an EC_{50} value of 0.005 μg per mL was obtained and it had one of the highest selectivity indices recorded for anti-HIV agents.[11] At physiological pH, each cyclam ring carries an overall 2^+ charge and can adopt the stable *trans*-III (*RRSS*) configuration with respect to the four nitrogens. It is suggested that negatively-charged aspartate residues found in the CXCR4 receptor (Asp171, Asp262), may provide crucial binding sites for interaction with the positively charged bicyclam rings *via* hydrogen bonding.[25] Using bovine rhodopsin as a template for CXCR4 (PDB Code 1HZX), in-silico docking predictions showed that two nitrogens of one cyclam ring can interact with two carboxylate oxygens of an aspartate residue, Asp262 and two nitrogens of the other cyclam ring with two carboxylate oxygens of a glutamate residue, Glu288.[26]

Although AMD3100 binds specifically to CXCR4 and is effective as an anti-HIV agent, it was withdrawn from Phase II clinical trials in May 2001 due to cardiotoxicity. It has been suggested that toxicity may result from

metal complexation affecting ring coordination through isomer configurational binding.[24] A particular disadvantage was its lack of oral bioavailability. Several analogues have been prepared retaining the aromatic linker while substituting one or both rings by *N*-containing basic centres capable of binding to acidic residues.[24, 27] Varying levels of activity suggested the possibility of spatial importance of the aromatic ring. Replacement by a saturated cyclohexane ring rendered the analogues completely inactive leading to the conclusion that a central linker with planar or near planar geometry is crucial for maintaining activity.[24]

1.3.3.4. Metal Complexes

A study into protein recognition of macrocycles has shown how the affinity of bicyclam for CXCR4 is enhanced further by binding to Ni(II) or Zn(II).[28] It can be illustrated that anti-HIV activity is very much dependent upon the bound metal and a Zn(II)-bicyclam complex showed slightly higher biological activity than the metal-free ligand. Experiments predict an order of activity for the following metals tested: Zn(II) > bicyclam ~ Ni(II) > Cu(II) > Co(III) >>> Pd(II). The Pd(II) complex is shown to be virtually inactive.[29-31] This is discussed further in Section 1.4.2.

By exploring the structure of protein-cyclam adducts, structural insight into specific hydrophilic and hydrophobic interactions involved in the binding of bicyclam to CXCR4 can be gained. In addition to known interactions with aspartate and glutamate residues there is a distinct possibility that the hydrocarbon backbone of the bicyclam rings is involved in hydrophobic interactions with tryptophan residues, Trp195 and Trp283.[32] This particular interaction is comparable to that of the hydrophobic contact

of the side-chains of proline with tryptophan found at some protein-protein interfaces, commonly described as a Trp-Pro-Trp sandwich. If these macrocycles exist as metal complexes *in vivo*, then it is pertinent to ask how this would affect levels of essential elements in the body and what the long-term effect may be. Cyclam has a high affinity for Zn(II) (log K = 15.5) [33] and it has been calculated that in the case of AMD3100 nearly all the drug would exist as a Zn(II) complex at physiological pH of 7.4. The kinetics of Zn(II) binding with cyclam at pH7 show that uptake is relatively rapid.[34] Competitive experiments show that Zn(II) has a higher uptake rate than Cu(II) - important information as Cu(II) may be a competitor for bicyclam. Cu(II) is shown to have a stronger affinity for cyclam than zinc and so could form preferentially *in vivo*, but the complexes are biologically less active. The ability of Zn(II) to exert kinetic control over the uptake of Cu(II) into specific binding sites is shown and a rate for the disappearance of "free" Cu(II) on addition to cyclam is determined.[34] The uptake of Cu(II) appears to be markedly slower in the presence of Zn(II) under these particular experimental conditions and suggests that Zn(II) binds more rapidly to cyclam at physiological pH of 7.4. Further investigation is therefore required in regard to the wider significance in biology for these complexes and their interactions with proteins.

The selectivity of CXCR4 for bicyclams is well researched and the affinity for CXCR4 is enhanced through metal ion binding of an AMD3100 complex to the aspartate residue, Asp262. [28, 35] An investigation [36] into the structure and dynamics of metallo-macrocycles showed how the CXCR4 receptor binds preferentially to a zinc complexed bicyclam and that the two macrocyclic rings in a perchlorate complex exist as two major configurations, *trans*-I and *trans*-III (Figure 1.9) in aqueous solution. Addition of acetate to

represent the carboxylate side chains of Asp171 and Asp262 induced a major structural change such that the two rings exist in aqueous solution as *cis*-V/*trans*-I. A definition of the six possible configurations cyclam can adopt on complexing with a metal ion was proposed over 40 years ago[37] and it is generally regarded that the *trans*-III configuration is the most thermodynamically stable isomer. An homology model of CXCR4 was produced using the structure of bovine rhodopsin as a template and *cis*-V/*trans*-I Zn_2-bicyclam was docked with the *cis*-V macrocycle coordinated to Asp262 through a Zn(II)-carboxylate interaction, and through double N-H H-bonds to the oxygens of Glu288. The *trans*-I macrocycle is bound to the oxygens of Asp171 through a Zn(II)-carboxylate interaction (Figure 1.10). It is thought that the high anti-HIV activity of Zn(II)-bicyclam may arise through retention of the *cis*-V configuration in one of the macrocycles.[36]

Recently, a configurationally restricted bismacrocyclic CXCR4 receptor antagonist showed increased levels of activity against HIV.[38] The zinc complex of an ethylene bridged analogue of AMD3100 revealed a lower EC_{50} value than AMD3100 and $[Zn_2\text{-AMD3100}]^{4+}$ and showed the highest recorded activity against HIV to date (0.0025 μM *vs* 0.08 μM).

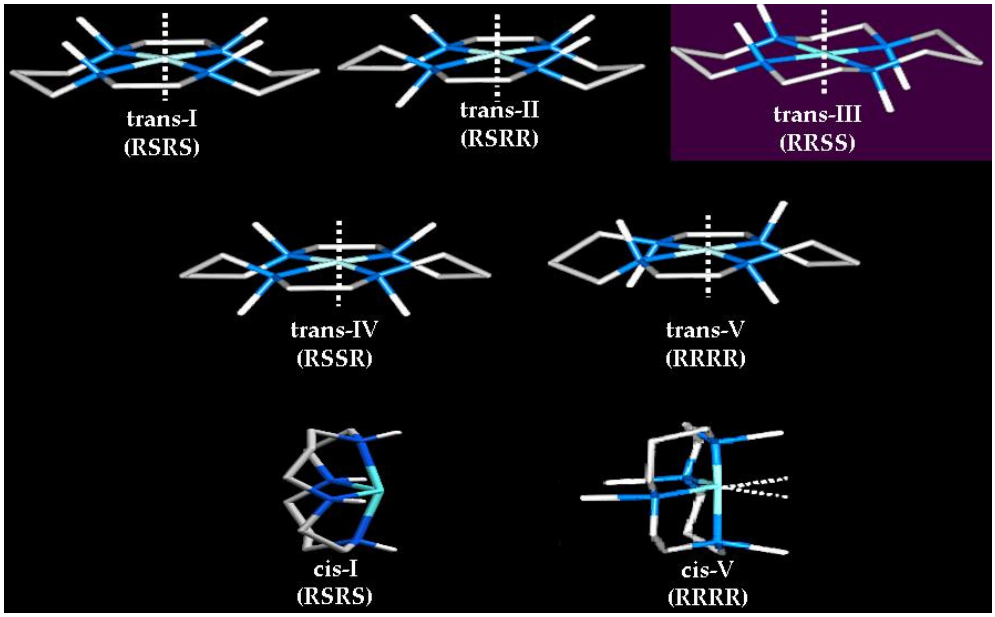

Figure 1.9 *Configurations of metal-cyclam*
The trans-III configuration is highlighted as the most stable configuration in octahedral complexes.

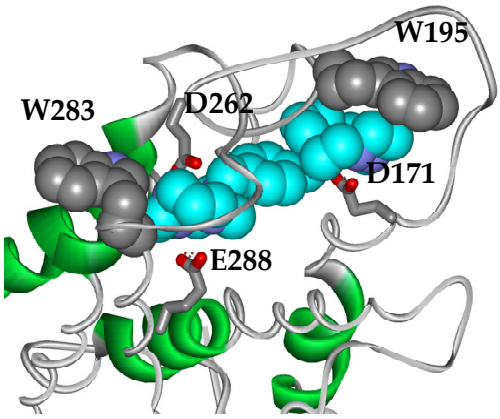

Figure 1.10 *Model of Zn_2-bicyclam bound to CXCR4* [39]

AMD3100 (xylyl-bicyclam, Figure 1.8, **16**) has now made an impact in stem cell research. CXCR4 receptors are also expressed in bone marrow and by binding to the receptor the drug promotes the release of stem cells from bone marrow into the blood stream. The natural ligand of CXCR4 is stromal cell-derived factor-1 (SDF-1), responsible for directing migration of hematopoietic cells from foetal liver to bone marrow.[40] Blocking of SDF-1 by AMD3100 triggers a rapid movement of stem cells from the bone marrow to the circulating blood where they can be easily collected for transplant purposes. Stem cell mobilisation is presently at the forefront of scientific research in the pursuit of non-invasive methods to treat the depressed immune systems of post-chemotherapy patients. In fact, any physiological tissue or muscle where cells do not normally regenerate after destruction or injury could potentially benefit from this type of therapy, such as cardiac therapy. Another major area of interest that would benefit from stem cell treatment is brain disease such as Alzheimer's. AMD3100 has been re-launched commercially as *Mozobil* and is currently undergoing its second set of Phase III clinical trials against Hodgkin's and Non-Hodgkin's Lymphoma as a stem cell mobiliser.

1.4. Cyclam and bicyclam

Macrocycles such as cyclam and bicyclam are highly protonated and bind transition ions to form a range of *trans* (I-V) and *cis* configurations (Figure 1.9). These configurations may be recognised independently by different coreceptor proteins. Reported pK_a values for cyclam show a high affinity for the first two protonations (average pK_{a1} 11.4, pK_{a2} 10.3).[41-44] Values of pK_{a3} and pK_{a4} show much weaker affinities (1.6 and 1.9 respectively) due to steric restrictions and electrostatic repulsions from the first two protonations. The

restricted geometry may allow the nitrogen lone pairs to overlap, resulting in high electron density within the cavity.

Table 1.1 Protonation values for cyclam

pK_{a1}	pK_{a2}	pK_{a3}	pK_{a4}	Conditions	Ref
11.49	10.24	1.64	0.86	Unknown	39
11.585	10.624	1.611	2.415	0.5 M KNO_3, 25˚C	40
11.3	10.23	1.43	2.27	0.1 M $NaNO_3$, 25 ˚C	41
11.29	10.19	1.61	1.91	0.1 M KCl, 25 ˚C	42

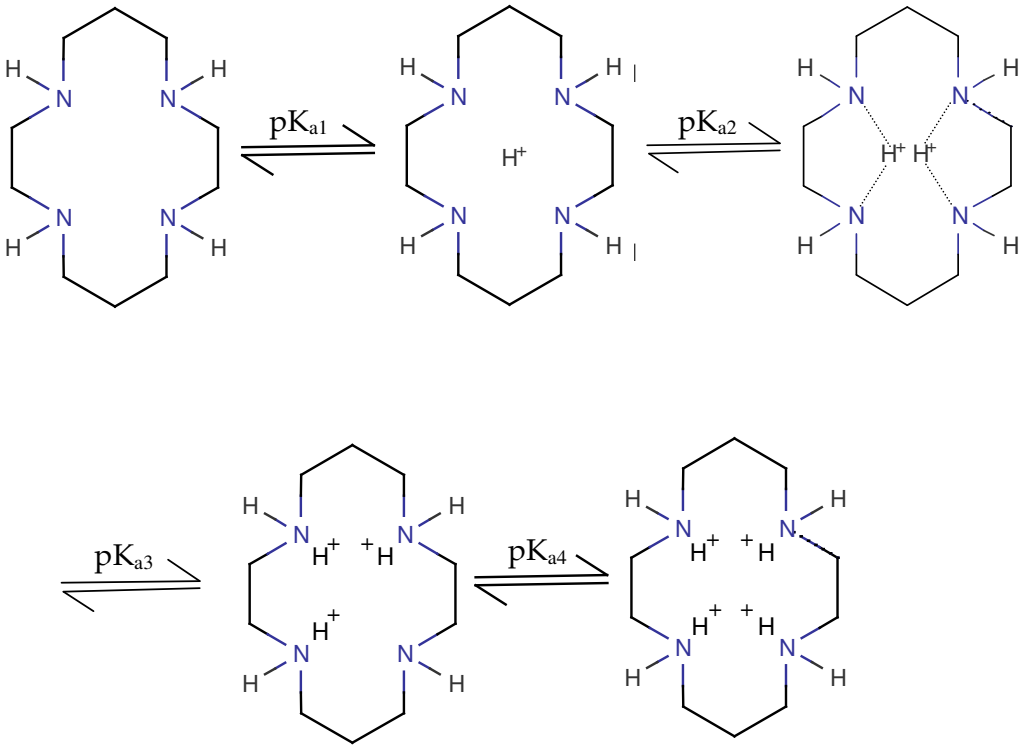

Figure 1.11 Protonation steps for cyclam and bicyclam complexes

Macrocyclic amines form stable complexes with almost all transition metal ions.[45] The stability is associated with the "chelate effect" and an example of how an increase in the number of chelate rings is related to the entropic factor. Other contributions arise from metal ion size and ring cavity area. Cu(II)-cyclam is more stable (log K = 30.5) than the equivalent 15-membered macrocycle complex (log K = 24.4).[45] The stability of these complexes reveals why cyclam is not used in selective metal extraction.

1.4.1. Configurational isomers and transition metal complexes

It is expected that particular ring configurations play a crucial part in determining the antiviral activity of macrocyclic complexes. Metallo-complexes of cyclam and bicyclam in solution give rise to several different configurational isomers, each dependent on the chirality of the 4 ring nitrogens.[3] Metal coordination to cyclam (or bicyclam) gives rise to 5 possible ring configurations, the stereochemistry of the NH protons described as *RSRS, RSRR, SSRR, RSSR* and *RRRR.* These five configurations are designated *trans*-I to *trans*-V respectively. Two *trans*- isomers show NH protons across the macrocycle cavity diagonal pointing in the same direction (*trans*-I and *trans*-V).[36] It is expected in this instance that the macrocycle is able to fold across such a diagonal leading to the isomers, *cis*-I and *cis*-V (Figure 1.9). Research has shown that *trans*-I, II, III and *cis*-V configurations are significant for potential bioactivity in metallo-macrocyclic antiviral compounds.[36, 38, 46] Antiviral activity of cyclam and its derivatives is thought to be significantly influenced by metal complexation and subsequent binding with carboxylate oxygens of acidic amino acid residues in the binding site of CXCR4.

Transition metal complexes favouring square planar geometries are found predominantly in the *trans*-I configuration while octahedral complexes favour *trans*-III. Analysis of all nickel(II) cyclam complexes in the Cambridge Structural Database (CSD) shows the most common configuration to be *trans*-III, so deemed the most stable configuration. Less than 23% of octahedral nickel(II) complexes with a 1,4,8,11-substituted cyclam backbone adopted the *trans*-I configuration compared with more than 75% preferring *trans*-III.[47] This situation is reversed for square-planar, square-pyramidal and trigonal-bipyramidal complexes with less than 30% adopting *trans*-III and the majority showing a preference for the *trans*-I configuration. Repeated analyses for copper(II) complexes resulted in similar findings.[48] Different metal complexes show varying levels of anti-HIV activity revealing a relationship between the metal-cyclam geometry and the number of binding site interactions possible.

Studies undertaken[49] also assume the biological target to be the coreceptor protein CXCR4 and experimental work employed the use of acetate ligands to represent carboxylate oxygens. Pd(II)-cyclam retains a *trans*-III configuration in both solid state and solution.[49] Varying the counterion had no effect on ring configuration and addition of acetate did not induce any configurational change in the bicyclam analogue. Ni(II)-cyclam adopted the thermodynamically stable *trans*-III configuration in the solid state with axial counterions, but in solution produced both a diamagnetic square-planar *trans*-I configuration in addition to a paramagnetic isomer. The bicyclam analogue contained a mixture of paramagnetic-paramagnetic, paramagnetic-diamagnetic and diamagnetic-diamagnetic species with different configurations for each combination. Both Cu(II)-cyclam and bicyclam were found to be *trans*-III in the solid state

(H_2O axial ligands, acetate counter ion) and in solution. Co(III)-cyclam adopted the *trans*-III configuration in the solid state (acetate axial ligands), but solution studies showed the existence of three different configurations (*trans*-III, *trans*-I and a further unidentified *trans*- configuration). The bicyclam analogue formed intermediate species on reacting with acetate that equilibrated to the *trans*-III isomer with time.[49] All complexes showed a marked contrast to results found for Zn(II)-cyclam and bicyclam where addition of excess acetate produced a higher proportion of the *cis*-V isomer. Zn(II)-bicyclam has been shown to exist in three configurations in solution, *trans*-I, *trans*-II and *cis*-V and formation of the *cis*-V configuration is driven by addition of excess acetate.[36]

1.4.2. Constrained Cyclam Complexes

Various analogues of cyclam have been prepared using a range of substituent functional groups and examples include dioxocyclams and cross-bridged cyclams.[3] The constraining bridge is of particular interest as a means of retaining a rigid structure in one configuration, as cyclam is known to exist as several isomers in solution (Figure 1.9). It has been suggested[34] that studies using configurationally-restrained cyclams may provide some insights into the mechanism of action of (apo) cyclam drugs *in vivo* and the role of metal complexation.

Some tetra*aza* macrocyclic ligands containing pendant arms with varying organic groups have been synthesised.[50] The rate of metal complex formation of these compounds is shown to be retarded due to the steric congestion around the macrocycle by the introduction of pyridylmethyl or phenylmethyl pendant arms. A zinc complex of a constrained cyclam bearing two cyclohexane rings and two methyl groups shows an unusual

crystal structure in that the Zn(II) ion is found in an axially-elongated octahedral environment with two *trans*- water molecules and four equatorial nitrogen atoms from the macrocycle.[51] This contrasts with previous work on mononuclear complexes of macrocyclic polyamines where coordination environments are usually found to be distorted tetrahedron or square pyramidal with only one water molecule bound to zinc(II) ions.[45, 52, 53]

In bicyclam, addition of an ethylene bridge between adjacent nitrogens results in formation of a piperazine ring on each macrocycle.[38] The induced steric restriction keeps the ring configuration as *trans*-II on metal complexation. Studies have shown how such a restriction may favour a five-coordinate Cu(II) species on protein binding, in contrast to a distorted octahedral zinc(II) species for the same ligand.[54] Solution studies analysed by NMR spectroscopy showed that the zinc complex was present in a single configuration and showed the highest recorded activity to date against HIV. The mechanism of antiviral activity is expected to be the same as for the bicyclams, through binding interactions with CXCR4.[38] The trigonal bypyramidal geometry of the Cu(II) complex provides an interesting perspective on expected protein binding interactions and this study correlates antiviral activity with associated binding strength of carboxylates.

Configurational restriction of the macrocycle in some cases appears to increase antiviral activity[54] and may even provide increased kinetic stability *in vivo*.[55, 56] This led to the idea explored in this thesis that it would be interesting to study *cis*-V constrained macrocycles in this context due to the high antiviral activity recorded for this predominant configuration in Zn_2-bicyclam.

1.4.3. Proposed mechanism of antiviral activity

It is suggested that viral gp120 (the glycoprotein envelope) is an indirect target of bicyclam compounds. Using time-of-addition experiments, results indicate that bicyclams interact with an early post-adsorption stage in the replication cycle of the virus and that the mode of action is through entry inhibition of HIV into the cell.[11] No viral DNA was detected in PCR (polymerase chain reaction) experiments after infection of cells with HIV in the presence of AMD3100. The inhibitory effect was concentration-dependent, leading to possible viral uncoating as the target. However, this step cannot be assayed directly and so studies have been directed toward the binding and fusion of the virus.[57] It is well documented that one mode of entry for HIV into the cell is through interaction with a specific receptor expressed on the surface of white blood cells (Helper T-cells) and explains why HIV affects the immune system.

Bicyclams are targeted at CXCR4, the coreceptor for T-tropic HIV-1 and HIV-2 strains and competitive binding experiments between the bicyclam AMD3100 and monoclonal antibody 12G5 mAb that reacts specifically with CXCR4 have been carried out.[58] By blocking the interaction with CXCR4, the virus is denied access to the cell preventing the onset of infection. At 25 μg/mL, AMD3100 completely inhibits the binding of the 12G5 mAb by binding directly and specifically to CXCR4.[58] At a concentration of 0.2 μg/mL AMD3100 still affects the binding of 12G5 mAb to CXCR4. The specificity of AMD3100 for the CXCR4 receptor has been determined acting on the premise that the compound should only be active against viruses that use CXCR4 as a coreceptor to enter the target cells. AMD3100 is active against T-tropic viruses (IC_{50} between 0.003 and

0.01 μg/mL) but not active against M-tropic viruses (IC_{50} > 25 μg/mL). M-tropic viruses are known to preferentially use the CCR5 receptor, although some can also use CCR2 and/or CCR3 (but not CXCR4) to enter cells. It has also been shown that there is no interaction of AMD3100 with any of the chemokine receptors CXCR1 through CXCR3, or CCR1 through CCR9.[19] It is interesting to note that no reports in the literature give any indication of whether AMD3100 could be involved in binding to other receptors from the same superfamily of proteins; the 7-helix transmembrane family, for example D6 (CCPB2).

1.4.4. Metalloporphyrins

Porphyrins are macrocycles comprised of four pyrroles linked by four methine bridges. Although metalloporphyrins exhibited potential as anti-HIV agents, in terms of potency and selectivity they were analogous to polyoxometallates[11], somewhat less than that of the serendipitously discovered macrocycle, bicyclam.

There are several reported accounts of particular porphyrins that display antiviral activity against HIV infection, with results obtained using viral replication inhibition assays.[59, 60] One investigation involved the possible antiviral activity of natural porphyrins related to protoporphyrin and other associated structures. None of the compounds tested met the criteria for successful inhibition of HIV infection.[61] Metalloderivatives were subsequently evaluated; compounds with no axial ligands were more effective at preventing infection. A possible mechanism for activity may involve porphyrin binding to the V3 loop of viral envelope glycoprotein gp120, thereby blocking access to the CD4 receptor. It would appear that the axial ligands are involved in steric restrictions with the biological target.

Expanded porphyrins are mimics of natural porphyrins, designed in such a way as to incorporate an array of metal ions. These ligands have such a large degree of structural freedom that they are able to accommodate all sizes of metal ion, including small ions like vanadium(V).[62] Such high-oxidation state vanadium compounds are thought to hold promising medicinal properties, including anticancer, antiviral and insulin-mimetic activity.[63-67]

1.5. Vanadium as a bioactive metal

1.5.1. Vanadium

Vanadium was named after Vanadis, the Norse goddess of beauty, due to its tendency to form compounds and solutions with a wide variety of colours. Although a range of oxidation states from -1 to +5 exist, biologically relevant oxidation states are limited to +3 to +5. Table 1.2 shows the reduction potentials of vanadium in aqueous solution.[68]

Table 1.2 Reduction potentials in aqueous solution [68]

Reduction reaction	E° (V *vs*. NHE)
$O_2 + 4H^+ + 4e^- \longrightarrow 2H_2O$	1.229
$VO_2^+ + 2H^+ + e^- \longrightarrow VO^{2+} + H_2O$	0.991
$VO^{2+} + 2H^+ + e^- \longrightarrow V^{3+} + H_2O$	0.337
$V^{3+} + e^- \longrightarrow V^{2+}$	-0.225

Vanadium is known to be of essential importance in some biological processes and described as an essential mineral or trace element in human physiology. Haloperoxidases are enzymes that catalyze the oxidation of halides (iodide, bromide and chloride) by hydrogen peroxide, resulting in halogenation of organic substrates. Two classes of haloperoxidases are known, the vanadium- and Fe-heme-containing enzymes. Within the class of vanadium-haloperoxidase enzymes, both vanadium bromoperoxidases (V-BrPO) and vanadium chloroperoxidases (V-ClPO) have been identified.[69] Ascidians (sea-squirts) accumulate vanadium from the surrounding sea and concentrate it 10^3 to 10^6-fold. Vanadium is as abundant as zinc in the earth's crust (0.015%). More importantly, a high concentration of vanadium(V) is found in sea water in the form of contact ion pairs $Na^+H_2VO_4^-$ in an average concentration of 30 nM.[63] It is reduced from V(V) to V(III) possibly by tunichromes (peptide pigments consisting of hydroxy-dopa units) for storage in blood vacuoles at very acidic pH values.[63, 70, 71] Vanadium-binding metallo-proteins (vanabins) found in the blood of such creatures are assumed to be involved in the transport of oxygen but no scientific evidence is available to substantiate this. At present there is no real understanding of why vanadium is collected and accumulated in this manner and no biological explanation is available. The Amanita mushroom is another example of an organism containing unusually high levels of vanadium with concentrations of nearly 400 ppm being observed in some species.[68] This particular vanadium compound was isolated in 1972 and given the name amavadin (or amavadine).[68] Identification of the organic ligand present in amavadin was revealed through IR and EPR analysis, although initially an absorption in the IR spectrum at 980 cm^{-1} was wrongly identified as a V=O

stretching frequency. This led to the proposed structure shown as Figure 1.12, **19**.

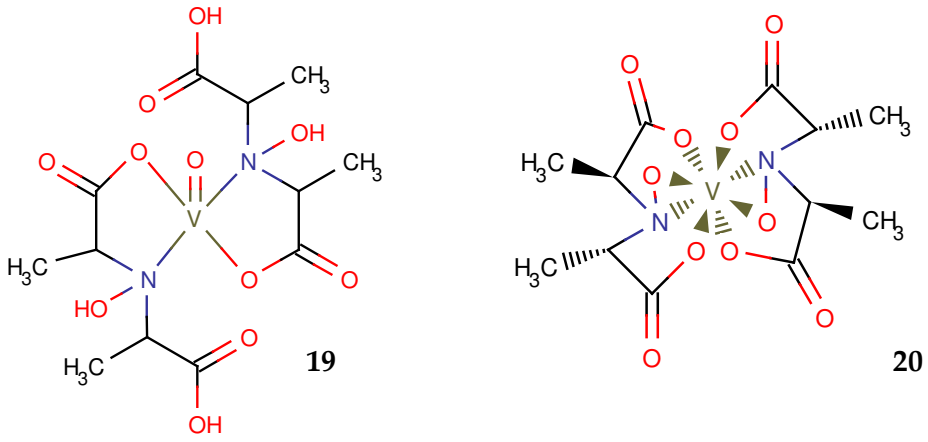

Figure 1.12 Structure of amavadin: originally proposed structure 19, and the experimentally determined and revised structure, 20

Again, the role is unknown but thought perhaps to be associated with a defence mechanism. The discovery of the role of vanadium as an insulin mimic in 1979 increased scientific interest in the coordination chemistry and reactivity of this Group 5 transition metal.[72] Pioneering work by many groups[73] has made a significant contribution to the understanding of the solution chemistry, coordination chemistry and bioinorganic chemistry of vanadium. An insulin mimic is a substance that alleviates some or all of the symptoms of diabetes. The ability of vanadate to act as a phosphate analogue may be the reason why such coordination complexes are so successful as insulin mimics, although it is not certain whether V(V) or V(IV) (or both) are responsible for the bioactivity.[68]

1.5.2. Vanadium in macrocycles

Recently, macrocycles in the form of expanded porphyrins have been used to accommodate vanadium[62], the coordination chemistry of which is a relatively unexplored area. In these complexes, the dioxovanadium(V) cation VO_2^+, is coordinated to three pyrrolic nitrogens.

Vanadium(IV) porphyrins have been shown to be physiologically stable as a new class of anti-HIV agents and demonstrate solution stability against glutathione reduction.[74] As potential therapeutics, vanadium complexes are possible anticancer and antidiabetic agents, and there is growing awareness in their antiviral properties. It is found[74] that macrocyclic dianionic porphyrinato ligands stabilise the vanadium ion by providing a rigid square planar scaffold. No demetallation resulting in free porphyrin ligand was observed.

Vanadium macrocycles offer new possibilities for design of antivirals against HIV.

1.6. Aims of thesis

Xylyl-bicyclam is a CXCR4 receptor antagonist. Antiviral activity has been linked to the existence of particular isomers in solution and is thought to be associated with metal complexation in the body. Several metal complexes have been characterised that display varying levels of activity and different ring configurations. It is suggested that cardiac toxicity may be linked to complexation with particular metals. The aim of this study is to investigate oxo-vanadium complexes of cyclam and bicyclam and their possible interaction with the CXCR4 receptor. Another aspect of the project is to investigate the antiviral activity of constrained macrocycles that may retain a particular configuration in solution. Specific aims are as follows.

1. To synthesise and characterise the organic macrocyclic ligand, xylyl-bicyclam (1-1'-[1,4-phenylenebis(methylene)]-bis(1,4,8,11-tetra*aza* cyclotetradecane)).

2. To synthesise and characterise vanadium complexes of xylyl-bicyclam and cyclam (1,4,8,11-tetra*aza*cyclotetradecane) with substitution of the axial ligand *trans*- to the oxygen of the V=O group by biologically relevant ligands Examples include thiocyanate (prevalent in plasma in the lungs of smokers) and cyclic GMP (guanosine monophosphate), a cyclic nucleotide. EPR spectroscopy will be used to investigate the behaviour of cyclams and bicyclams in aqueous solution and solution studies will be used to investigate the binding strength of the axial ligand. Investigations using IR with resonance Raman spectroscopy, X-ray crystallography and EXAFS/XANES will be used to give information on the solid state.

3. To synthesise and characterise zinc complexes of the constrained analogues of 1,4,8,11-tetra*aza*cyclotetradecane. Solution studies using 2D NMR spectroscopy will allow ring configurations to be assigned and compared to those in the solid state. The role of both zinc and the ring nitrogens in the binding of axial ligands will be investigated.

4. To investigate the binding of xylyl-bicyclam and related complexes to 7-helix transmembrane G-protein coupled receptors such as CXCR4 and D6, using molecular modelling. In-silico docking of complexes known to be either active or inactive may reveal the existence or alternatively the absence of possible axial ligand interactions.

1.7. Bibliography

[1] L. F. Lindoy, *The Chemistry of Macrocyclic Ligand Complexes*, Cambridge University Press, Melbourne, **1989**.

[2] E. C. Constable, *Coordination Chemistry of Macrocyclic Compounds, Vol. 72*, Oxford University Press Inc., , New York, **1999**.

[3] X. Liang, P. J. Sadler, *Chem. Soc. Rev.*, **2004**, *33*, 246.

[4] T. Le Goff, J. Braven, L. Ebdon, D. Scholefield, *Anal. Chim. Acta* **2004**, *510*, 175.

[5] C. M. Carey, W. B. Riggan, Jr., *Anal. Chem.*, **1994**, *66*, 3587.

[6] C. J. Anderson, M. J. Welch, *Chem. Rev.*, **1999**, *99*, 2219.

[7] S. S. Jurisson, J. D. Lydon, *Chem. Rev.*, **1999**, *99*, 2205.

[8] T. Storr, K. H. Thompson, C. Orvig, *Chem. Soc. Rev.*, **2006**, *35*, 534.

[9] R. Delgado, V. Félix, L. M. P. Lima, D. W. Price, *Dalton Trans.*, **2007**, 2734.

[10] www.unaids.org.

[11] E. De Clercq, *Nat. Rev. Drug Discov.*, **2003**, *2*, 581.

[12] E. De Clercq, *Biochim. Biophys. Acta* **2002**, *1587*, 258.

[13] O. S. Pedersen, E. B. Pedersen, *Antivir. Chem. Chemother.*, **1999**, *10*, 285.

[14] A. K. Ghosh, P. R. Sridhar, L. Sofiya, A. K. Hussain, J. Li, A. Y. Kovalevsky, D. E. Walters, J. E. Wedekind, V. Grum-Tokars, D. Das, Y. Koh, K. Maeda, H. Gatanaga, I. T. Weber, H. Mitsuya, *J. Med. Chem.*, **2006**, *49*, 5252.

[15] Y.-F. Wang, Y. Tie, P. I. Boross, J. Tozser, A. K. Ghosh, R. W. Harrison, I. T. Weber, *J. Med. Chem.*, **2007**, *50*, 4509.

[16] S. Rusconi, M. Moonis, D. P. Merrill, P. V. Pallai, E. A. Neidhardt, S. K. Singh, K. J. Willis, M. S. Osburne, A. T. Profy, J. C. Jenson, M. S. Hirsch, *Antimicrob. Agents Chemother.*, **1996**, *40*, 234.

[17] A. G. Dalgleish, P. C. L. Beverley, P. R. Clapham, D. H. Crawford, M. F. Greaves, R. A. Weiss, *Nature* **1984**, *312*, 763.

[18] D. Klatzmann, E. Champagne, S. Chamaret, J. Gruest, D. Guetard, T. Hercend, J.-C. Gluckman, L. Montagnier, *Nature* **1984**, *312*, 767.

[19] S. Hatse, K. Princen, G. Bridger, E. De Clercq, D. Schols, *FEBS Letters* **2002**, *527*, 255.

[20] M. Lu, S. C. Blacklow, P. S. Kim, *Nat. Struct. Biol.*, **1995**, *2*, 1075.

[21] J. K. Judice, J. Y. K. Tom, W. Huang, T. Wrin, J. Vennari, C. J. Petropoulos, R. S. McDowell, *Proc. Natl. Acad. Sci., USA* **1997**, *94*, 13426.

[22] S. Oishi, S. Ito, H. Nishikawa, K. Watanabe, M. Tanaka, H. Ohno, K. Izumi, Y. Sakagami, E. Kodama, M. Matsuoka, N. Fujii, *J. Med. Chem.*, **2008**, *51*, 388.

[23] www.pfizer.co.uk/Media/Press/2007/Pages/HIVlaunch.aspx.

[24] W. Zhan, Z. Liang, A. Zhu, S. Kurtkaya, H. Shim, J. P. Snyder, D. C. Liotta, *J. Med. Chem.*, **2007**, *50*, 5655.

[25] H. Tamamura, H. Tsutsumi, H. Masuno, S. Mizokami, K. Hiramatsu, Z. Wang, J. O. Trent, H. Nakashima, N. Yamamoto, S. C. Peiper, N. Fujii, *Org. Biomol. Chem.*, **2006**, *4*, 2354.

[26] V. I. Pérez-Nueno, D. W. Ritchie, O. Rabal, R. Pascual, J. I. Borrell, J. Teixido, *J. Chem. Inf. Model.*, **2008**, *48*, 509.

[27] S. Hatse, K. Princen, E. De Clercq, M. M. Rosenkilde, T. W. Schwartz, P. E. Hernandez-Abad, R. T. Skerlj, G. Bridger, D. Schols, *Biochem. Pharmacol.*, **2005**, *70*, 752.

[28] L. O. Gerlach, J. S. Jakobsen, K. P. Jensen, M. M. Rosenkilde, R. T. Skerlj, U. Ryde, G. Bridger, T. W. Schwartz, *Biochemistry* **2003**, *42*, 710.

[29] J. A. Esté, C. Cabrera, E. De Clercq, S. Struyf, J. Van Damme, G. Bridger, R. T. Skerlj, M. J. Abrams, G. Henson, A. Gutierrez, B. Clotet, D. Schols, *Mol. Pharmacol.*, **1999**, *55*, 67.

[30] Y. Inouye, T. Kanamori, T. Yoshida, X. Bu, M. Shionoya, T. Koike, E. Kimura, *Biol. Pharm. Bull.*, **1994**, *17*, 243.

[31] Y. Inouye, T. Kanamori, T. Yoshida, T. Koike, M. Shionoya, H. Fujioka, E. Kimura, *Biol. Pharm. Bull.*, **1996**, *19*, 456.

[32] T. M. Hunter, I. W. McNae, X. Liang, J. Bella, S. Parsons, M. D. Walkinshaw, P. J. Sadler, *Proc. Natl. Acad. Sci., USA* **2004**, *102*, 2288.

[33] M. Kodama, E. Kimura, *J. Chem. Soc. Dalton Trans.*, **1977**, 2269.

[34] S. Paisey, P. J. Sadler, *Chem. Commun.*, **2004**, 306.

[35] E. De Clercq, *Mol. Pharmacol.*, **2000**, *57*, 833.

[36] X. Liang, J. A. Parkinson, M. Weishaupl, R. O. Gould, S. J. Paisey, H.-s. Park, T. M. Hunter, C. A. Blindauer, S. Parsons, P. J. Sadler, *J. Am. Chem. Soc.*, **2002**, *124*, 9105.

[37] B. Bosnich, C. K. Poon, M. L. Tobe, *Inorg. Chem.*, **1965**, *4*, 1102.

[38] G. C. Valks, G. McRobbie, E. A. Lewis, T. J. Hubin, T. M. Hunter, P. J. Sadler, C. Pannecouque, E. De Clercq, S. J. Archibald, *J. Med. Chem.*, **2006**, *49*, 6162.

[39] T. M. Hunter, Edinburgh (Edinburgh), **2005**.

[40] C. H. Kim, H. E. Broxmeyer, *Blood* **1998**, *91*, 100.

[41] F. P. Hinz, D. W. Margerum, *Inorg. Chem.*, **1974**, *13*, 2941.

[42] M. Micheloni, A. Sabatini, P. Paoletti, *J. Chem. Soc. Perkin Trans. II* **1978**, 828.

[43] V. J. Thom, G. D. Hosken, R. D. Hancock, *Inorg. Chem.*, **1985**, *24*, 3378.

[44] R. D. Hancock, R. J. Motekaitis, J. Mashishi, I. Cukrowski, J. H. Reibenspies, A. E. Martell, *J. Chem. Soc. Perkin Trans. II* **1996**, 1925.

[45] E. Kimura, *Tetrahedron* **1992**, *48*, 6175.

[46] X. Liang, M. Weishaupl, J. A. Parkinson, S. Parsons, P. A. McGregor, P. J. Sadler, *Chem. Eur. J.*, **2003**, *9*, 4709.

[47] M. A. Donnelly, M. Zimmer, *Inorg. Chem.*, **1999**, *38*, 1650.

[48] M. Bakaj, M. Zimmer, *J. Mol. Struct.*, **1999**, *508*, 59.

[49] T. M. Hunter, S. J. Paisey, H.-s. Park, L. Cleggorn, A. Parkin, S. Parsons, P. J. Sadler, *J. Inorg. Biochem.*, **2004**, *98*, 713.

[50] S.-G. Kang, S.-J. Kim, *Bull. Korean Chem. Soc.*, **2003**, *24*, 269.

[51] K.-Y. Choi, I.-H. Suh, C. J. Kim, *Polyhedron* **1997**, *16*, 1783.

[52] E. Kimura, T. Koike, *Comm. Inorg. Chem.*, **1991**, *11*, 285.

[53] E. Kimura, M. Shionoya, A. Hoshino, T. Ikeda, Y. Yamada, *J. Am. Chem. Soc.*, **1992**, *114*, 10134.

[54] G. McRobbie, G. C. Valks, C. J. Empson, A. Khan, J. D. Silversides, C. Pannecouque, E. De Clercq, S. G. Fiddy, A. J. Bridgeman, N. A. Young, S. J. Archibald, *Dalton Trans.*, **2007**, 5008.

[55] M. Boiocchi, M. Bonizzoni, L. Fabbrizzi, F. Foti, M. Licchelli, A. Poggi, A. Taglietti, M. Zema, *Chem. Eur. J.*, **2004**, *10*, 3209.

[56] T. J. Hubin, J. M. McCormack, S. R. Collinson, N. W. Alcock, D. H. Busch, *Chem. Commun.*, **1998**, 1675.

[57] K. De Vreese, D. Reymen, P. Griffin, A. Steinkasserer, G. Werner, G. J. Bridger, J. Esté, W. James, G. W. Henson, J. Desmyter, J. Anné, E. De Clercq, *Antivir. Res.*, **1996**, *29*, 209.

[58] D. Schols, J. Esté, G. Henson, E. De Clercq, *Antivir. Res.*, **1997**, *35*, 147.

[59] A. K. Debnath, S. Jiang, N. Strick, K. Lin, P. Haberfield, A. R. Neurath, *J. Med. Chem.*, **1994**, *37*, 1099.

[60] A. K. Debnath, S. B. Jiang, N. Strick, K. Lin, S. B. Kahl, A. R. Neurath, *Med. Chem. Res.*, **1999**, *9*, 267.

[61] A. N. Vzorov, D. W. Dixon, J. S. Trommel, L. G. Marzilli, R. W. Compans, *Antimicrob. Agents Chemother.*, **2002**, *46*, 3917.

[62] J. L. Sessler, E. Tomat, V. M. Lynch, *Chem. Commun.*, **2006**, 4486.

[63] D. Rehder, *Inorganic Chem. Commun.*, **2003**, *6*, 604.

[64] Y. Shechter, I. Goldwaser, M. Mironchik, M. Fridkin, D. Gefel, *Coord. Chem. Rev.*, **2003**, *237*, 3.

[65] K. H. Thompson, C. Orvig, *J. Inorg. Biochem.*, **2006**, *100*, 1925.

[66] A. Goc, *Central Eur. J. Biol.*, **2006**, *1*, 314.

[67] G. R. Willsky, A. B. Goldfine, P. J. Kostyniak, J. H. McNeill, L. Q. Yang, H. R. Khan, D. C. Crans, *J. Inorg. Biochem.*, **2001**, *85*, 33.

[68] C. Slebodnick, B. J. Hamstra, V. L. Pecoraro, *Modelling the biological chemistry of vanadium: Structural and reactivity studies elucidating biological function, Vol. 89*, Springer Verlag, Berlin, **1997**.

[69] A. Butler, A. H. Baldwin, *Vanadium bromoperoxidase and functional mimics, Vol. 89*, Springer Verlag, Berlin, **1997**.

[70] P. Frank, K. Kustin, W. E. Robinson, L. Linebaugh, K. O. Hodgson, *Inorg. Chem.*, **1995**, *34*, 5942.

[71] S. W. Taylor, B. Kammerer, E. Bayer, *Chem. Rev.*, **1997**, *97*, 333.

[72] K. H. Thompson, J. H. McNeill, C. Orvig, *Chem. Rev.*, **1999**, *99*, 2561.

[73] D. C. Crans, *Pure Appl. Chem.*, **2005**, *77*, 1497.

[74] S.-Y. Wong, R. Wai-Yin Sun, N. P.-Y. Chung, C.-L. Lin, C.-M. Che, *Chem. Commun.*, **2005**, 3544.

2. MATERIALS AND METHODS

2.1 Chemicals and instruments

2.1.1 Chemicals

Cyclam (1,4,8,11-tetra*aza*cyclotetradecane), *α*-*α'*-dibromo-*p*-xylene, ethyl trifluoroacetate, triethylamine, zinc acetate dihydrate, zinc chloride, barium chloride, vanadyl sulfate hydrate, vanadyl acetylacetonate, sodium bromide, potassium iodide, sodium thiocyanate, sodium ammonium phosphate tetrahydrate, silver hexafluorophosphate, guanosine 5'-monophosphate disodium salt hydrate (from yeast) guanosine 3',5-cyclic monophosphate sodium salt and NMR solvents, deuterium oxide (99.9%) and chloroform-*d* (99.9%) were purchased from Aldrich Chemical Co., and were reagent grade unless otherwise stated.

2.1.2 I R spectroscopy

Infrared spectra were recorded as KBr pellets in the range 4000 – 400 cm^{-1} on a Perkin-Elmer Paragon 1000 Fourier-transform spectrometer. Solution IR spectra were recorded on a Perkin-Elmer 100 Fourier-transform spectrometer and data were analysed using Spectrum software. Calibration for solution IR studies was carried out using a solution (275 mM) of $MgSO_4$ as a standard. All solutions for standard and complexes were made using double distilled water.

2.1.3 Conductivity measurements

Electrical conductivity was measured using the JENWAY Ltd Model 4310 conductivity meter with an electrode of surface area 1 cm^2. Calibration

of the instrument was acquired with the Hanna conductivity standard 1413 μS / cm prior to measurement of the sample. Solutions were prepared from double distilled water and recorded at ambient temperature.

2.1.4 Resonance Raman spectroscopy

Raman spectra were collected using a Labram 300 (Horiba Jobin Yvon, Stanmore, Middlesex, UK) 20mW HeNe laser with 632.817 nm wavelength, filter 0.1 – 100%, hole 500 micron, slit 300 micron, grating 1800 lateral (XY), spatial resolution < 1 mm, spectral resolution about 2.5 cm^{-1} and magnification 100 (numerical aperture about 0.95, Olympus UK, London, UK). Data were processed using LabSpec (Horiba Jobin Yvon) software, version 4.18.

2.1.5 NMR spectroscopy

NMR spectra were recorded either on a Bruker AVA 600 MHz spectrometer using a 5 mm RT (room temperature) TXI (triple resonance inverse) [^{1}H, ^{13}C, ^{15}N] probe equipped with xyz gradients, a Bruker Bio600 MHz spectrometer using a 5 mm TXI [^{1}H, ^{13}C, ^{15}N] cryo-probe equipped with z gradients, or a DMX500 MHz equipped with a TBI [^{1}H, ^{13}C, ^{15}N] z-gradient probe. All spectra were acquired at 298 K unless otherwise stated using standard pulse sequences for samples in 5 mm NMR tubes. ^{1}H shifts for D_2O solutions were referenced to 1,4-dioxane (3.75 ppm) and ^{1}H NMR signals for $CDCl_3$ solutions were referenced to the residual solvent peak, δ 7.27 ppm (chloroform). All spectra were recorded at 298 K and processed using XWIN-NMR (Version 3.6 Bruker UK Ltd) and TOPSPIN (Version 3.1 Bruker UK Ltd) software.

2.1.6 X-ray crystallography

X-ray crystallographic studies were carried out on a Bruker SMART-APEX CCD diffractometer equipped with an Oxford Cryosystems low-temperature device by Prof Simon Parsons, University of Edinburgh, UK. Crystal structure determination was also carried out by the ESPRC National Crystallographic Service, University of Southampton, UK.

2.1.7 CHNS analysis

CHNS analyses were carried out by University of St. Andrews, St. Andrews, UK, using a CE Instruments EA1110 CHNS analyser.

2.1.8 Electrospray ionisation-mass spectrometry (ESI-MS)

Positive-ion electrospray ionisation mass spectra were obtained on a Micromass Platform II mass spectrometer and solutions were infused directly at 10 μL/min. The capillary voltage was 3.5kV and the cone voltage was typically varied between 5 and 45 V. The source temperature was dependent on the solvent used. Data were processed using Masslynx (v3.5) Windows XP PC data systems.

2.1.9 Ultraviolet and visible spectroscopy (UV-Vis)

UV-Vis absorption spectra were acquired on a Varian Cary 50 Bio spectrometer using 1 cm pathlength quartz cuvettes. Spectra were acquired at room temperature, processed using Cary WinUV version 3.0 software and referenced to the solvent alone.

2.1.10 pH measurements

All pH values of solutions were determined using a Corning 145 pH meter equipped with a micro combination electrode and calibrated with Aldrich buffer solutions at pH 4, 7 and 10.

2.1.11 EPR spectroscopy

EPR spectra were recorded on an X-band Bruker ER200D-SCR spectrometer connected to a Datalink 486DX PC with EPR Acquisition System, version 2.42 software with the help of Dr Neil Robertson, University of Edinburgh, UK. Data were simulated using Bruker WINEPR Simphonia version 1.26 software by the National EPR Centre, University of Manchester, UK and corrected as for the DPPH standard.[1]

2.1.12 Absorption Near Edge Structure (XANES) and Extended X-ray Absorption Fine Structure (EXAFS)

2.1.12.1 V K Edge XANES/EXAFS

All data were collected and recorded by Danielle Covelli, University of British Columbia, Canada. X-ray absorption spectra were recorded at Stanford Synchrotron Radiation Laboratory (SSRL) on the 20-pole wiggler beam line 7-3, under ring operating conditions of 80-100 mA and 3 GeV. Data was collected using a Si (220) phi = 0° double crystal monochromator and the signal was detected using a 30 element Ge detector array. All samples were prepared by lightly grinding 5 mg of vanadium complex with boron nitride in a mortar and pestle until a fine uniform powder was formed. Vanadium metal reference foil was used for energy calibration.

XAS data were collected in the energy range from 5235-6485 eV using XAS Collect software. Ten scans of each compound were obtained at the V K edge, to ensure reproducibility. Energy calibration was performed using the V K-edge spectrum of a vanadium metal foil, assuming the lowest energy peak to be 5465 eV. Data processing, including averaging scans, energy calibration, background subtraction and normalisation was performed in SixPACK (Sam Webb, Stanford Synchrotron Radiation Laboratory). EXAFS analysis was carried out using Artemis (Bruce Ravel, Argonne National Laboratory).

Portions of this research were carried out at the Stanford Synchrotron Radiation Laboratory, a national user facility operated by Stanford University on behalf of the U.S. Department of Energy, Office of Basic Energy Sciences. The SSRL Structural Molecular Biology Program is supported by the Department of Energy, Office of Biological and Environmental Research and by the National Institutes of Health, National Centre for Research Resources, Biomedical Technology Program.

Some of the techniques in this section were used extensively throughout the project. These are discussed in more detail in the next section.

2.2 IR spectroscopy [2, 3]

Infrared (IR) absorption spectra provide a quick and simple means of confirming the presence or absence of a functional group in a molecule or compound. This technique is used routinely by vanadium chemists to look at the characteristic vibrational stretch of the V(IV)=O group, found to be in

the range 980 ± 50 cm^{-1}[4] and both solid state and solution IR have proved to have been invaluable in this work. IR is one of the few techniques available for acquiring informative structural data for paramagnetic vanadium compounds such as those synthesised in this thesis. Coordination of groups like acetate can take place with a metal in three different modes (unidentate, bidentate or bridging) and these modes may be identified through a comparison of frequencies with ionic acetate complexes. The technique has been used for both vanadium and zinc work in this thesis.

Spectra can be recorded in transmission or absorption mode and identifications made are unique to a particular molecule's structure. There are two types of fundamental vibrations in molecules and for each to be seen in an IR spectrum there must be a change in the electric dipole of the molecule. A stretch is a vibration between two atoms on the same bond axis and the distance between them can increase or decrease. A bend occurs when the position of the atoms change relative to the bond axis.

In a simple diatomic molecule both atoms are bonded by the overlap of a number of orbitals. At a particular internuclear distance a balance is met between attractive bonding forces and repulsive interaction between the remaining electrons of both atoms. This equilibrium bond distance (r_e) can be changed by applying energy and the system vibrates at a certain frequency, ώ defined by:

$$\acute{\omega} = \frac{1}{2\pi}\sqrt{\frac{k}{\mu}}$$

where μ is the reduced mass of the two objects.

$$\mu = \frac{(m_1 * m_2)}{(m_1 + m_2)}$$

The vibrational frequency will depend on the mass of the two atoms at either end of the bond and the strength of the bond, or *force constant*, holding them

together. Heavier atoms held by weaker bonds should vibrate at lower frequencies than lighter atoms and those held by multiple bonds. The vibrational frequency also alters with charge on a molecule. As the number of electrons changes, the occupation of the bonding and nonbonding molecular orbitals varies. An increase of bond order and strength leads to an observed increase in vibrational frequency.

2.3 Resonance Raman spectroscopy [2, 5]

Resonance Raman and infrared spectroscopies are complimentary techniques. Polar bonds result in a large dipole and absorb strongly in the infrared, whereas more easily polarised covalent bonds absorb strongly in Raman spectra. These techniques can be used together to determine the presence or absence of a centre of symmetry in a molecule. Compounds with a centre of symmetry will not display any common peaks in their Raman and infrared spectra and this is described by the *mutual exclusion principle*. For solution studies, the choice of solvent is important in vibrational spectroscopy. As water is a poor Raman scatterer, aqueous solutions are more amenable to study by Raman than infrared spectroscopy.

Raman spectra originate in the electronic polarisation caused by ultraviolet or visible light. When light of energy less than that required to promote a molecule into an excited electronic state is absorbed by a molecule a *virtual excited state* is created.

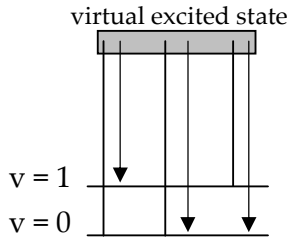

Figure2.1 Energy levels involved in Raman spectroscopy

The lifetime of this virtual state is very short and the majority of the light is re-emitted over 360° at the same energy. This re-emitted light is known as *Rayleigh scattering*. A small proportion of this re-emitted light differs in energy from the incident radiation (ν_0) by energy gaps that correspond to some of the vibrational modes. The probability for a ground state molecule to be excited into a vibrationally excited state is high due to the population density of the ground state. This leads to peaks with high intensity being observed at a lower frequency than the incident radiation (Stokes lines). Peaks derived from excited vibrational states at higher energy are called anti-Stokes lines and will be much lower in intensity as a result of the much smaller population density.

The selection rule for Raman spectroscopy differs from that of infrared. Raman activity is determined by a change in polarisability of the molecule during a vibration. The polarisability is a measure of the ease with which the electron cloud may be distorted, or polarised.

2.4 NMR spectroscopy [6-9]

Some atomic nuclei have a nuclear spin (I) that results in observed behaviour not unlike that of bar magnets. When a magnetic field is applied, these magnets can orient themselves in $2I + 1$ different ways. The most important nuclei for NMR analysis are ^{1}H and ^{13}C with spins of ½ and these nuclei adopt one of two possible orientations. The low energy orientation is aligned with the magnetic field and the high energy orientation is aligned against the applied field. The difference in energy is given by

$$\Delta E = h\gamma B_0/2\pi$$

where γ = gyromagnetic ratio (a proportionality constant that measures the strength of the nuclear magnets). This constant is different for each nucleus. B_0 is the strength of the applied field and the number of nuclei in the low energy state (N_α) and in the high energy state (N_β), will differ by an amount determined by the Boltzmann distribution:

$$N_\beta/N_\alpha = \exp(-\Delta E/kT)$$

Nuclear spins of $^1/_2$, $^3/_2$, or $^5/_2$, ….., etc. belong to nuclei with an odd mass number.

Table 2.1 ***NMR magnetic properties of nuclei studied in this thesis***

Nucleus	**Spin quantum number, *I***	**Magnetic moment, μ (μ_N)**	**Gyromagnetic ratio, γ (10^7 rad $T^{-1}s^{-1}$)**	**Natural Abundance (%)**	**Sensitivity (relative to ^{1}H)**
^{1}H	½	4.84	26.75	99.99	1.000
^{13}C	½	1.22	6.73	1.11	0.016
^{15}N	½	0.49	-2.71	0.37	0.001
^{*51}V	$^7/_2$	5.1514	7.0453	99.76	0.382

****^{51}V not studied by NMR in this thesis, but relevant to EPR studies***

2.4.1 Nuclear spin and chemical shift

The spin quantum number of NMR active nuclei must be equal to, or greater than ½ for the nucleus to possess a magnetic moment, generated by the spinning of the nucleus. The magnitude of the magnetic moment varies between atoms and is defined as

$$\mu = \gamma h/2\pi I$$

where h = Planck's constant. The spin states of nuclei are characterised by magnetic quantum numbers $m_I = I, I\text{-}1, I\text{-}2, \ldots, -I$. In the presence of a magnetic field the orientation of the magnetic moment μ, to the field direction (z-axis) is quantised and depends on I such that

$$\mu_z = \gamma h/2\pi m_I$$

where m_I has $2I + 1$ values. The energy of a transition is dependent upon the strength of the magnetic field and the magnetogyric ratio, γ. The frequency ν, of such a transition is given by

$$\nu_0 = \gamma B_0/2\pi$$

In the absence of a magnetic field, all $2I + 1$ orientations of a spin-I nucleus have the same energy. This degeneracy is removed on the application of B_0.

The position of the chemical shift describes the chemical environment of a nucleus. In a molecule, the magnetic field B, experienced by a nucleus differs from B_0 due to a small magnetic field B′, induced by the electrons of the molecule circulating in the direction of the magnetic field. The motion of B opposes B_0 shielding the nucleus to some extent such that

$$B = B_0 - B'$$

A definition of the chemical shift δ, is given in terms of the difference in resonance frequencies between the nucleus being studied (ν) and a reference nucleus (ν_{ref}).

$$\delta = 10^6 [(\nu - \nu_{ref})/\nu_{ref}]$$

The term δ is quoted in parts per million to scale the numerical value to a convenient size. The signals for deshielded nuclei are seen on the left hand side of the spectrum due to a larger ν and δ. Deshielding effects can be seen as a result of hydrogen bonding and, in particular, intramolecular hydrogen

bonds can shift a signal to a higher chemical shift than its expected resonance.

2.4.2 Spin-spin coupling and quadrupolar relaxation

Interactions between the spins of neighbouring nuclei result in the splitting of the NMR signal, the pattern of which is characteristic of the nuclear environment under investigation. Spin-spin coupling is measured using the *coupling constant*, *J* (Hz) and is observable up to 4 bond lengths (W coupling). This is seen in aromatic systems where the planarity of the ring allows specific nuclei to "see" each other across a further distance than usually observed in an NMR spectrum. These spectra show splitting patterns characterised by the presence of weak couplings. Normally, *J* (Hz) is only observable up to 3 bond lengths between nuclear centres.

Coupling constant values are affected by interbond angles and increase with increasing angles. In the case of olefinic *cis*- and *trans*- coupling, for two-bond coupling a *trans*- coupling is normally observed with a larger *J*(Hz) value than a corresponding *cis*- coupling. For three-bond coupling, the dihedral angle ϕ, is important between planes containing coupling nuclei and bonds associated with them. The dihedral angle can be derived from the Karplus equation

$$^{3}J = C\cos^{2}\phi + B\cos\phi + A$$

Quadrupolar relaxation is electric rather than magnetic in origin. In contrast to nuclei with values of I = ½ where the charge distribution is spherical, nuclei with a quadrupole moment are ellipsoidal in charge distribution (I > ½). An electric field is generated from the motion of an unsymmetrical field for these species, creating a fluctuating electric field or

electric quadrupole. If a quadrupole moment is large enough, it can influence both its own nucleus and adjacent nuclei. Line broadening is seen for nuclei attached to atoms with larger relative electric quadrupole moments. Often, NH protons cannot be observed (or are very broad) due to the quadrupole effect. Relaxation refers to the processes that allow nuclear spins to lose energy and drop from the excited state to the ground state without emitting an NMR signal.

2.4.3 Paramagnetic effects in NMR spectra [10]

The unpaired electrons in paramagnetic compounds such as high spin Fe(II), Fe(III), Co(II), Ni(II), Cu(II) and Ru(III) have a severe effect on chemical shift and linewidths of signals observed in spectra of biomolecules that contain one or more paramagnetic transition metals. The extent of line broadening observed, as seen with NH protons, is a major drawback for analysis using high-resolution NMR spectroscopy. In some compounds the extent of delocalisation of an unpaired electron is such that severe line broadening results in no signal being seen. Relaxation of the unpaired electron(s) is the main cause of line-broadening effects seen in solution spectra due to a dipolar or contact coupling with the resonating nucleus *i.e.* through-space or through-bond. No NMR analysis was possible for the vanadium complexes in this thesis as paramagnetic signals were too broad to detect.

2.4.4 2D NMR spectroscopy

In 2D NMR, a second dimension is introduced that allows for more detailed structural determination. The most important benefit is that individual chemical shifts and all coupling constants can be measured

without ambiguity, even when multiplets are overlapping. 2D NMR data is especially valuable to completely assign the signals of a compound for which the structure is already known. There are now several two-dimensional experiments available for molecular structural studies and those used in this thesis are listed in Table 2.2.

Table 2.2 2D NMR experiments used in this thesis

Information desired	**Experiment**
Proton-proton couplings	[^{1}H,^{1}H] COSY
Long range proton-proton couplings	[^{1}H,^{1}H] TOCSY
Unknown proton assignments from that of known carbons, or *vice versa*	[^{1}H,^{13}C] HSQC
Unknown NH proton assignments	[^{1}H,^{15}N] HSQC

2.4.4.1 COrrelation SpectroscopY (COSY) and TOtal Correlation SpectroscopY (TOCSY)

Most 2D experiments can be divided into auto-correlated or cross-correlated types. Auto-correlated experiments refer to homonuclear spin systems where a magnetisation (or coherence) transfer occurs. A common auto-correlation experiment is [^{1}H, ^{1}H] COSY that produces *off-diagonal* correlation peaks. In cross-correlation experiments the magnetisation of one nucleus is modified by the coupling effects of other nuclei. The 2D peaks appear at the intersection of f_1 and f_2, *i.e.* both axes are in frequency units which may be converted to ppm.

In [^{1}H, ^{1}H] COSY experiments, signals from couplings are viewed as cross-peaks between the two frequency domains and are dominated by geminal and vicinal coupling. In [^{1}H, ^{1}H] TOCSY experiments, all mutually coupled proton spins can be grouped from the cross-peaks present. This experiment contains much more information than the [^{1}H, ^{1}H] COSY as correlations between protons up to seven bonds are possible. The transfer of magnetisation occurs from H_a to H_b, from H_b to H_c and so on until all mutually coupled protons have been connected. Relationships can be established between protons that are actually far removed. An advantage of this experiment is the ability to identify the number of isomers or different products in a sample.

Information	Groups	Experiments
Vicinal proton connectivities		[^{1}H, ^{1}H] COSY
All proton connectivities in one spin system	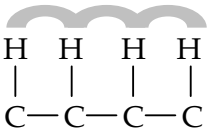	[^{1}H, ^{1}H] TOCSY

2.4.4.2 Heteronuclear Single-Quantum Correlation (HSQC)

These experiments enable identification of protons directly coupled to other NMR active nuclei (H-X). Examples include [^{1}H, ^{13}C] and [^{1}H, ^{15}N] HSQC experiments. Proton resonances may also be more spread out depending on the chemical shifts of coupled heteronuclei. This allows assignment of protons that may be overlapping in 1D or 2D proton spectra.

A useful practice for [^{1}H, ^{13}C] HSQC is the identification of NH protons through their absence in the spectrum. Broadened NH peaks that show up in a 1D spectrum can be verified in this way, leading to easier identification of the remainder of the molecule by acquiring this as a starting point for assignment of the peaks.

2.4.4.3 ^{15}N NMR spectroscopy [9]

Proton resonances have been detected from NH protons with ^{14}N present in natural abundance (99.6 %) but they are often broadened as ^{14}N is a quadrupolar nucleus (I=1) and quadrupolar relaxation occurs. For aqueous experiments, D_2O is usually unsuitable due to NH/ND exchange and it is often necessary to work in H_2O. Despite the low natural abundance of ^{15}N (0.37 %), it has spin ½ and can be utilised in experiments using polarisation transfer from ^{1}H. This leads to an intensity increase in signal, given by the ratio of magnetogyric ratios, γ_H/γ_X. For ^{15}N, a gain of 9.8 (γ_H/γ_X) in signal intensity is achievable by such a polarisation transfer.

2.5 EPR spectroscopy [11-17]

EPR (Electron Paramagnetic Resonance) or ESR (Electron Spin Resonance) is a magnetic resonance method used to characterise and investigate properties of paramagnetic materials, those containing unpaired electrons. Materials such as free radicals, donor and acceptor impurities in semiconductors, metal ions in crystals and inorganic metal complexes can be studied using this method. The fundamental physical concepts are related to that of nuclear magnetic resonance (NMR), the main contrast being that the

excited spins are those of electrons rather than nuclear spins. Information on the structure and environment of radicals can be gained from important parameters such as g-factors, hyperfine (hf) splitting (electron-nucleus coupling) and zero field splitting. Investigations at different temperatures can provide information on the dynamics of a system.

2.5.1 Spin-lattice relaxation

Magnetic energy is absorbed by the paramagnetic ion and transferred to the lattice. Lattice motions result in a fluctuating magnetic field to which the spin magnetic moment of the electron couples, and magnetic energy is emitted. This simple loss of energy means that a particular spin spends less time in the excited state resulting in a broadened resonance line. Line-widths are predicted from spin-lattice relaxation $(2\pi T_1)^{-1}$, where T_1 is the relaxation time for the transfer of energy from the spin system to the lattice. T_1 is particularly sensitive to temperature and the presence of nearby electronic excited states. A decrease in temperature reduces molecular tumbling and interatomic motion, resulting in longer relaxation times and subsequent narrower lines. Nearby electronic excited states (~ 100 cm^{-1}) result in short relaxation times and lower temperatures are required to reduce the width of the lines.

2.5.2 Hyperfine splitting

Magnetic interactions that occur between electron spins and nuclear spins in a molecule give rise to a specific number of lines in the EPR spectrum. This arrangement is the *hyperfine structure* of the spectrum. From the number of lines and relative intensities, interpretation of the number and

spins of the nuclei that interact with an unpaired electron can be made. The strength of the interaction and the magnetic moments of the nuclei give rise to the separations between the lines. The hyperfine separation can be used to describe the number of equivalent nuclei in the molecule.

2.5.3 Line widths and intensities

The line width is a result of magnetic interactions between the electron spin and the environment in the sample. As electrons can interact magnetically with their environment in the sample, the resultant magnetic field experienced by a population of electron spins is not evenly distributed. The resonance absorption line obtained for a given value of this resultant field is obtained over a range of values of the applied field. This results in a finite line width from which information regarding the spin environment can be obtained. One such example of these effects is the ability to make an order of magnitude estimate of the distance between paramagnetic centres and chemical exchange between a paramagnetic molecule and its surroundings.

Several parameters affect the intensity of a signal which is the total area under the resonance curve. A combination of frequency (usually 9.5 GHz), concentration of paramagnetic sample and temperature all determine the intensity of the observed signal. The intensity can be used to determine the concentration of paramagnetic centres in the sample.

2.5.4 Magnetic moment and g-factor

The fundamental properties of an electron are its mass, charge, intrinsic angular momentum (also known as the spin) and its magnetic

moment. The magnetic moment μ, can be thought of as arising from the spinning motion of the electron's charge and has the spin quantum number s = ½ with magnetic components $m_s = +½$ and $m_s = -½$. The magnetic moment of the electron is aligned either parallel ($m_s = +½$) or antiparallel ($m_s = -½$) to the magnetic field (B_0) and different energies apply to each. A lower energy is associated with the anti-parallel alignment and the energy difference between the two states is given by:

$$\Delta E = g_e \mu_B B_0$$

Figure 2.3 shows how energy levels are split with increasing magnetic field, B_0.

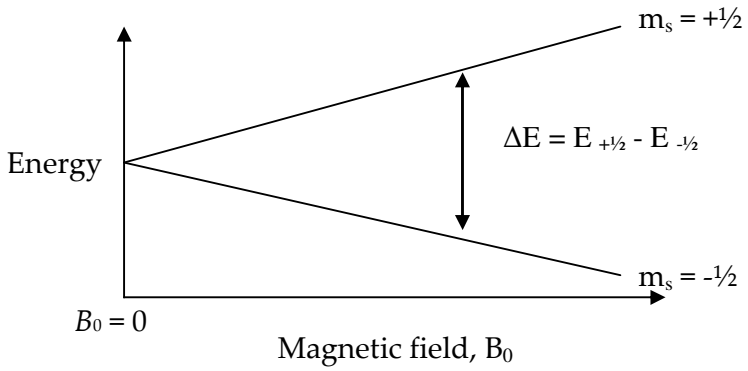

Figure 2.3 Splitting of energy levels is directly proportional to strength of magnetic field

Equations of ΔE with $h\nu$ gives a resonance condition that is satisfied through irradiation with photons. Transitions are subsequently induced between the two levels and the populations of the energy levels can be shown as:

$$\frac{n_+}{n_-} = e^{-\Delta E/kT}$$

in which n_+ and n_- represent populations of upper and lower level energy states, respectively. It is this population difference caused by the energy separation that is detected as an absorption. An EPR spectrometer achieves resonance using a fixed frequency ν, while sweeping the magnetic field. Experiments typically employ microwave frequencies of approximately 9 GHz in X-band spectrometers and spectra are commonly presented as first or second derivatives. Higher field W-band spectrometers operate at 95 GHz and the improved spectral resolution can reveal small couplings not seen with X-band analysis. Recent developments have resulted in spectrometers operating up to THz (very high frequency (VHF) EPR) and are most prominently used in structural biology.[18]

The g-factor represented by g_e, is a physical property of the electron and a proportionality constant between the magnetic moment and the angular momentum where g_e = 2.002319 for unpaired electrons. Different metal ions have varying g-values and published values for some examples of d^1 Ti^{3+}, Zr^{3+}, Nb^{4+}, Cr^{5+}, Mo^{5+} and W^{5+} ions are listed in Table 2.4. Published values for some examples of d^1 V^{4+} ions are listed in Table 2.5. In addition to its spin, an electron can have additional angular momentum as it moves not only around its own axis but also in an orbit and is called orbital angular momentum. Orbital angular momentum also has a magnetic moment associated with it.

Table 2.4 Listed g-values for d^1 metal ions [19]

Metal ion	g_{iso}	$g_{\parallel}$	$g_{\perp}$
CpTiX, X = C_3H_5,			
$C_3H_3Me_2$, C_3H_4Et	1.991	-	-
$[Cp_2Zr(PPh_2)_2]^-$	1.989	-	-
$[Nb(OCH_3)Cl_5]^{2-}$	1.869	1.923	1.842
$[CrOCl_5]^{2-}$	1.988	2.008	1.974
$[MoOCl_5]^{2-}$	1.947	1.96	1.938
$[MoOBr_5]^{2-}$	1.993	2.090	1.945
$[WOCl_5]^{2-}$	1.773	1.804	1.758
$[WOBr_5]^{2-}$	1.830	1.940	1.775

Table 2.5 Listed g-values for d^1 V^{4+} ions [19]

Metal ion	g_{iso}	$g_{\parallel}$	$g_{\perp}$
VO^{2+}			
in KNO_3	1.966	1.9352	1.974
in $CsNO_3$	1.964	1.919	1.984
$V(NEt_2)_4$	1.976	1.946	1.991
$VOSO_4$			
in H_2O	1.961	-	-
$VO(acac)_2$			
in CH_3OH	1.969	-	-
VO(picolinate)$_2$	1.970	-	-
VOTPP		-	-
in $CHCl_3$	1.979	1.966	1.985

2.5.5 EPR of V^{4+} and VO^{2+}

^{51}V has a natural abundance of 99.8% and a nuclear spin I = $^7/_2$. In solution, eight hyperfine lines are observed and couplings are usually large (~ 100 gauss). As almost all vanadium compounds have symmetry less than O_h and T_d, EPR signals are easily observed due to a longer relaxation time.[19] At room temperature there is free rotation of the vanadyl group (V=O) resulting in an isotropic spectrum. At lower temperatures anisotropy becomes apparent and axial or rhombic spectra can be identified. Lower A_{iso} values are seen with increasing basicity due to greater delocalisation of the unpaired electron and vanadium systems are sensitive to solvation. The

decrease in A_{iso} with basicity of any 6th axial solvent ligand can be compared with the same decrease in stretching frequency of the V=O group as the basicity of the 6th axial ligand increases. Higher A_{iso} (^{51}V) values are associated with greater localisation of the electron on the metal when ligands are electrophilic in nature.[19]

2.6 Bibliography

[1] S. A. Al'tshuler, B. M. Kozyrev, *Electron Paramagnetic Resonance*, C P Joole, Jr., ed., Academic Press, New York, **1964**.

[2] A. K. Brisdon, *Inorganic Spectroscopic Methods*, University Press, Oxford, **1998**.

[3] J. B. Lambert, H. F. Shurvell, D. A. Lightner, R. G. Cooks, *Organic Structural Spectroscopy*, Prentice-Hall, New Jersey, **1998**.

[4] J. Selbin, *Chem. Rev.,* **1965**, *65*, 153.

[5] K. Nakamoto, *Infrared and Raman Spectra of Inorganic and Coordination Compounds*, 4 ed., Wiley - interscience, Canada, **1986**.

[6] G. Bodenhausen, D. J. Ruben, *Chem. Phys. Lett.,* **1980**, *69*, 185.

[7] P. Crews, J. Rodriquez, M. Jaspers, *Organic Structure Analysis* Oxford University Press, New York, **1998**.

[8] D. H. Williams, I. Fleming, *Spectroscopic Methods in Organic Chemistry*, 5 ed., University Press, Cambridge, **1995**.

[9] S. J. Berners-Price, P. J. Sadler, *Coord. Chem. Rev.,* **1996**, *151*, 1.

[10] L. Ronconi, P. J. Sadler, *Coord. Chem. Rev.,* **2008**, *doi:10.1016/j.ccr.2008.01.016*.

[11] N. M. Atherton, *Principles of Electron Spin Resonance*, Ellis Horwood, Chichester, **1993**.

[12] A. J. Hoff, *Advanced EPR Applications in Biology and Biochemistry*, Elsevier, Amsterdam, **1989**.

[13] M. Bersohn, J. C. Baird, *An Introduction To Electron Paramagnetic Resonance*, W A Benjamin, Inc., New York, **1966**.

[14] J. R. Pilbrow, *Transition Ion Electron Paramagnetic Resonance*, Clarendon Press, Oxford, **1990**.

[15] G. R. Eaton, S. S. Eaton, K. M. Salikhov, *Foundations of Modern EPR*, World Scientific, Singapore, **1998**.

[16] J. A. Weil, J. R. Bolton, J. E. Wertz, *Electron Paramagnetic Resonance. Elementary Theory and Practical Applications*, Wiley, New York, **1994**.

[17] F. E. Mabbs, *Chem. Soc. Rev.,* **1993**, *22*, 313.

[18] M. Bennati, T. F. Prisner, *Rep. Prog. Phys.,* **2005**, *68*, 411.

[19] B. A. Goodman, J. B. Raynor, *Electron spin resonance of transition metal complexes. In: Advances in Inorganic Chemical Radiochemistry (H.J. Eneleus, A G Sharpe)*, Academic Press, London, **1970**.

3. OXOVANADIUM(IV) CYCLAM COMPLEXES

This chapter describes the syntheses of oxovanadium(IV) cyclam complexes, **21**-**29**. Numbers in bold after compound names refer to experimental data in Chapter 7. Two complexes, oxovanadium(IV) cyclam sulfate **21** and chloride **22** were investigated further with bicyclam analogues, oxovanadium(IV)-xylyl-bicyclam sulfate **30** and chloride **31** (Chapter 4) to explore the chemistry of oxovanadium(IV) in macrocycles.

Cyclam exhibits high thermodynamic and kinetic stability on complexation with a variety of cations, including transition metals.[1] The particular macrocycle ring configurations of isomers in solution are dependent upon the geometry of the complex in question. The stereochemistry is dictated by the chirality of the ring nitrogens giving rise to the five *trans*- and two *cis*- configurations shown in Figure 1.9 and Figure 3.1(a).

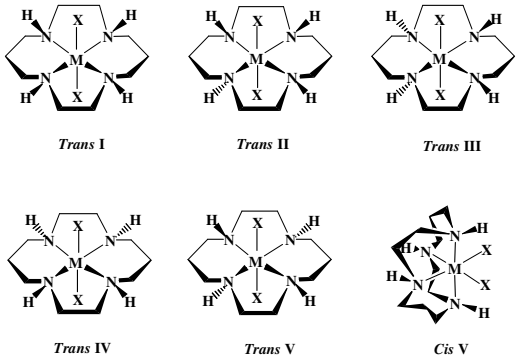

Figure 3.1(a) Configurations of metal cyclam

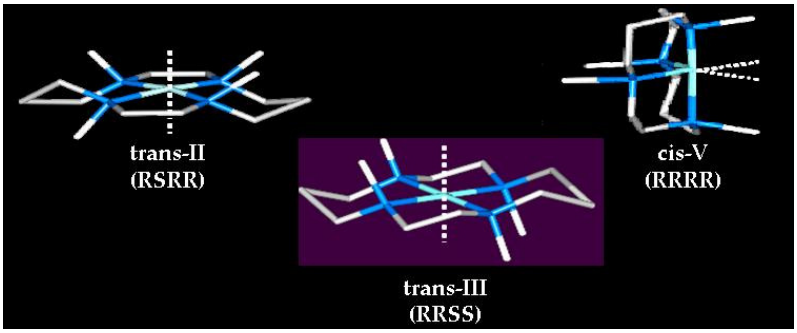

Figure 3.1(b) Some major configurations of metallo-cyclam complexes.

Square planar complexes prefer to adopt the *trans*-I configuration while octahedral complexes show a preference for *trans*-III.[2, 3] It is thought that *trans*-I and *trans*-III configurations may interconvert in solution due to the flexibility of the ring and investigation of the relative strain energies reveals that the *trans*-III isomer is the most stable.[3, 4] Configurational isomers thought to exhibit antiviral activity against HIV include *trans*-I/*trans*-III, *trans*-II and *cis*-V, shown in Figure 3.1(b).

3.1. Experimental

Oxovanadium(IV) cyclam complexes were synthesised as shown in Scheme 3.2.

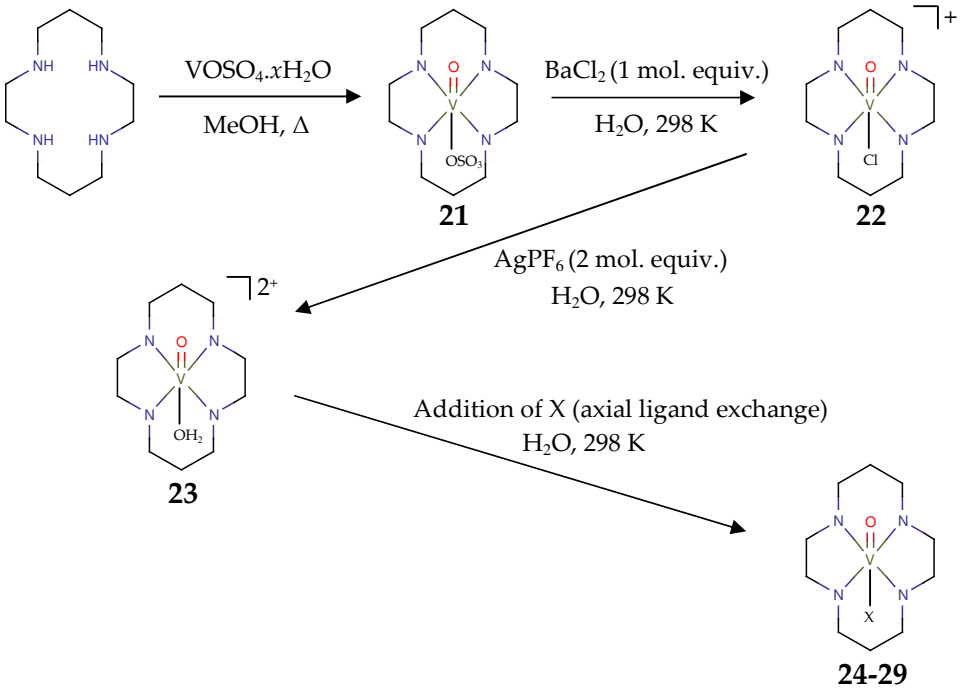

Scheme 3.2 General preparative route to oxovanadium(IV) macrocycle complexes where X = Br (24), I (25), NCS (26), $HOPO_3$ (27), GMP (28) and cGMP(29) (experimental details are found in Chapter 7).

3.2. Materials

Starting materials were purchased from Sigma-Aldrich as detailed in Chapter 2. The solvent used for all synthetic work was anhydrous quality methanol from Sigma-Aldrich. HPLC Grade methanol and reagent grade diethyl ether were used for crystallisations.

3.3. Results

3.3.1. Magnetic measurements

Bulk magnetic properties can be analysed by measuring the magnetic polarisation *M*, in an applied magnetic field, *H*. The sensitivity of *M* to *H* is defined as the magnetic susceptibility X, where X = d*M*/d*H* which in low fields can be approximated to *M*/*H*, and values of X are comprised of two components. The parameter X consists of a diamagnetic component which is very small resulting from paired electrons and a paramagnetic component which is much larger and results from unpaired electrons. The small diamagnetic component is subtracted to give a net susceptibility such that $X_{para} = X_{total} - X_{dia}$. In subsequent discussion, X will be taken to mean X_{para}. The parameter X_{para} holds the most useful information of the sample, and significantly, above any bulk magnetic ordering temperature can be generally represented by the equation:

$$X_{para} = \frac{g^2\mu_B^2\mu_o S(S+1)N_A}{3k_B T}$$

where $\mu_o = 1$ in c.g.s. units (permeability), $N_A/3k_B = 1/8$ in c.g.s. units and μ_B = the Bohr Magneton. The magnetic moment, $\mu_{eff} = g\sqrt{(S(S+1))}\mu_B$ such that X_{para} can be described as:

$$\frac{(\mu_{eff})^2}{8} \times \frac{1}{T} = \frac{C}{T} \quad \text{and} \quad X = \frac{C}{T} \text{ is known as the Curie Law.}$$

Data from paramagnetic compounds with no interacting magnetic moments will therefore give a straight line plot for 1/X vs T. The slope of the line gives the Curie constant from which the g-value is derived. This Law is further refined to include the parameter Θ, the Weiss constant, where $X = \frac{C}{T-\Theta}$ is referred to as the Curie-Weiss Law. Dominant ferromagnetic interactions will generally lead to $\Theta > 0$ and anti-ferromagnetic interactions which are much more common will lead to $\Theta < 0$. Data can be presented in different forms dependent upon the parameter used for the y-axis. In Figure 3.3(a) a plot of X vs T shows how the data fit well to the Curie Law for the cyclam chloride complex **22**. The same fit can also be made for the cyclam sulfate complex **21** and parameter values of g, C and Θ for both complexes are listed in Table 3.4. An alternative representation of the data would be to show a straight line plot using 1/X on the y-axis, where $\Theta = 0$ would pass through the origin, $\Theta < 0$ would give a negative intercept and $\Theta > 0$, a positive intercept on the x-axis. Data for complex **22** in this format is displayed in Figure 3.3(b).

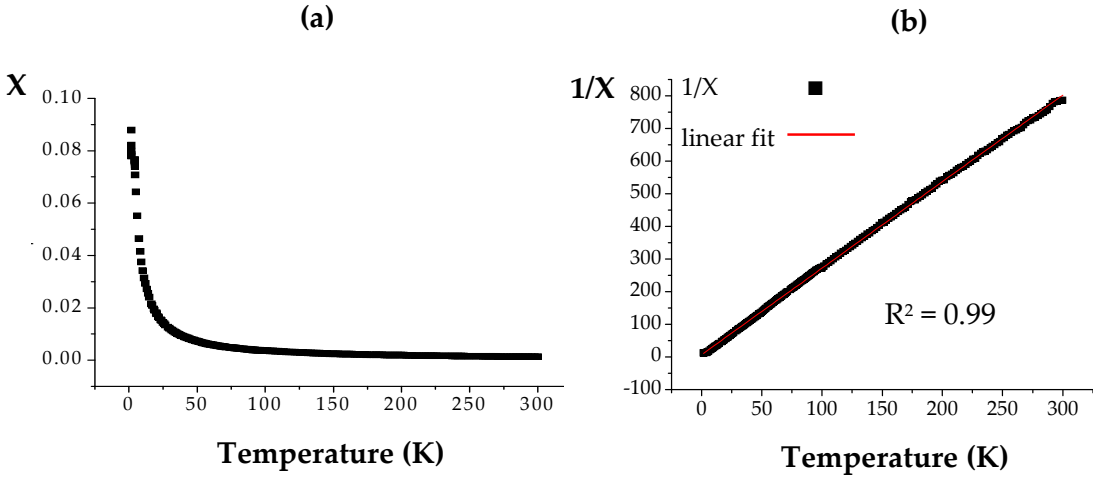

Figure 3.3 Plots of Curie Law fits for vacuum dried single crystals of oxovanadium(IV) cyclam chloride 22, in powder form. Graph (a) shows X vs T and graph (b) shows the reciprocal plot, 1/X vs T.

The good fit of the data for both complexes **21** and **22** to the Curie Law confirms the presence of an oxovanadium(IV) metal centre with negligible interactions between vanadium centres.

Table 3.4 Magnetic parameters for oxovanadium(IV) cyclam complexes, sulfate 21 and chloride 22

Complex	**g**	**C**	**Θ**	**μ_{eff}**
sulfate, 21	1.927	0.348	-0.05	1.67
chloride, 22	2.005	0.377	-2.61	1.73

3.3.2. X-ray crystallography

Four X-ray crystal structures of oxovanadium(IV) cyclam complexes were achieved in this work. Three structures were determined at 150 K (complexes **21**, **22** and **26**) and complex **25** was determined at 120 K. Data for the latter was collected by the EPSRC National Crystallography Service, University of Southampton, UK. All structures show the cyclam ring in the *trans*-III configuration. Selected bond lengths and angles are detailed in Table 3.5 with supporting crystallographic data in Table 3.6.

Table 3.5 Selected bond lengths (Å) and angles (°) for oxovanadium(IV) cyclam complexes. Italics apply to complex 25, where atom numbering different for comparison of identical bonds/angles.

Axial ligand *trans*- to V=O (except 25, I^- = counter ion)		**Sulfate (SO_4^{2-}), 21**	**Chloride (Cl^-), 22**	**Iodide (I^-), 25**	**Thiocyanate (NCS^-), 26**
V-N bond lengths	N(1)-V(15) N(4)-V(15) N(8)-V(15) N(11)-V(15)	2.107(2) 2.114(2) 2.0841(19) 2.0976(19)	2.097(4) 2.097(4) 2.081(4) 2.082(4)	2.097(2) *(N1-V1)* 2.093(2) *(N5-V1)* 2.111(2) *(N8-V1)* 2.0977(19) *(N12-V1)*	2.0907(18) 2.108(2) 2.0994(18) 2.0861(19)
V=O bond lengths	V(15)-O(16)	1.6093(17)	1.599(3)	1.6009(19)	1.6004(16)
V-L* bond lengths		2.1359(16) V(15)-O(17)	2.6501(12) V(15)-Cl(17)	2.6044(7) V(15)-Cl	2.2053(19) V(15)-N(17)
Bond angles	N(1)-V-N(11)	95.98(8)	95.67(16)	95.95(8) *(N8-V-N12)*	92.14(8)
	N(4)-V-N(1)	84.27(9)	83.91(15)	84.14(8) *(N12-V-N1)*	84.18(7)
	N(4)-V-N(8)	92.92(8)	92.12(15)	93.11(8) *(N1-V-N5)*	95.97(7)
	N(8)-V-N(1)	166.88(7)	165.46(16)	168.51(8)*(N5-V-N12)*	166.46(7)
	N(1)-V-L*	93.92(9)	83.39(12)	85.67(6) *(N12-V-L*)*	82.69(7)
	L-V=O	177.83(9)	176.99(12)	176.91(7)	178.74(8)

** L = bonding atom of axial ligand trans- to V=O.*

Table 3.6 X-ray crystallographic data for oxovanadium(IV) cyclam complexes

Axial ligand *trans-* to V=O	**Sulfate (SO_4^{2-}), 21**	**Chloride (Cl^-), 22**	**Iodide (I^-), 25**	**Thiocyanate (NCS^-), 26**
Formula	$C_{34}H_{84}N_{12}O_{19}S_3V_3$	$C_{11}H_{31}C_{l2}N_4O_{3.5}V_1$	$C_{10}H_{24}Cl_1I_1N_4O_1V_1$	$C_{11}H_{24}F_6N_5O_1P_1S_1V_1$
Formula weight	1214.13	397.24	429.62	470.31
Crystal system	Trigonal	Monoclinic	Monoclinic	Monoclinic
Space group	*R* 3 *c*	*C* 1 *c* 1	*P* 1 2_1/*n* 1	*P* 1 2_1/*n* 1
a / Å	25.2262(2)	15.3070(6)	10.0293(4)	9.4176(10)
b / Å	25.2262(2)	13.2387(6)	10.3318(4)	19.597(2)
c / Å	15.1963(3)	18.7031(8)	15.9990(5)	10.9379(12)
α / °	90	90	90	90
β / °	90	101.165(2)	90.704(3)	111.405(4)
γ / °	120	90	90	90
Cell vol. / $Å^3$	8374.76(19)	3718.4(3)	1657.70(11)	1879.4(4)
Z	6	8	4	4
Density (Calc) mg/m^3	1.444	1.419	1.721	1.662
Abs. coeff. mm^{-1}	0.680	0.838	2.618	0.792
Reflections collected	55545	8887	23623	19947
Independent reflections	5575 [R(int) = 0.037]	8887 [R(int) = 0.048]	3800 [R(int) = 0.0432]	4854 [R(int) = 0.040
R1 (obs/all refl)	0.0292 [3992 data]	0.0543 [8478 data]	0.0277 [3250 data]	0.0408 [4186 data]
wR2 (obs/all refl)	0.0849	0.1491	0.0724	0.1078

[$V^{(IV)}O(cyclam)SO_4$]·1.33CH_3OH], 21

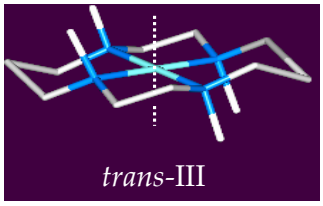

Complex **21** crystallised as the *trans*-III isomer, the most thermodynamically stable ring configuration (Figure 3.7). The geometry is distorted octahedral and one of the methanol molecules of crystallisation is disordered (Figure 3.8). Complex **21** is neutral and the sulfate group coordinates as a monodentate ligand. Two of the remaining sulfate oxygens form hydrogen bonds to two NH protons of the cyclam ring. The oxo-vanadium(IV) bond length is short (1.6093(19) Å) and comparable with the V=O bond in the square pyramidal oxovanadium(IV) complex [$V^{(IV)}O(acac)_2$] (1.58 Å).[5] The V-O(sulfate) bond length of 2.1359(16) Å, is slightly longer than the V-O bonds in [$V^{(IV)}O(acac)_2$] (1.97 Å).[5]

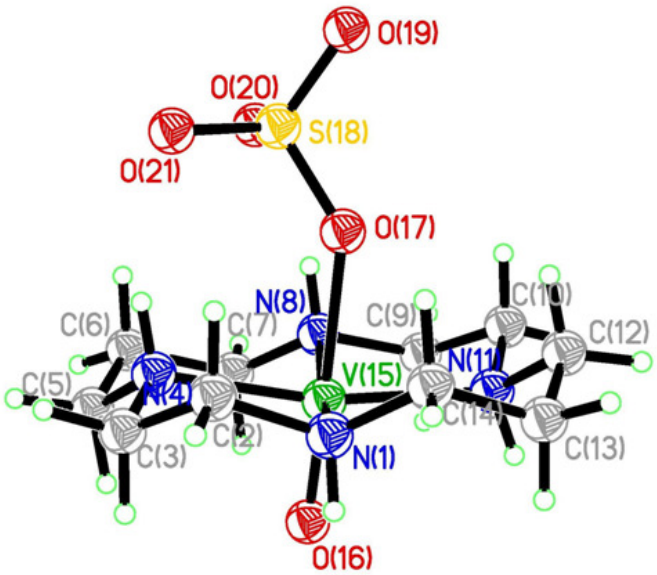

Figure 3.7 $V^{(IV)}O(cyclam)$ sulfate, 21

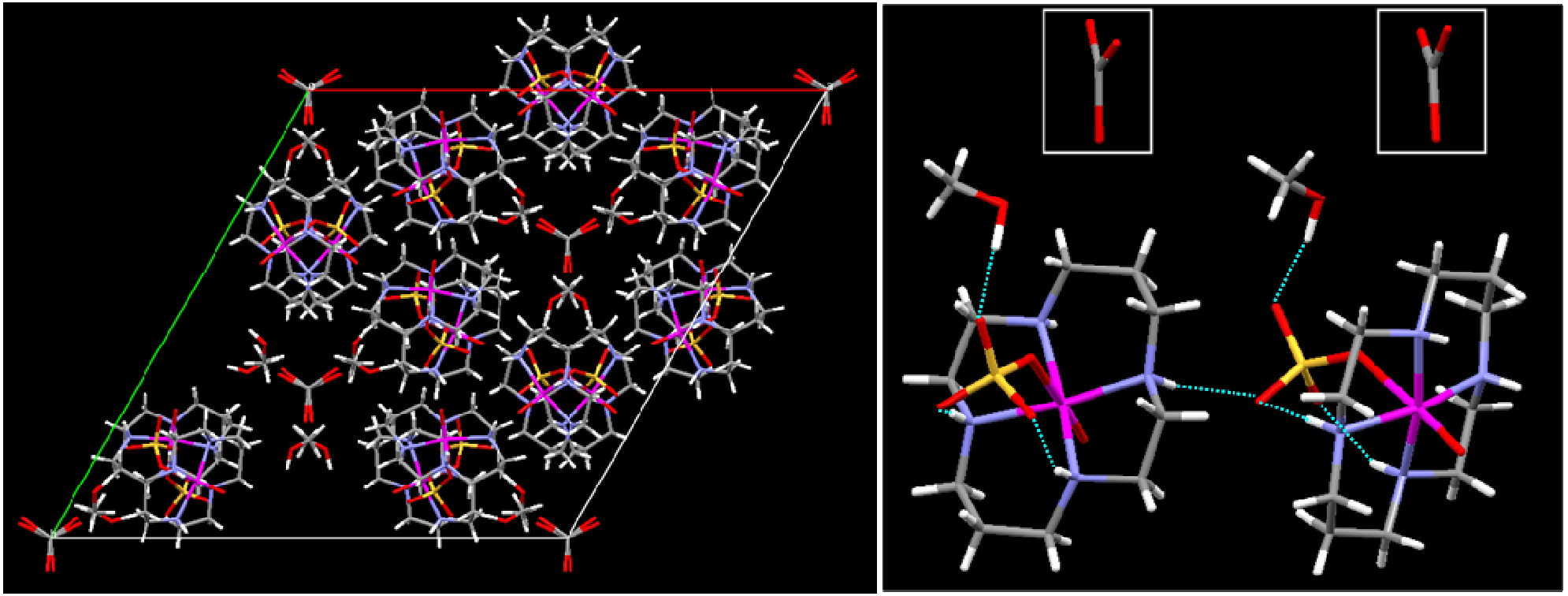

Figure 3.8 Crystal packing of [$V^{(IV)}O$(cyclam)SO_4·1.33 CH_3OH] 21, projected along the c axis of the unit cell. Hydrogen bonds are shown (cyan) between methanol, sulfate and NH groups, leading to stabilisation of the trans-III configuration. Methanol molecules with 100% carbon occupancy and disordered oxygens are highlighted in boxes.

[$V^{(IV)}$O(cyclam)Cl]·CH_3OH·1.5H_2O]Cl, 22

Complex **22** crystallised as the *trans*-III isomer, in a distorted octahedral geometry (Figure 3.9). There are two molecules in the asymmetric unit and the V-Cl bond is significantly longer than published examples for octahedral vanadium(IV) complexes of chloride ligands *trans*- to V=O[6, 7] (2.465 Å, 2.468 Å). Hydrogen bonds exist between chloride atoms, ring protons and solvent molecules, adding to the stability of the *trans*-III configuration (Figure 3.10). The angle Cl-V=O (176.99(12) Å) is significantly smaller than the corresponding O_3SO-V=O angle in the sulfate complex, **21** (177.83(9) Å). The N(1)-V(15)-N(8) angle (165.46(16) Å) is also significantly smaller than the corresponding angle in complex **21** (166.88(7) Å).

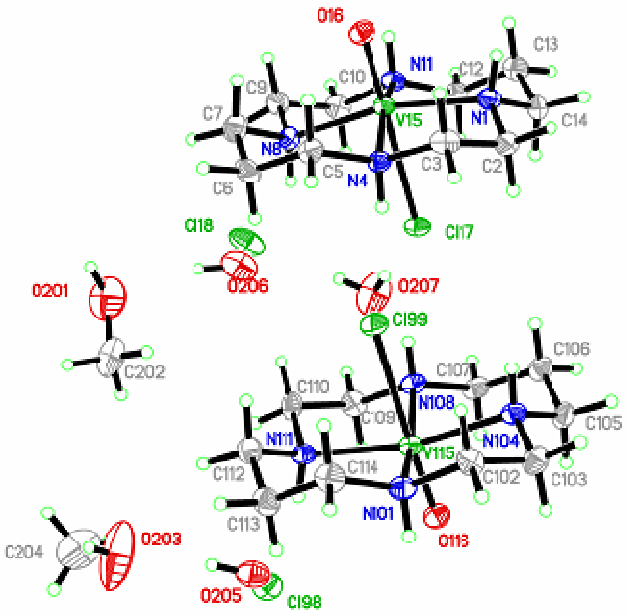

Figure 3.9 $V^{(IV)}$O(cyclam) chloride, 22

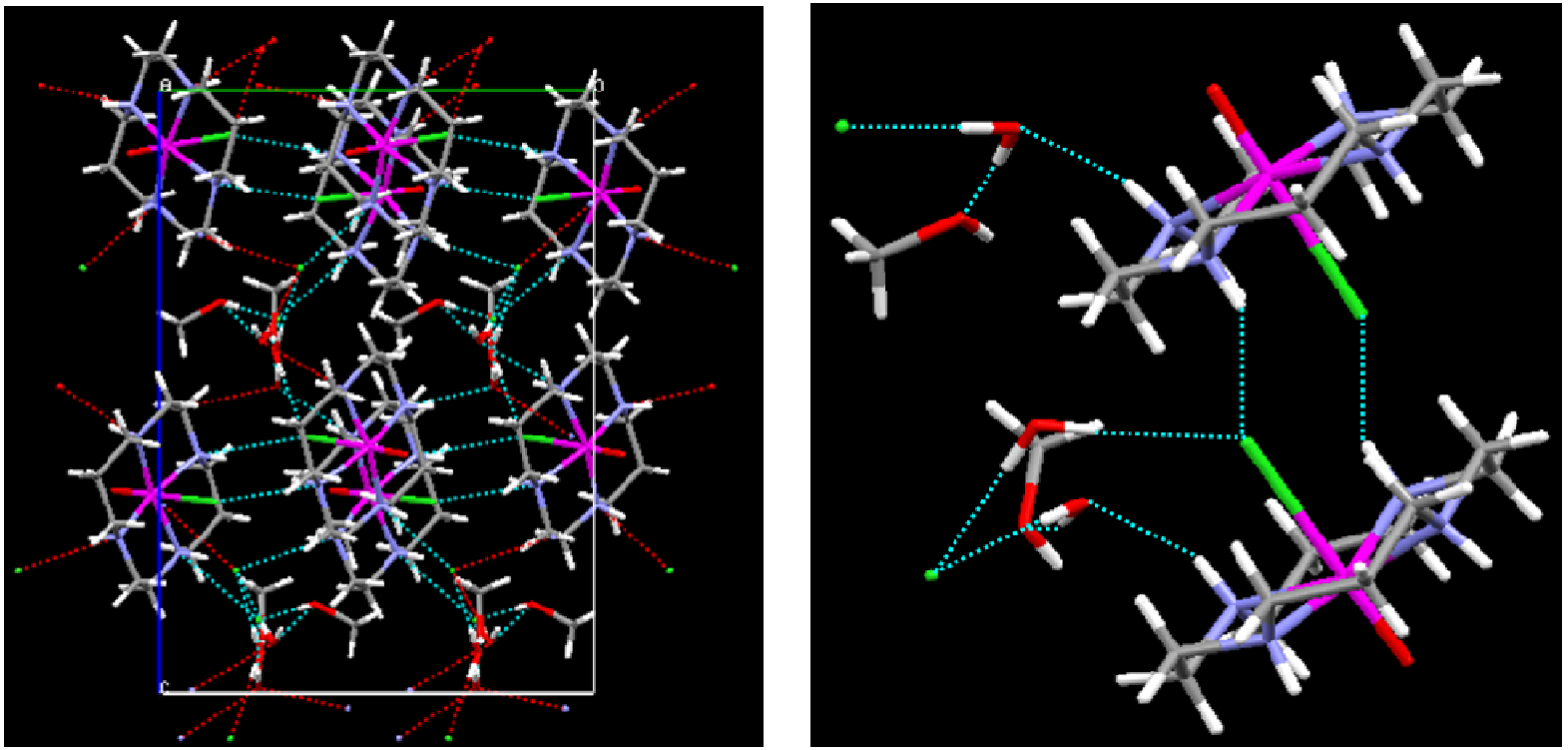

Figure 3.10 Crystal packing of $[V^{(IV)}O(cyclam)Cl]^{+}\cdot CH_3OH\cdot 1.5H_2O]Cl$, 22 showing networks of hydrogen bonding between chloride groups, NH groups, methanol and water. These interactions provide extra stability for the trans-III configuration.

[$V^{(IV)}$O(cyclam)Cl]I, 25

Complex **25** crystallised as the *trans*-III isomer, in a distorted octahedral geometry. The axial chloride and counter ion iodide ions were refined isotropically and are drawn as spheres instead of ellipsoids. During recrystallisation, the iodide ligand appears to have exchanged with the chloride. A small amount of chloride ion must have been present in the recrystallisation powder and shows an interesting preference of vanadium as a hard metal centre for a hard ligand. Mass spectrometry gave the molecular ion as m/z = 394.1 $[M]^+$ for $[VO(cyclam)I]^+$ which shows the iodide is bound. The iodide ion is seen as the counter ion in the crystal structure and it may be that the crystal chosen for X-ray analysis was part of a mixture of crystals with both chloride and iodide axial ligands. The V-Cl bond length (2.6044(7) Å) of **25** is significantly shorter than the V-Cl bond length of **22** (2.6501(12) Å). Distances were measured between axial chlorides of one molecule and the ring NH protons of a neighbouring molecule in complex **22** and compared with **25**. The former shows calculated distances of 2.491 Å and 2.590 Å, while the latter displays a much longer distance of 2.736 Å. There is no hydrogen bonding seen in complex **25** and the angle N-V-N is correspondingly larger than that seen for complex **22**. The angle Cl-V=O (176.91(7) Å) is comparable with that of complex **22** (176.99(12) Å).

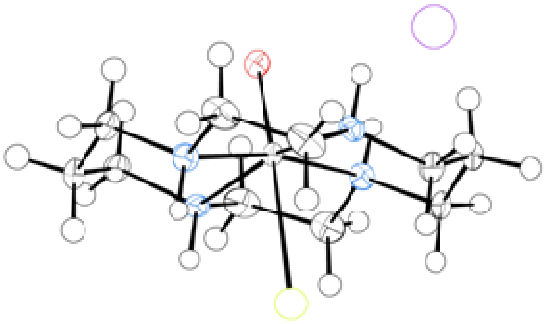

Figure 3.11 $V^{(IV)}$O(cyclam) iodide, 25

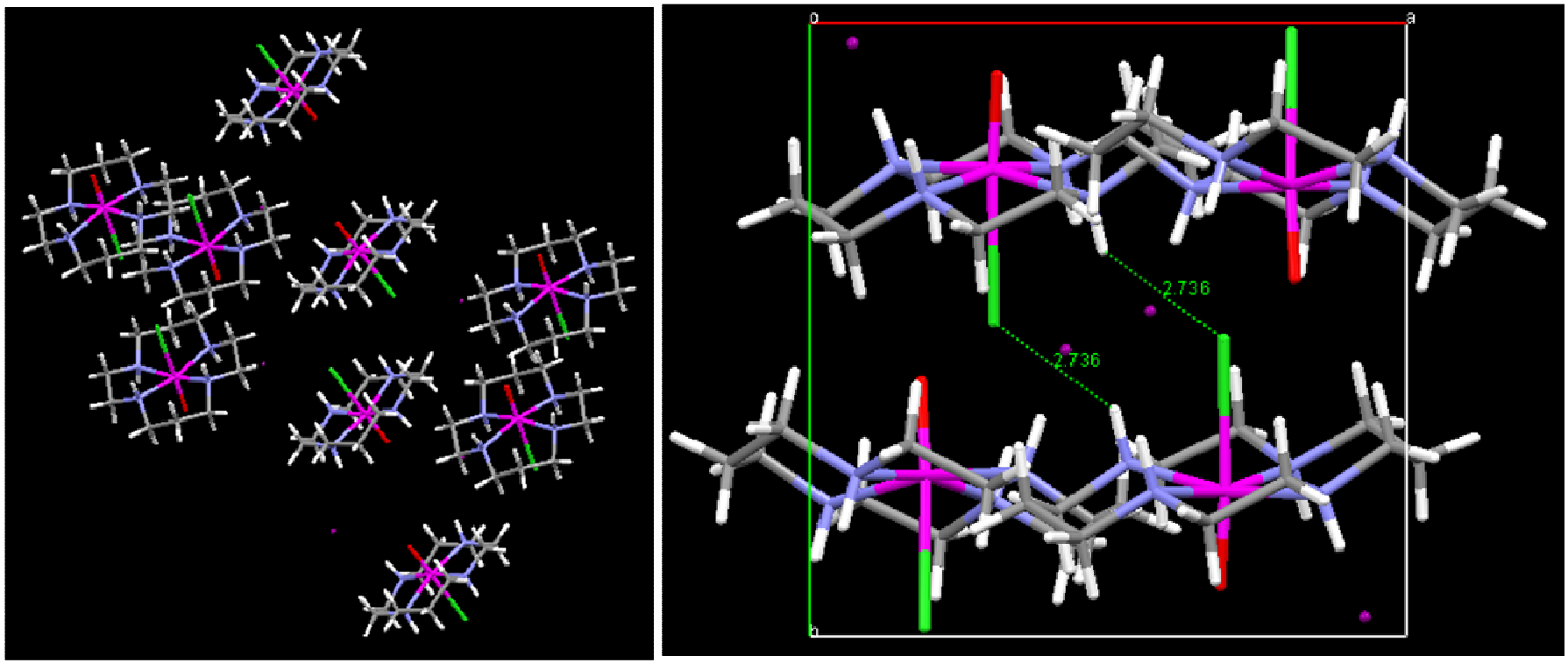

Figure 3.12 Crystal packing of [$V^{(IV)}$O(cyclam)Cl]I, 25. No hydrogen bonds exist between molecules and only short contacts (sum of van der waals radii) are seen between chlorides groups, NH groups and iodide counter ions.

[$V^{(IV)}$O(cyclam)NCS]PF_6, 26

Complex **26** crystallised as the *trans*-III isomer, in a distorted octahedral geometry. This complex crystallised with one cyclam ring in the asymmetric unit and PF_6 as the counter ion for charge balance. No hydrogen bonding is seen between the axial sulfur atom of the thiocyanate ligand and NH protons of the ring, or between the ring and the counter ion. The SCN-V=O angle (178.74(8) Å) is significantly larger than that of any other crystal structure in this chapter and vanadium shows an expected preference for the harder nitrogen ligand than the softer sulfur.

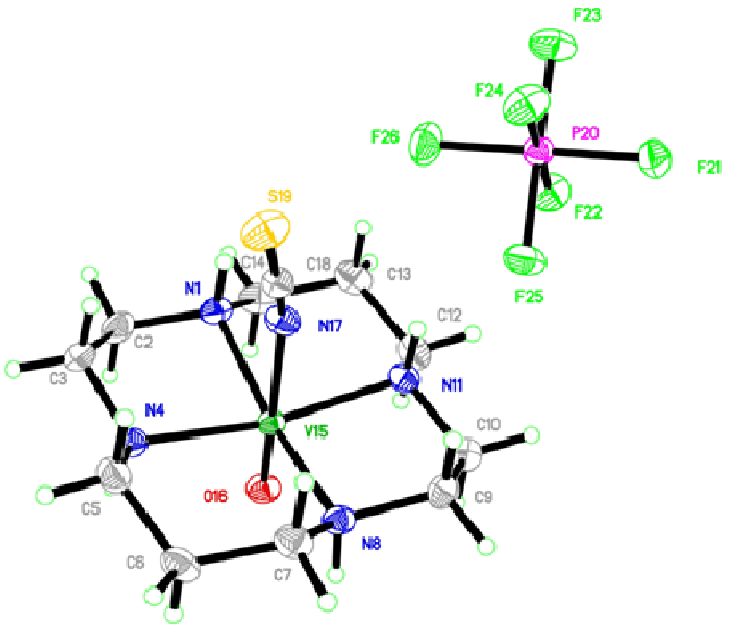

Figure 3.13 VO(cyclam) thiocyanate, 26

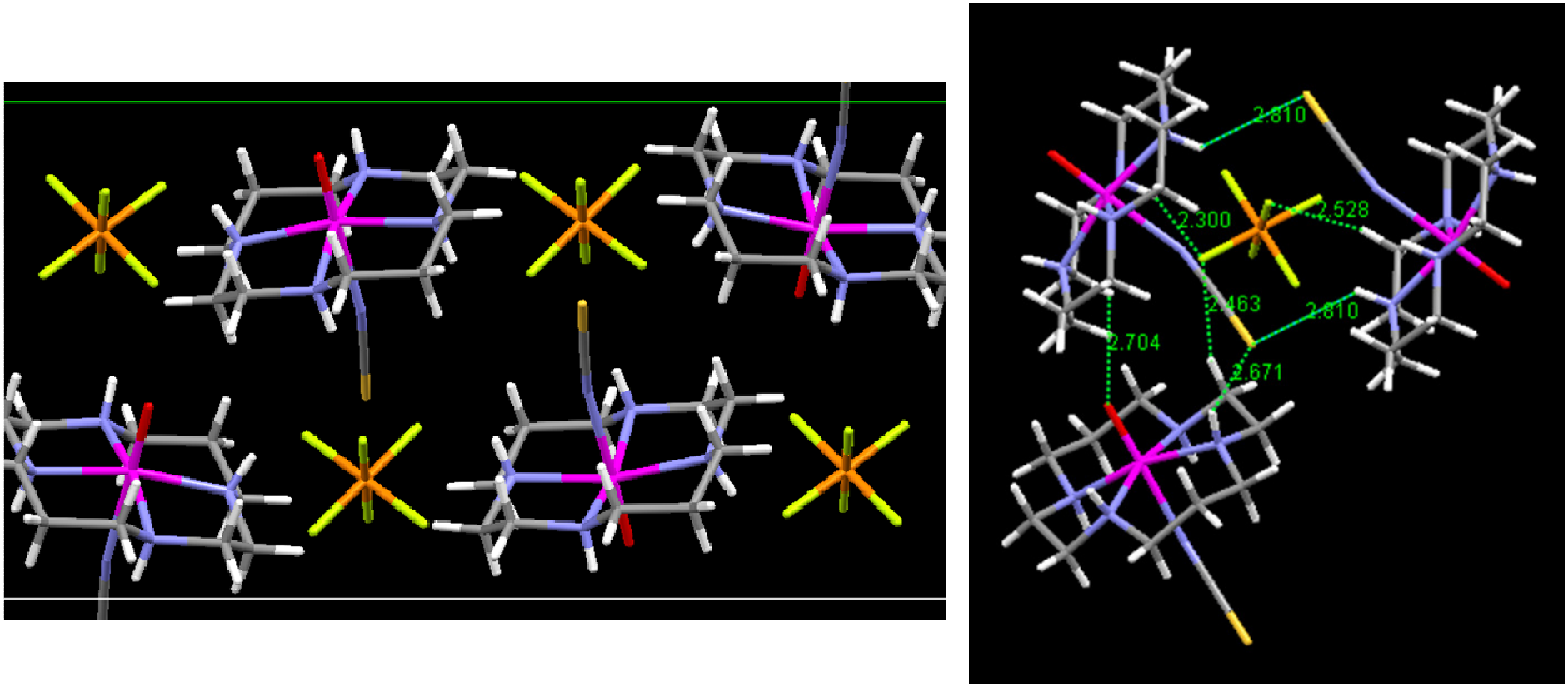

Figure 3.14 Crystal packing of [V$^{(IV)}$O(cyclam)NCS]PF$_6$, 25. No hydrogen bonds exist between molecules and only short contacts (sum of van der waals radii) are seen between thiocyanate groups, NH groups and PF$_6$ counter ions.

3.3.3. FTIR and resonance Raman spectroscopy

All complexes were analysed by solid state and solution IR and selected complexes by resonance Raman spectroscopy. The shift of the V(IV)=O vibrational stretch, a characteristic probe for the axial ligand *trans*- to V=O[8, 9] was recorded for each complex and data are listed in Table 3.16. The vibrational stretches of NH groups are listed and found to be consistent for all complexes. Solution IR was carried out by the Department of Chemistry, University of Warwick, Gibbet Hill Road, Coventry, UK, for oxovanadium(IV) cyclam sulfate **21** and chloride **22**, to investigate displacement of the axial ligand in an aqueous environment.

Raman spectra are shown in Figure 3.15. Problems were encountered using single crystals for Raman analysis as the red laser (632 nm) charred the sample extensively. Cracking and scarring were observed and the damage to the crystal is shown in Figure 3.17. Replacement of the laser light with one of lower absorption wavelength (blue laser, 432 nm) resulted in the same damage to the crystal, only to a lesser degree. This made analysis difficult as scans were required to be collected very quickly. The nature of the technique often requires several scans for good data collection and samples became charred before enough data could be collected. Spectra were acquired using a 0.1 % laser filter aperture for the first collection of data points, increasing to 100 % for each complex to see which bands could be found. Not all of the complexes were suitable for analysis as varying degrees of damage to the structures was incurred through absorption of the laser light. The samples were moved around on the microscope slide so that the laser was focused on a fresh part of the sample each time the filter aperture was increased, ensuring spectra were not acquired from a previously damaged portion.

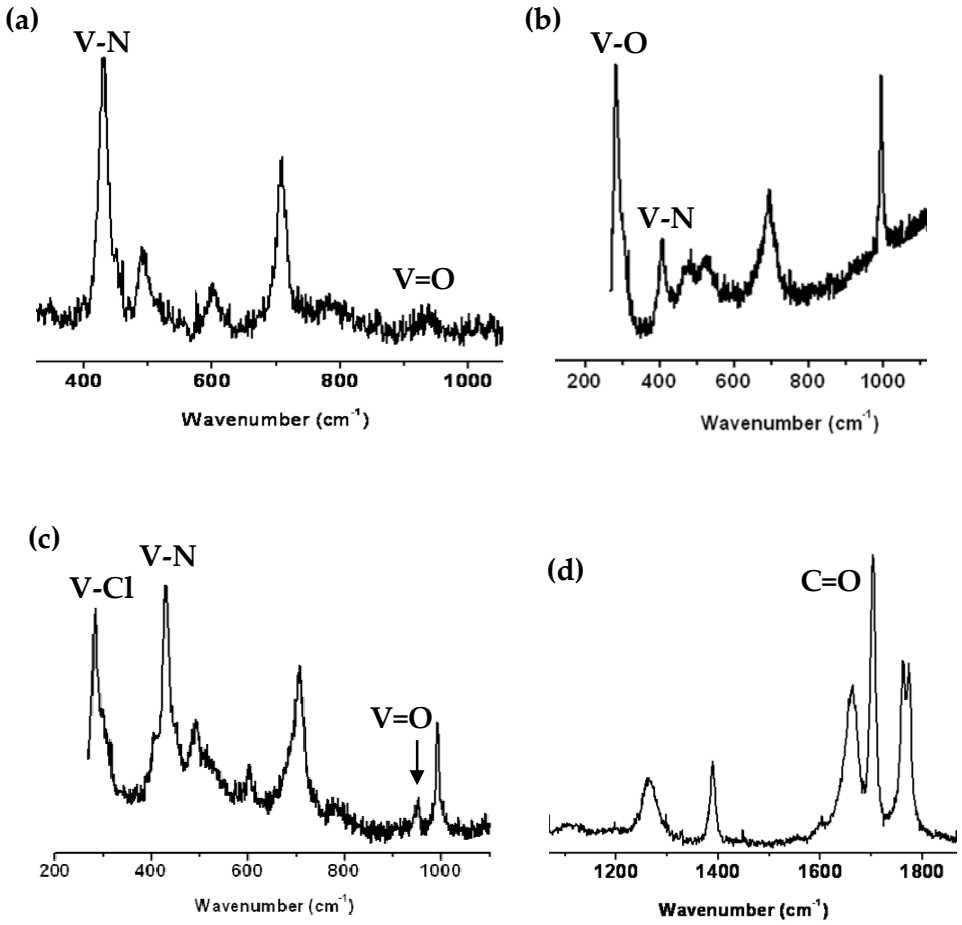

Figure 3.15 Selected Raman spectra of (a) VO(cyclam)sulfate 21, 10% laser filter aperture; (b) VO(cyclam)sulfate 21, 100% laser filter aperture; (c) VO(cyclam)chloride 22, 100% laser filter aperture and (c) VO(cyclam)cGMP 29, 0.1% laser filter aperture.

Table 3.16 Infrared and Raman absorptions for powder samples of oxovanadium(IV) cyclam complexes, 21 - 29

Axial ligand *trans-* to V=O	**Sulfate (SO_4^{2-}), 21**	**Chloride (Cl^-), 22**	**H_2O, 23**	**Bromide (Br^-), 24**	**Iodide (I^-), 25**	**Thiocyanate (NCS^-), 26**	**Phosphate (PO_4^{3-}), 27**	**GMP, 28**	**cGMP, 29**
V=O	974, **974 (w, br)**	988, **988 (w)**	949	949	948	964	933	985	968
N-H	3167, 3059	3195, 3159, 3054	3286, 3265, 3207	3284, 3263, 3205	3286, 3265, 3153	3248, 3230, 3188	3298, 3209	3213, 3128	3292, 3145
PO_4^{3-}	-	-	-	-	-	-	1093	1095	1092
C=O#	-	-	-	-	-	-	-	1693	1698
$S0_4^{2-}$ ν_3 - - ν_4 -	1106 1064 1028 619 598	-	-	-	-	-	-	-	-
N≡C	-	-	-	-	-	2084	-	-	-
V-N	**445**	**445**	**445**	**445**	**445**	**-**	**445**	**-**	**445**
V-L*	**295**	**300**	-	-	-	-	-	-	**1710**

** L = bonding atom of axial ligand trans- to V=O group. Values in bold represent Raman absorptions*
 # Functional group as part of axial ligand, but not directly bonded to vanadium centre

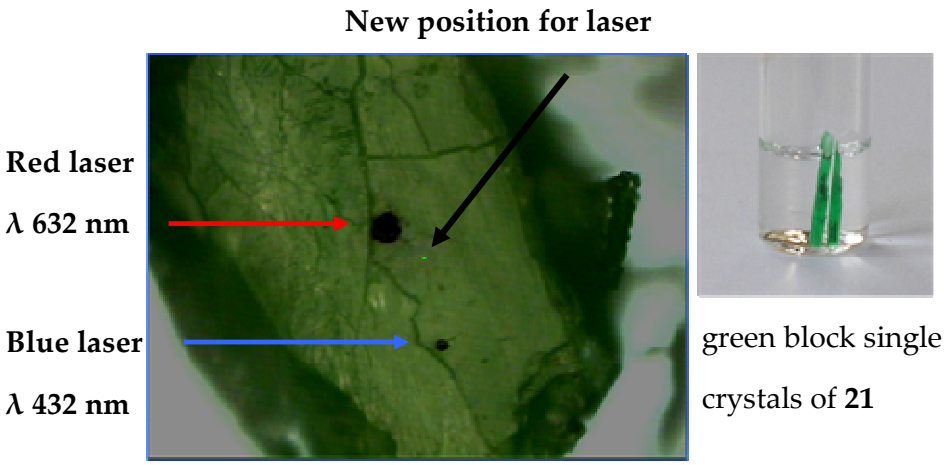

Figure 3.17 Single crystals of VO(cyclam)sulfate, 21 and damage by laser on Raman analysis

Solution IR revealed a change in the V=O stretch for complexes **21** (957 cm^{-1}) and **22** (980 cm^{-1}) and spectra are shown in Figure 3.18. Using $MgSO_4$ (275 mM solution, 10 μL drop, 1024 scans) the resonant frequency for the ν_3 vibration of free sulfate was found to be 1102 cm^{-1}. This was repeated after several hours to check the consistency of the data. The spectrum remained unchanged in this time. Solutions of the $MgSO_4$ standard and complexes **21** (275 mM) and **22** (296 mM) were made using double distilled water. The solutions for complexes **21** and **22** were made by dissolving 3 mg of the complex in 30 μL of double distilled water. The spectra remained unchanged on repeating the experiments over a few hours.

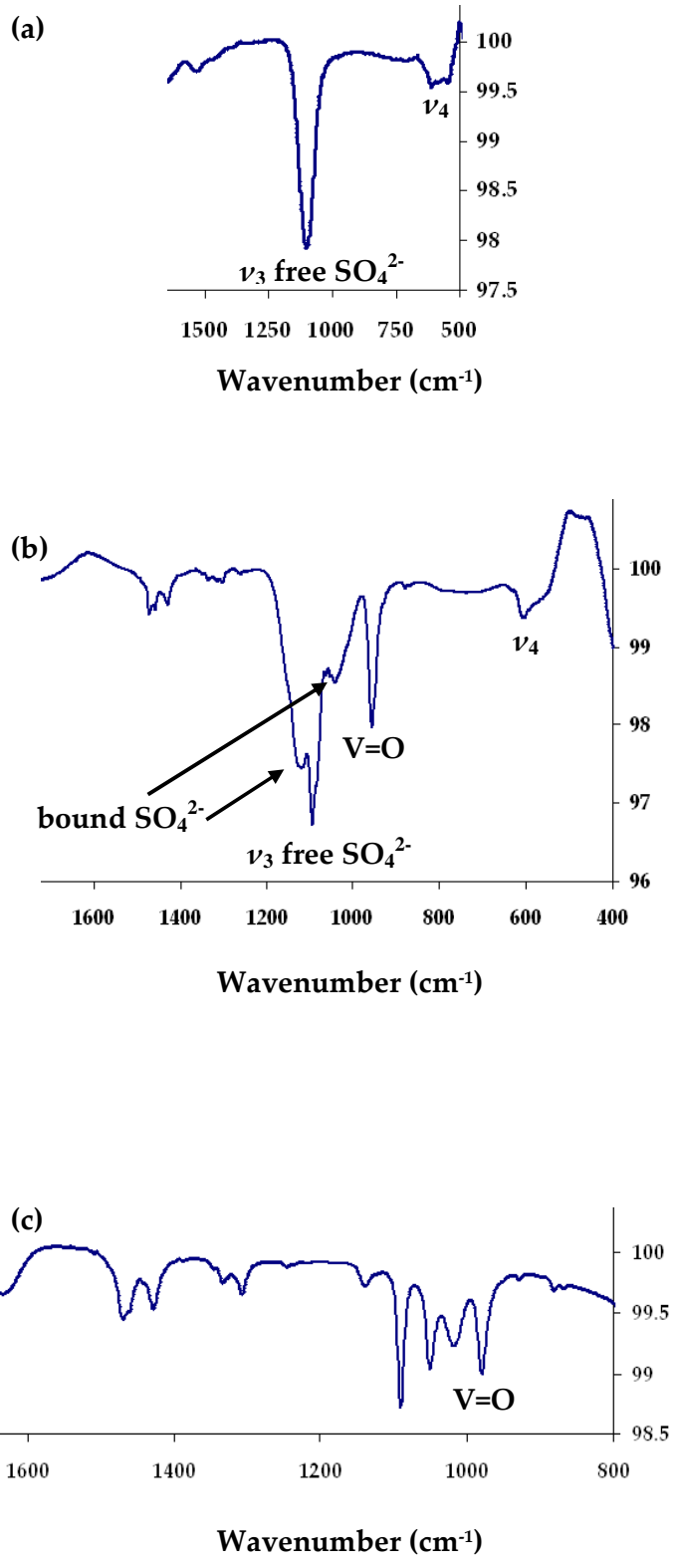

Figure 3.18 Solution IR spectra for (a) $MgSO_4$ (standard) and oxovanadium(IV) cyclam complexes (b) 21 (sulfate) and (c) 22 (chloride)

3.3.4. Conductivity Measurements

Electrical conductivity was measured using the JENWAY Ltd Model 4310 conductivity meter with an electrode of surface area 1 cm^2. Calibration of the instrument was acquired with the Hanna conductivity standard 1413 μS / cm prior to measurement of the sample. Solutions (1 mM) of complexes **21** and **22** were prepared from double distilled water and recorded at ambient temperature.

Published experimental values for conductivity measurements of electrolytes in water are given in Table 3.19[10] and provide an indication of ranges that may be expected from different ratios of electrolytes in solution.

Table 3.19 Expected Molar Conductance (Λ_M) Ranges[a] for 2, 3, 4 and 5 Ion Electrolytes (~10^{-3} M) at 298 K

Solvent	Dielectric Constant	Electrolyte Types			
		1:1	**2:1**	**3:1**	**4:1**
Water [11]	78.4	118-131	235-273	408-435	~560

[a] *Units on all molar conductivities are Ω^{-1} cm^2 mol^{-1}*

An example of the order of magnitude expected for neutral complexes is described in the literature as 5-6 Ω^{-1} cm^2 mol^{-1} for mixed-ligand complexes (1 x 10^{-3} M) of formula [M(bpy)(cbdca)] where M is Pd(II) or Pt(II).[12] Values for complexes **21** and **22** are listed in Table 3.20. Conductivity is directly linked to the concentration of ions in solution and the values show an increase in conductivity for solutions of the order: complex **22** > $MgSO_4$ ~ NaCl > complex **21**.

Table 3.20 Conductivity measurements for oxovanadium(IV) cyclam complexes (21, 22) and standards

	1 mM	0.1 mM
NaCl		
t = zero	135 (135)	160 (16)
t = 24 h	139 (139)	150 (15)
t = 60 h	140 (140)	160 (16)
t = 84 h	138 (138)	160 (16)
$MgSO_4$		
t = zero	186 (186)	-
t = 24 h	182 (182)	-
21		
t = zero	61 (61)	150 (15)
t = 24 h	61 (61)	150 (15)
22		
t = zero	247 (247)	-
t = 24 h	247 (247)	-

Units on all molar conductivities are Ω^{-1} cm^2 mol^{-1} and values in brackets represent measured conductivities, κ.

3.3.5. EPR spectroscopy

EPR spectroscopy revealed 8-line spectra for the ^{51}V (I = $^7/_2$, 99.76% natural abundance) quadropolar nucleus, $3d^1$ complexes (no. lines = 2n*I*+1). All calculated A and g-values for 298 K and 77 K spectra are shown in Tables 3.22 and 3.23 respectively. Spectra representative of all the cyclam complexes are shown in Figure 3.21 for room temperature analyses (water and methanol) and for frozen samples. Data were simulated using Bruker WINEPR Simphonia version 1.26 software by the National EPR Centre, University of Manchester, UK and corrected as for the DPPH standard.[13] Spectra were compared with a reference complex **23** where the 6th axial ligand *trans*- to the V=O group is expected to be a solvent molecule, synthesised by abstraction of the chloride from complex **22** using $AgPF_6$. All A and g-values for complexes **21**-**29** are identical.

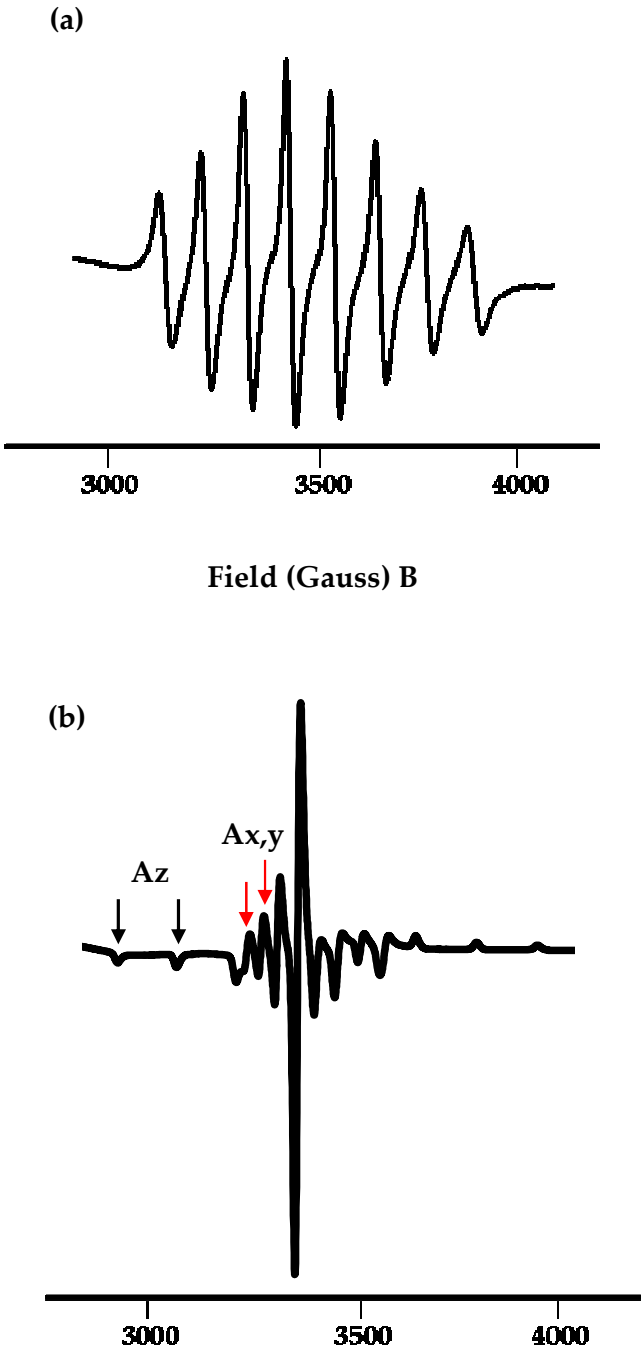

Figure 3.21 Representative spectra of all oxovanadium(IV) cyclam complexes 21-29 showing (a) solution spectrum in water, 298 K and (b) frozen spectrum in methanol, 77 K.

Table 3.22 EPR parameters A(G) and g-values calculated for all complexes in water

Axial ligand *trans*- to V=O	**Sulfate (SO_4^{2-}), 21**	**Chloride (Cl^-), 22**	**H_2O, 23**	**Bromide (Br^-), 24**	**Iodide (I^-), 25**	**Thiocyanate (NCS^-), 26**	**GMP, 28**	**cGMP, 29**
A_{iso} (G), 298 K	88	88	88	88	88	88	88	88
g-value, 298 K	1.972	1.972	1.972	1.972	1.972	1.972	1.972	1.972

Table 3.23 EPR parameters A(G) and g-values calculated for all complexes in methanol

Axial ligand *trans*- to V=O	**Sulfate (SO_4^{2-}), 21**	**Chloride (Cl^-), 22**	**H_2O, 23**	**Bromide (Br^-), 24**	**Iodide (I^-), 25**	**Thiocyanate (NCS^-), 26**	**GMP, 28**	**cGMP, 29**
A_{iso} (G), 298 K	88	88	88	88	88	88	88	88
$A_{\perp}$(G), 77 K	53 xx 53 yy	53 xx 53 yy	53 xx 53 yy	53 xx 53 yy	53 xx 53 yy	53 xx 53 yy	53 xx 53 yy	53 xx 53 yy
$A_{\parallel}$ (G), 77 K	167 zz	167 zz	167 zz	167 zz	167 zz	167 zz	167 zz	167 zz
g-value, 298 K	1.972	1.972	1.972	1.972	1.972	1.972	1.972	1.972
g-value, 77 K	1.983 xx 1.983 yy 1.968 zz	1.983 xx 1.983 yy 1.968 zz	1.983 xx 1.983 yy 1.968 zz	1.983 xx 1.983 yy 1.968 zz	1.983 xx 1.983 yy 1.968 zz	1.983 xx 1.983 yy 1.968 zz	1.983 xx 1.983 yy 1.968 zz	1.983 xx 1.983 yy 1.968 zz

3.3.6. EXAFS/XANES

Spectra were obtained by Danielle Covelli, University of British Columbia at the Stanford Synchrotron Radiation Laboratory, for oxovanadium(IV) cyclam complexes **21** (sulfate) and **22** (chloride) and compared with the bicyclam analogues **30** (sulfate) and **31** (chloride) having identical axial ligands *trans*- to the V=O group. The data for **30** and **31** are shown in Chapter 4. Vanadium K-edge EXAFS data for cyclam complexes **21** and **22** are shown in Figure 3.24. EXAFS parameters obtained from R-space fits for **21** (k^3, Δk = 2-13 $Å^{-1}$, Δr = 0.7-2.5 Å) and **22** (k^3, Δk = 1.7-12.5 $Å^{-1}$, Δr = 0.7-2.5 Å) are listed in Table 3.25 and statistical parameters from best R-space fits are given in Table 3.26. The XANES spectrum is shown in Figure 3.27 and includes data for the bicyclam analogues **30** and **31**.

These spectra will not be discussed in any detail in this chapter as they will be included with the EXAFS and XANES data for the bicyclams and discussed fully in Chapter 4.

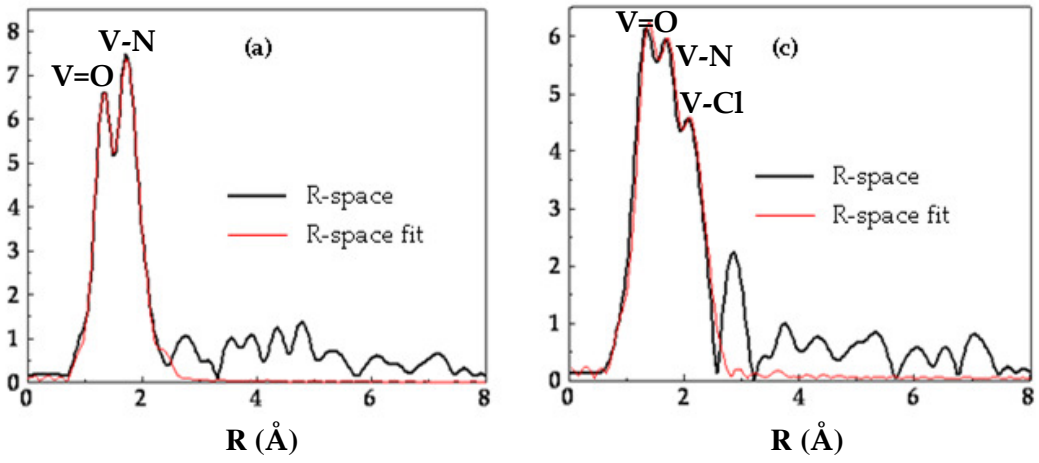

Figure 3.24 R-space (non-phase shift corrected) with calculated fits EXAFS data for (a) VO(cyclam)sulfate 21 and (c) VO(cyclam)chloride, 22. (Figures (b) and (d)not shown relate to the bicyclam data in Chapter 4).

Table 3.25 EXAFS parameters for oxovanadium(IV) complexes 21 (sulfate) and 22 (chloride)

Complex	Scattering Pair	N[a]	R (Å)[a]	σ^{2a}	SO_2^a	ΔE_o^a	CN[c]	Global SO_2^d
21	V-O	1[b]	1.63	0.00096	0.88	0.88	0.88	1.0
	V-N	4[b]	2.11	0.0016	0.96	0.19	3.84	
	V-O(sulfate)	1[b]	2.46	0.0023	0.84	1.37	0.84	
22	V-O	1[b]	1.63	0.0034	1.23	6.94	1.23	1.0
	V-N	4[b]	2.11	0.0017	0.81	5.69	3.24	
	V-Cl	1[b]	2.58	0.0044	1.43	-3.38	1.43	

Definitions from Table 3.25

[a]N = path degeneracy, R = distance in Å, σ^2 = bond variance (related to Debye-Waller factor), SO_2 = amplitude reduction parameter and ΔE_o = internal reference energy.
[b] These parameters were fixed during the fitting procedures.
[c] Estimated coordination number for each path, where CN = N*SO_2*(GSO_2)
[d] Global SO_2 (GSO_2) is defined as a global amplitude reduction factor (equivalent for all paths). GSO_2 was adjusted in cases where CN for V-O deviated significantly from 1.

Table 3.26 Statistical parameters obtained from the best R-space fits given in Table 3.25 for complexes 21 and 22

Sample	Number of Independent Variables	Chi Square	Reduced Chi Square	R-Factor
21	12	34.5	85.4	0.0027
22	12	49.2	22.4	0.0031

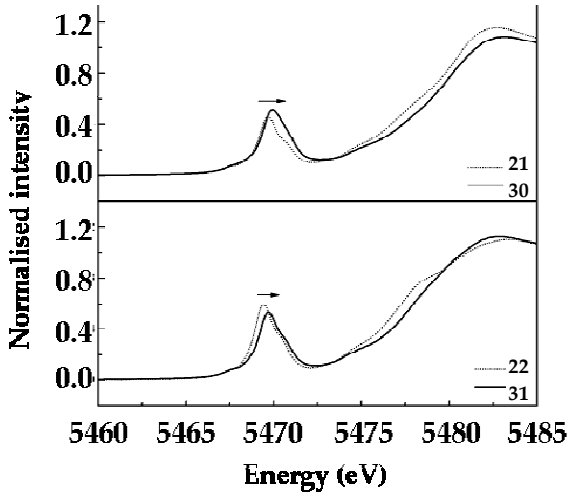

Figure 3.27 XANES pre-edge data for (top) oxovanadium(IV) cyclam (21) and bicyclam (30) sulfate, and (bottom) oxovanadium(IV) cyclam (22) and bicyclam (31) chloride

3.3.7. Antiviral HIV Tests

Anti-HIV activity tests on complexes **21** (sulfate) and **22** (chloride) were carried out by Professor Dr Erik De Clercq, Rega Institute, Katholieke Universiteit Leuven, Minderbroedersstraat 10, B-3000 Leuven, Belgium. Both cyclam complexes were found to be completely inactive against both HIV-1 and HIV-2. Results from the antiviral and cytotoxicity evaluations are detailed in Table 3.28. The complexes were tested against a range of virus strains in addition to HIV and found to be completely inactive against all cell lines. Results from these evaluations are detailed in Tables 3.29 – 3.32.

Table 3.28 Anti-HIV and cytotoxicity evaluation in III_B and ROD cell cultures

Complex	Strain	IC_{50} (μM)	CC_{50} (μM)	SI	Max Prot %	Appr	av. IC_{50} (μM)	av. CC_{50} (μM)	SI
21	III_B	**> 340**	**> 340**	x1	5	1			
		> 340	**> 340**	x1	4	1	**> 340**	**> 340**	x1
	ROD	**> 340**	**> 340**	x1	27	2			
		> 340	**> 340**	x1	24	2	**> 340**	**> 340**	x1
22	III_B	**> 360**	**> 360**	x1	4	1			
		> 360	**> 360**	x1	7	1	**> 360**	**> 360**	x1
	ROD	**> 360**	**> 360**	x1	14	2			
		> 360	**> 360**	x1	14	2	**> 360**	**> 360**	x1

Table 3.29 Cytotoxicity and antiviral activity in HeLa cell cultures

Compound	Minimum cytotoxic concentration[a] (μM)	EC_{50}[b] (μM)		
		Vesicular stomatitis virus	Coxsackie virus B4	Respiratory syncytial virus
21	> 100	> 100	> 100	> 100
22	> 100	> 100	> 100	> 100

[a] *Required to cause a microscopically detectable alteration of normal cell morphology*
[b] *Required to reduce virus-induced cytopathogenicity by 50%*

Table 3.30 Cytotoxicity and antiviral activity in Vero cell cultures

Compound	Minimum cytotoxic concentration[a] (μM)	EC_{50}[b] (μM)				
		Para-influenza-3 virus	Reovirus-1	Sindbis virus	Coxsackie virus B4	Punta Toro virus
21	> 100	> 100	> 100	> 100	> 100	> 100
22	> 100	> 100	> 100	> 100	> 100	> 100

[a] *Required to cause a microscopically detectable alteration of normal cell morphology*
[b] *Required to reduce virus-induced cytopathogenicity by 50%*

Table 3.31 Anti-Feline Corona Virus (FIPV) and anti-Feline Herpes Virus activity and cytotoxicity in CRFK cell cultures

Compound	CC_{50}[a] (μM)	EC_{50}[b] (μM)	
		Feline corona virus (FIPV)	Feline Herpes virus
21	> 100	> 100	> 100
22	> 100	> 100	> 100

[a] *50% cytotoxic concentration, as determined by measuring cell viability with the colorometric formazan-based MTS assay*
[b] *50% effective concentration, or concentration producing 50% inhibition of virus-induced cytopathic effect, as determined by measuring the cell viability with the colorometric formazan-based MTS assay. CRFK cells: Crandell-Rees Feline kidney cells*

Table 3.32 Cytotoxicity and antiviral activity in HEL cell cultures

Compound	Minimum cytotoxic concentration[a] (μM)	EC_{50}[b] (μM)				
		Herpes simplex virus-1 (KOS)	Herpes simplex virus-2 (G)	Vaccinia virus	Vesicular stomatitis virus	Herpes simplex virus-1 TK^- KOS ACV^r
21	> 100	> 100	> 100	> 100	> 100	> 100
22	> 100	> 100	> 100	> 100	> 100	> 100

[a] *Required to cause a microscopically detectable alteration of normal cell morphology*
[b] *Required to reduce virus-induced cytopathogenicity by 50%*

Oxovanadium(IV) cyclam complexes were also tested for CXCR4 binding activity using an alternative assay. An investigation was carried out using antibody competition binding tests for complexes **23** (oxovanadium(IV) cyclam aqua) and **29** (oxovanadium(IV) cyclam cGMP) as an indirect measure of the amount of complex successfully bound to CXCR4. The extent of binding was detected by fluorescence and these experiments were carried out by Dr Steve Archibald, Departments of Chemistry and Biological Sciences, University of Hull, Hull, UK.

Details are listed in Table 3.33 and Figure 3.35 shows the plot obtained for complex **29** which is representative of both complexes tested. It is of course possible that, in solution, complex **29** is the same as complex **23** as the EPR results would suggest. The plot shows the fluorescence lies in the region of the positive control suggesting that none of the complex was found to be strongly bound to CXCR4. This suggests that binding of the complexes to CXCR4 is weak, and that the natural antibody is largely favoured and may have displaced the antagonist molecule.

Table 3.33 Antibody competition binding studies

Compound	**Antibody inhibition (%)**	
Saturated with 20 μM	**Duplicate 1**	**Duplicate 2**
23	2.93	0
29	5.67	3.15

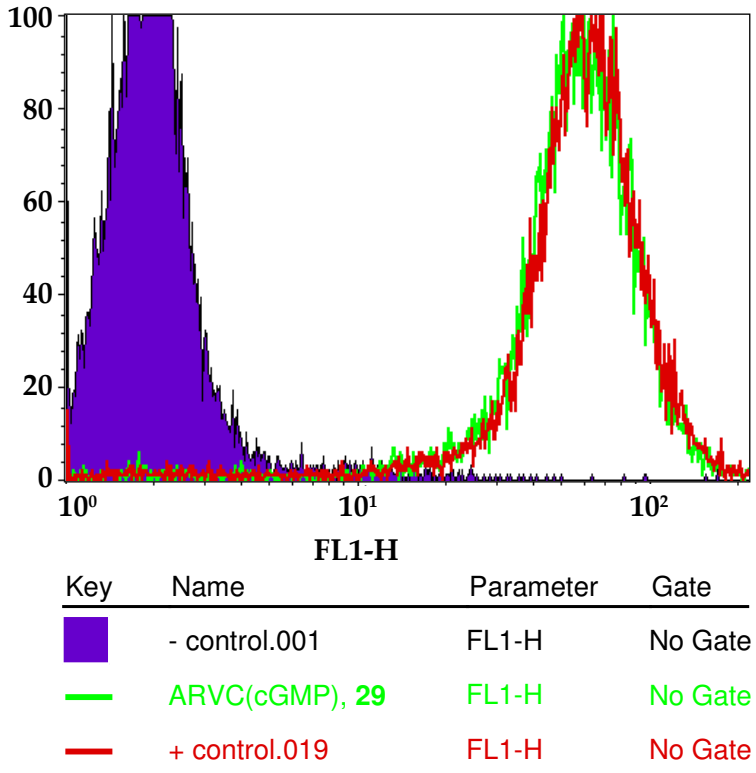

Figure 3.35 Fluorescence plot from antibody competition binding studies

3.3.8. In-silico docking of metallomacrocycles with bovine rhodopsin template

Until recently[14, 15] the only 7-helix transmembrane G-protein coupled receptor for which the crystal structure is known is bovine rhodopsin, a photoreceptor of the vertebrate visual system, and has typically been used as a template for all known 7-helix transmembrane GPCRs. The seven transmembrane alpha helices are linked together sequentially by extracellular and cytoplasmic loops.[16] A molecule of the chromophore retinal (retinylidene) is represented by red spheres and located in the binding site, found closer to the extracellular section.[17] The rhodopsin structure is commonly used to model 7-helix transmembrane proteins such as CXCR4, the coreceptor for HIV.

Figure 3.36 X-ray crystal structure of bovine rhodopsin [17]

A model was achieved using Modeller release version 8 and version 2 and this work was carried out with the help of Dr Dinesh C Soares, Department of Medical Genetics, Western General Hospital, Edinburgh. CXCR4 shows 33% sequence alignment identity with bovine rhodopsin and from the model it is possible to manually dock an antagonist molecule in the relevant binding site. This method can be used to study possible binding interactions between the functional groups of amino acid residues and that of the antagonist molecule, gaining some insight into how a particular antagonist shows anti-HIV activity *in vivo*. Figure 3.37 shows a modelled

representation of the CXCR4 coreceptor and the relevant amino acid residues thought to be associated with the binding of zinc(II)-(xylyl-bicyclam)[18] are highlighted. Complex **21** (sulfate) was chosen as the antagonist for potential docking due to the available crystal structure.

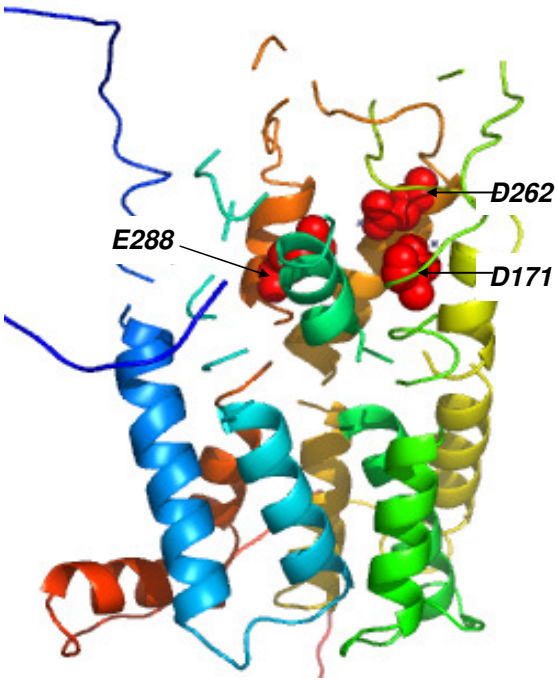

Figure 3.37 Representation of CXCR4 and antagonist binding sites (carboxylate residues are shown as red spheres)

Manual docking of this compound was performed under SYBYL version 6.9 (Tripos Associates, St. Louis, MO, USA). Complex **21** was first superimposed onto one ring of the previously docked [Zn_2-xylyl-bicyclam]-CXCR4 protein receptor interaction[18] using all equivalent Cα atoms. This provided a similar initial relative orientation and position of the cyclam ring

with respect to CXCR4 (*cf.* [Zn_2-xylyl-bicyclam]). The vanadium cyclam compound was then merged with the CXCR4 protein model into a separate MOL2 file using SYBYL v6.9.

Expected clashes were observed between Asp171 and the sulfate group, which was subsequently removed to free the axial 6th position of the octahedral geometry. The EPR data from Section 3.3.5 suggest that the 6th ligand is labile and may be exchanged in water and this assumption is used in the modelling exercise. Parameters were set with a view to investigate the possibility of metal-carboxylate interactions with Asp171 in the binding site. In this case, the vanadium centre was fixed relative to the receptor. A distance restraint (1.609 Å) was set between V=O to maintain the bond length and prevent stretching during the minimisation process. Bad contacts and geometries were then relieved by energy minimising the region of the CXCR4 receptor surrounding the oxovanadium(IV) cyclam complex **21**, (all amino acid residues 5Å from the cyclam ligand).

Figure 3.38 shows a model of one of the known binding sites for CXCR4, highlighting how an oxovanadium(IV) cyclam complex might bind to the site.

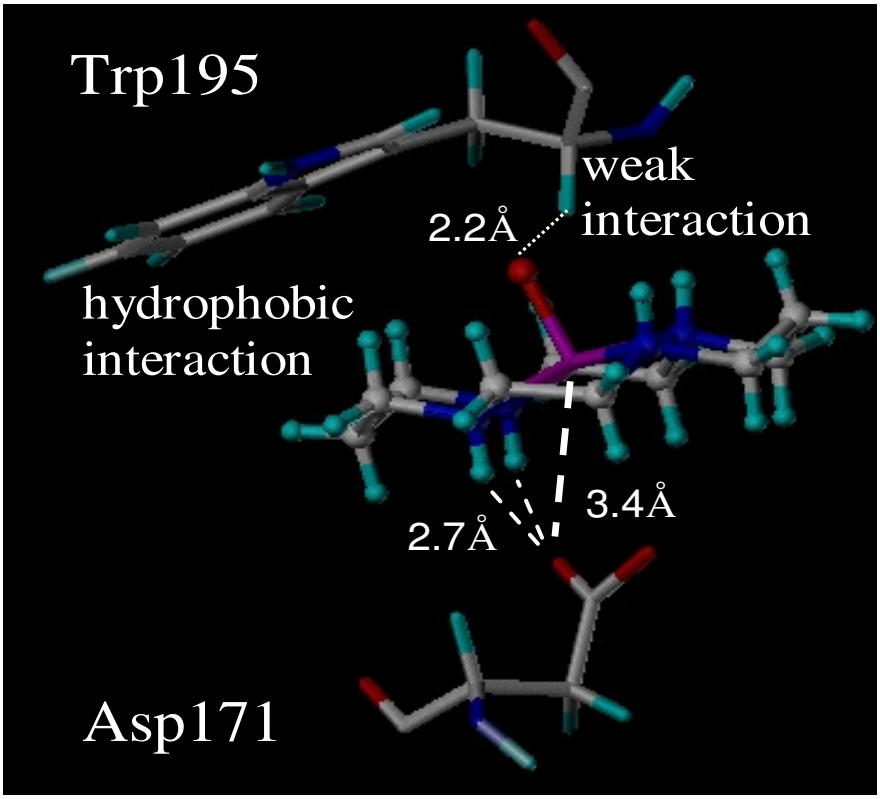

Figure 3.38 Model of an oxovanadium(IV) complex in one of the CXCR4 binding sites

A weak interaction between the oxygen atom of the V=O group and the proton of the α-carbon of a tryptophan residue (Trp195) is seen in addition to a hydrophobic interaction with the hydrocarbon backbone of the cyclam ring. Hydrogen bonding may also be possible between carboxylate oxygens of an aspartate residue (Asp171) and NH protons of the macrocycle which is in the *trans*-III configuration. This provides a suitable geometry for hydrogen bonding due to the downward oriented protons. A distance of 3.4 Å is measured between the vanadium metal centre and carboxylate oxygens of Asp171.

3.4. Discussion

3.4.1. Oxovanadium(IV) cyclam complexes in the solid state

3.4.1.1. Magnetic measurements

Analysis by SQUID (Superconducting Quantum Interference Device) provided magnetic measurements for complexes **21** (sulfate) and **22** (chloride) and reveal the complexes to be dominated by antiferromagnetic interactions in each case. Magnetic susceptibility has been measured in the temperature range 0-300 K and calculated μ_{eff} values (Table 3.4) confirm the presence of one vanadium centre for each complex. The g values for V(IV) are expected to be slightly less than 2 and calculated values are consistent with this, although the sulfate complex is slightly lower than the chloride. This lower value most likely arises from either a slight impurity or perhaps a small amount of water or other solvent not accounted for in the molecular weight. Theta values for both complexes are small and for sulfate it is essentially zero indicating negligible intermolecular interactions. For the chloride complex, the interactions look to be small and antiferromagnetic.

3.4.1.2. X-ray crystallography

X-ray crystallography shows all 4 oxovanadium(IV) cyclams crystallise with the thermodynamically stable *trans*-III ring configuration. The vanadium centre sits outwith the plane of the 4 ring nitrogen atoms and the angle N-V-N differs between complexes. This difference appears to be dependent upon the extent of both intra- and intermolecular hydrogen bonding between the axial ligand, NH protons and solvent molecules. Significant differences are also seen between bond lengths of the axial ligand and V=O groups and angles (L-V=O). Table 3.39 lists the values found.

Table 3.39 X-ray crystal structures of oxovanadium(IV) cyclams in order of increasing ligand-vanadium (L-V) bond length and angles (1 = largest, 4 = smallest)

Complex ID	L-V bond length (Å)	Order	L-V=O angle (deg)	Order	N-V-N angle (deg)	Order
21	2.1359(16)	4	177.83(9)	2	166.88(7)	2
22	2.6501(12)	1	176.99(12)	3	165.46(16)	3
25	2.6044(7)	2	176.91(7)	3	168.51(8)	1
26	2.2053(19)	3	178.74(8)	1	166.46(7)	2

The values show that the V-Cl bond length of complex **22** is significantly longer than any of the other complexes. The complex also exhibits the smallest angles for L-V=O and N-V-N. In comparison with complex **25** where the axial ligand is also chloride, the values show that changing the counter ion affects the N-V-N angle. The larger iodide ion keeps the molecules sufficiently far enough apart that no hydrogen bonding takes place between the chloride axial ligand and NH protons of adjacent molecules. This particular hydrogen bond is seen extensively in complex **22** (Figure 3.10) and results in a significant decrease of the N-V-N angle from the non-hydrogen-bonded analogue, **25**. The axial ligands of complexes **21** and **26** are bonded to the vanadium metal through atoms with similar electronegativity values. Complex **21** (O_3SO-V) exhibits both intra- and inter-molecular hydrogen bonding between the sulfate, NH protons and solvent molecules, and has a smaller L-V=O bond angle than that of complex **26** (SCN-V) which shows no hydrogen bonding in the crystal matrix. There appear to be no previous reports of 6-coordinate oxovanadium(IV) structures of cyclam in the CSD[19], nor for any other oxidation state of vanadium in cyclams. A 5-coordinate square pyramidal oxo-vanadium(IV) cyclam has been reported[20] but no crystal structure is available for comparison of V-N bond lengths. It would be interesting to compare how the bond length of

V=O may be affected by this geometry. Attempts to crystallise complex **23** which may also be a 5-coordinate structure have not been successful so far.

3.4.1.3. Infrared and Resonance Raman spectroscopy

For all complexes, the strong V(IV)=O vibrational stretch was found to lie in the range 933 – 988 cm^{-1}, in good agreement with literature values of 985 ± 50 cm^{-1}.[21] NH stretches were compared and found to be within expected values of 3000 – 3500 cm^{-1} with small variations between the complexes.[22] It would not be expected that the axial ligand *trans*- to the V=O group would affect the strength of the NH bonds nor the subsequent V-N bond as the electronic structure of the vanadium(IV) metal centre does not change with alternating axial ligand. Complex **21** shows the characteristic V(IV)=O vibrational stretch at 974 cm^{-1}, unusually high for a 6-coordinate complex and would indicate the sulfate binds weakly. Complex **22** shows the V(IV)=O stretch at 988 cm^{-1} suggesting that the chloride ligand is also weakly bound and this is borne out by the long V-Cl bond length (2.6501(12) Å) found in the X-ray structure.

Raman spectroscopy revealed additional signals on increasing the percentage of laser light allowed through the filter. The V=O stretch was seen only for the sulfate **21** and chloride **22** complexes and weak signals in the region 950-980 cm^{-1} are in good agreement with the strong infrared absorption values for this group. Assignments were made for vibrations of bonds between the oxovanadium(IV) atom with the nitrogens of the macrocycle ring (V-N) at 445 cm^{-1}.[23] It is documented for V(0) and V(II) compounds that the V-N stretch occurs between 385 – 370 cm^{-1}.[24] V(0) and V(II) compounds have d^5 and d^3 electronic structures respectively. An

increase in oxidation state from 0 to II gives a slight increase in the V-N stretch from 371 cm^{-1} to 385 cm^{-1}. Further oxidation to V(IV), with a d^1 configuration, may be expected to show a more significant change in frequency due to the higher concentration of charge on the vanadium having a stronger electron-withdrawing effect on the nitrogen lone pair, resulting in a stronger bond. Raman signals were also seen in the range 350–250 cm^{-1} for two of the complexes and these have been assigned to the oxovanadium(IV)-axial ligand bond, *trans*- to the V=O group. These signals were seen only for complexes **21** (V-O, 295 cm^{-1}) and **22** (V-Cl, 300 cm^{-1}) when applying the 100% filter. The assigned V-O and V-Cl signals became apparent on increasing the filter aperture of the laser from 10% to 100%, but the result was decomposition of the complex. This was confirmed by visual inspection which revealed charring in addition to a new signal *circa*. ~1000 cm^{-1} and cannot be assigned to any functional group within the complexes.

3.4.1.4. EXAFS

EXAFS data were Fourier-transformed over a k-range varying from 1.6-13 $Å^{-1}$. The data shows two main first-coordination shells for the sulfate complex **21** and the scattering pathways are assigned as V=O and V-N. No signal is seen for V-O of the sulfate complex and it is thought to be hidden under the large signal for V-N. The data clearly shows three main first-coordination shells for the chloride complex **22** and the scattering pathways are assigned as V=O, V-N and V-Cl respectively. These data will be discussed more fully in Chapter 4 when discussion of the bicyclam EXAFS and XANES data are used to compare the electronic structures of the oxovanadium(IV) sulfate and chloride bicyclams with the cyclam analogues of this chapter.

3.4.2. Oxovanadium(IV) cyclam complexes in solution

3.4.2.1. Infrared spectroscopy

Solution infrared spectroscopy was used to investigate the possibility of displacement of the axial ligand. Comparison of the vibrational stretch for the V=O group with that of the solid state values may show differences in terms of binding strength of the axial ligands. For complex **21**, exchange of the sulfate group with water can be investigated through the vibrational modes related to the symmetry of the sulfate group. The free sulfate ion belongs to the high-symmetry point group T_d and of the four fundamentals, only v_3 and v_4 are infrared active. [24, 25] If the symmetry of the ion is lowered by complex formation, the degenerate vibrations split and Raman-active modes appear in the infrared spectrum.[24] In complex **21**, the symmetry of the sulfate ion belongs to the C_{3v} point group in the solid state, confirmed by X-ray crystallography.

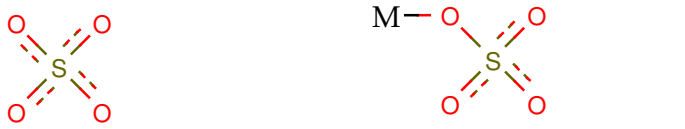

Free ion (T_d) Unidentate complex (C_{3v})

Figure 3.40 Sulfate coordination environments for free and bound ions

The spectrum acquired for complex **21** revealed that the v_3 vibration mode was split into two signals at 1119 and 1043 cm^{-1} in addition to a signal at 1095 cm^{-1} assigned to free sulfate. The free sulfate signal appears to be overlaid with the split signal of the complex. A bidentate or bridged

bidentate structure of C_{2v} symmetry would split the v_3 vibration into 3 separate bands, but the range is outwith that seen for complex **21.** The v_4 vibration is unchanged at 600 cm^{-1} from that of the free sulfate. This would also be split into three bands if the structure was bidentate or bridged bidentate. The V=O stretch at 957 cm^{-1} occurs at a lower wavenumber than the solid state sample (974 cm^{-1}). For a mixture of bound and unbound sulfate species in solution, a second signal for V=O would be expected. This would be likely to occur at a higher wavenumber ($VOSO_4$ = > 1000 cm^{-1}) and is suspected to be hidden beneath the broad signal for free sulfate at 1095 cm^{-1}. The spectrum acquired for complex **22** also shows a decrease in the V=O stretch at 980 cm^{-1} from the solid state sample (988 cm^{-1}), although much smaller than that seen for the sulfate complex, **21.** The strong band at 1100 cm^{-1} is assigned to the C-O_{as} stretch of methanol.

3.4.2.2. Conductivity measurements

The binding strength of axial ligands for complexes **21** and **22** was investigated by analysing the concentration of ions in an aqueous solution to see if the vanadium-axial ligand bond strength could be correlated with the extent of ligand displacement. Three different concentrations of NaCl were used to standardise the experiment and readings were recorded over several hours to ensure the solution had stabilised. For a 1 mM concentration, values for NaCl and $MgSO_4$ show that both salts fully dissociate to give 1:1 electrolytes in solution. These values lie slightly outwith the 1:1 range quoted in Table 3.19 and show that the ranges given can only provide an indication of expected values as both NaCl and $MgSO_4$ are 1:1 electrolytes. The experimental result for **21** suggests that the complex may be partially hydrolysed. The dilution factor is significant as a change in concentration

should result in a large difference in conductivity for weak (partially dissociated) electrolytes. The value of 61 Ω^{-1} cm^2 mol^{-1} is too low for a 1:1 electrolyte/complex (full hydrolysis) in solution and too high for a neutral complex (no hydrolysis) according to the value ranges expected for these two possibilities. The value for complex **22** suggests that full hydrolysis has taken place, as 247 Ω^{-1} cm^2 mol^{-1} is in the correct range for a 2:1 electrolyte/complex according to the published values listed in Table 3.21. As there are two chloride atoms (axial ligand and counter ion) in this structure, a 2:1 ratio would be expected if the complex is fully hydrolysed.

3.4.2.3. EPR spectroscopy

EPR spectroscopy revealed 8-line spectra due to coupling of the unpaired electron with the ^{51}V (I = $^7/_2$, 99.76% natural abundance) quadropolar nucleus, $3d^1$ complexes (no. lines = 2n*I*+1). Spectra for all complexes show the g-values are close to 2 in all cases as expected, as the unpaired electron is in a non-degenerate orbital. In addition, there should also be negligible mixing in of an orbital component from excited states through spin-orbital coupling. The unpaired electron is in the *d*(xy) orbital and oriented between the N atoms in the cyclam plane. As *d*(xy) is essentially non-bonding, any interaction with the nitrogen orbitals is very small and no resolved coupling to nitrogen is seen. Any orbital angular momentum is subsequently quenched resulting in a "spin-only" system. In both methanol and water the cyclam complexes **21, 22** and **24-29** show identical spectra to the reference complex **23**, in which the 6th axial position is thought to be filled by a solvent molecule. This suggests that the 6th ligand for the complexes has been replaced by solvent and appears to be in agreement with X-ray crystal structure data (Table 3.5) where bond lengths

of the axial ligand *trans*- to the V=O group indicate that this ligand is weakly bound. It is of course possible that the ligand may still be attached and this can neither be discounted nor proved from X-band EPR analysis.

3.4.3. Oxovanadium(IV) cyclam complexes in-silico

There are two known strains of the HIV virus (HIV-1 and HIV-2). Although twelve different chemokine receptors are known to function as HIV coreceptors in cultured cells, only two are known to play an active part *in vivo*.[26] The first of these two receptors, CCR5, binds macrophage-tropic viruses associated with mucosal and intravenous transmission of HIV. The second, CXCR4, is active in the binding of T-cell-tropic viruses, often found in the later stages of disease. The CXCR4 coreceptor plays a crucial role in allowing the HIV virus to enter into the cell's cytoplasm where it discharges its DNA, effectively turning the cell into an HIV factory. The family of proteins to which both CCR5 and CXCR4 belong are known as 7-helix transmembrane proteins and these proteins characteristically span the lipid bilayer in a serpentine manner.

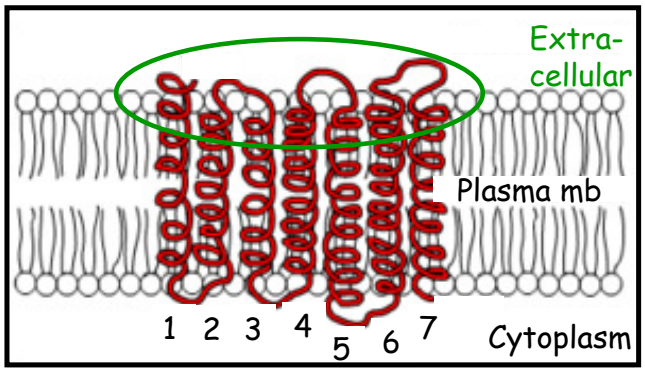

Figure 3.41 Representation of a 7-helix transmembrane protein

The literature shows that the bicyclam AMD3100 is most active as a zinc(II) complex[26] and in solution under physiological conditions the two macrocyclic rings exist in different configurations. One ring remains in the *cis*-V configuration found in the solid state crystal structure, but the other is thought to exist as *trans*-I (or possibly *trans*-III resulting from flexibility of the ring) in solution. Binding is through the zinc atom with carboxylate oxygen atoms of aspartate residues (Asp 171, Asp 262) and hydrogen bonding between the N-H protons of the *cis*-V configured macrocycle and carboxylate group of the glutamate residue (Glu 288). These interactions are shown schematically in Figure 3.42.

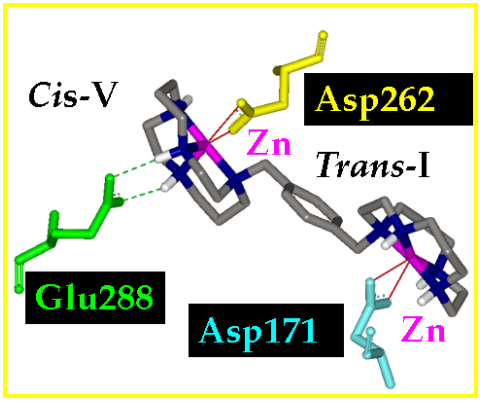

Figure 3.42 Proposed interactions between Zn(II)-bicyclam and the CXCR4 binding sites[16]

Molecular modelling can offer a representation of possible binding interactions in the CXCR4 active site. Previous studies show that activity may result from binding in an analogous fashion to zinc bicyclam[18], through important metal-carboxylate interactions with aspartate residues, Asp171 and Asp272, found in two separate binding sites. Complex **21** (sulfate) was used as a model to represent oxovanadium(IV) cyclam complexes **21**-**29**,

irrespective of the axial ligand *trans*- to V=O based on the assumption made from the results of the solution studies that the axial ligand undergoes either part or full exchange in an aqueous environment. Modelling of the complex is in a binding site thought to accommodate the *trans*-I configuration. The configurations *trans*-I and *trans*-III are likely to be interconvertible due to the flexibility of the ring and so the structure chosen (*trans*-III) was deemed to be a satisfactory model.

Potential hydrogen bonds were observed between carboxylate oxygen atoms of Asp171 with two NH protons of the cyclam ring (~2.0 Å and 2.7 Å) and a weak interaction observed between V=O---H (2.2 Å) of the α-carbon proton from Trp195 in the CXCR4 protein backbone. Trp195 was previously implicated in a putative stacking interaction with Zn_2-bicyclam and thought to provide hydrophobic interactions with the hydrocarbon backbone of the cyclam ring.[27]

The antiviral test results indicate that the oxovanadium(IV) complexes may not bind (or bind weakly) to the carboxylates of Asp171 in the CXCR4 binding site and the model indicates that the proposed weak interaction between the V=O group and the proton attached to the α-carbon of Trp195 could be anchoring the ring in an unfavourable position for successful binding of the axial ligand *trans*- to V=O. The distance between the vanadium centre and carboxylate oxygens of Asp171 (3.4Å) was found to be incompatible for formation of a coordination bond and this may be only one of a number of possible reasons for the inactivity of the oxovanadium(IV) cyclam complexes.

3.5. Conclusion

Infrared and Raman spectroscopy, EXAFS, magnetic measurements and X-ray crystallography were used to study oxovanadium(IV) complexes in the solid state and the presence of the oxovanadium(IV) ion is confirmed for all complexes. As seen in the recrystallisation of the iodide complex **25** (chloride axial ligand) and the binding of thiocyanate through the nitrogen atom of complex **26**, vanadium as a hard metal centre shows an interesting preference for hard ligands and all complexes form the *trans*-III configuration irrespective of ligand or counter ion.

The ring configuration is known to be of importance for antiviral activity of metallocyclam complexes, as seen for previously studied zinc complexes where interconversion between configurations is often facile.[18] Zinc complexes show higher antiviral activity than any other transition metal studied to date. The paramagnetic nature of the oxovanadium(IV) complexes has presented challenges for identification of the ring configurations in solution as NMR analysis has not been possible. It would seem that no other analytical technique available at this time can provide such information and at this point it is unknown whether the oxovanadium(IV) cyclams exhibit any interconversion of ring configuration in solution.

As antiviral activity is greatly influenced by metal complexation, it is of paramount importance to understand the factors that influence interactions between the coreceptor protein CXCR4 and metallocyclam complexes. Molecular modelling suggests that one possible reason for the inactivity of the cyclam complexes may be due to the unfavourable position

of the macrocycle in the binding site as a consequence of weak interactions between the V=O group with the protein backbone in one binding site.

3.6. Bibliography

[1] L. F. Lindoy, *The Chemistry of Macrocyclic Ligand Complexes*, Cambridge University Press, Melbourne, **1989**.

[2] P. J. Connolly, E. J. Billo, *Inorg. Chem.*, **1987**, *26*, 3224.

[3] B. Bosnich, C. K. Poon, M. L. Tobe, *Inorg. Chem.*, **1965**, *4*, 1102.

[4] P. O. Whimp, M. F. Bailey, N. F. Curtis, *J. Chem. Soc. A* **1970**, *11*, 1956.

[5] Shriver, Atkins, *Inorg. Chem.*, 3 ed., Oxford University Press, **1999**.

[6] G. D. Triantafillou, E. I. Tolis, A. Terzis, Y. Deligiannakis, C. P. Raptopoulou, M. P. Sigalas, T. A. Kabanos, *Inorg. Chem.*, **2004**, *43*, 79.

[7] L. J. Calviou, J. M. Arber, D. Collison, C. D. Garner, W. Clegg, *J. Am. Chem. Soc. Chem. Comm.*, **1992**, *8*, 654.

[8] K. R. Asmis, G. Santambrogio, M. Brummer, J. Sauer, *Angew. Chem. Int. Ed.*, **2005**, *44*, 3122.

[9] K. R. Asmis, G. Meijer, M. Brummer, C. Kaposta, G. Santambrogio, L. Woste, J. Sauer, *J. Chem. Phys.*, **2004**, *120*, 6461.

[10] R. J. Angelica, *Synthesis and Technique in Inorganic Chemistry*, 2 ed., W B Saunders Company, Philadelphia, **1977**.

[11] M. Sneed, J. Maynard, *General Inorganic Chemistry*, Van Nostrand, New York, **1942**.

[12] H. Mansuri-Torshizi, S. Ghadimy, N. Akbarzadeh, *Chem. Pharm. Bull.*, **2001**, *49*, 1517.

[13] S. A. Al'tshuler, B. M. Kozyrev, *Electron Paramagnetic Resonance*, C P Joole, Jr., ed., Academic Press, New York, **1964**.

[14] V. Cherezov, D. M. Rosenbaum, M. A. Hanson, S. G. Rasmussen, T. F. S, K. T. S, H. J. Choi, P. Kuhn, W. I. Weis, B. K. Koblika, R. C. Stevens, *Science* **2007**, 1258.

[15] S. G. Rasmussen, H. J. Choi, D. M. Rosenbaum, T. S. Koblika, F. S. Thian, P. C. Edwards, M. Burghammer, V. R. Ratnala, R. Sanishvili, R. F. Fischetti, G. F. Schertler, W. I. Weis, B. K. Koblika, *Nature* **2007**, *450*, 383.

[16] T. P. Sakmar, *Curr. Opin. Cell Biol.*, **2002**, *14*, 189.

[17] T. Smith, *Nat. Struct. Biol.*, **2000**, *7*, 710.

[18] X. Liang, J. A. Parkinson, M. Weishaupl, R. O. Gould, S. J. Paisey, H.-s. Park, T. M. Hunter, C. A. Blindauer, S. Parsons, P. J. Sadler, *J. Am. Chem. Soc.,* **2002**, *124*, 9105.

[19] F. H. Allen, O. Kennard, *Chem. Des. Autom. News* **1993**, *8*, 31.

[20] M. Thirumavalavan, A. M. Martins, *Inorg. Chem. Commun.,* **2006**, *9*, 497.

[21] J. Selbin, *Chem. Rev.,* **1965**, *65*, 153.

[22] J. B. Lambert, H. F. Shurvell, D. A. Lightner, R. G. Cooks, *Organic Structural Spectroscopy*, Prentice-Hall, New Jersey, **1998**.

[23] E. J. Baran, A. H. Juberta, E. G. Ferrer, *J. Raman Spectrosc.,* **1992**, *23*, 489.

[24] K. Nakamoto, *Infrared and Raman Spectra of Inorganic and Coordination Compounds*, 4 ed., Wiley - interscience, Canada, **1986**.

[25] J. J. Wylde, G. C. Allen, I. R. Collins, *Appl. Spectrosc.,* **2001**, *55*, 1155.

[26] S. Hatse, K. Princen, G. Bridger, E. De Clercq, D. Schols, *FEBS Lett.,* **2002**, *527*, 255.

[27] T. M. Hunter, I. W. McNae, X. Liang, J. Bella, S. Parsons, M. D. Walkinshaw, P. J. Sadler, *Proc. Natl. Acad. Sci., USA* **2004**, *102*, 2288.

4. OXOVANADIUM(IV) BICYCLAM COMPLEXES

This chapter describes the synthesis and characterisation of oxovanadium(IV) bicyclam and cyclam complexes with aromatic pendant arm substituents. Numbers in bold after compound names refer to experimental data in Chapter 7.

In the late 1980's, the serendipitous discovery of an impurity in a batch of cyclam resulted in a compound that showed high antiviral activity against HIV.[1] The compound was characterised as the bicyclam JM1657 (**18**) and the structure was found to display a carbon-carbon bridge between two cyclam rings creating two chiral centres. This proved an obstacle in attempts to reproduce the compound due to the difficulty in forming the carbon-carbon bond between the two macrocycles. Alternative strategies were adopted and the synthesis of various linker molecules was attempted in an effort to find an improved or equally active product. This led to the discovery of JM2763, a bicyclam constructed of two cyclam rings joined by an aliphatic linker bridge consisting of 3 methylene groups. The compound showed similar antiviral activity to JM1657 (**18**).

Many derivatives were synthesised in an attempt to improve the activity of bicyclam and the most significant result came when an aromatic linker bridge was used. This work led to synthesis of the compound JM3100, later renamed AMD3100 (**16**) when a company called AnorMED (AMD) took over the development of the compound from Johnson Matthey (JM) and referred to as xylyl-bicyclam throughout this thesis. AMD3100 was successful as an entry inhibitor against HIV, reaching Phase II clinical trials but was not pursued further in light of cardiac problems experienced by two

patients.[2] An unexpected observation made during pharmacokinetic studies revealed highly elevated levels of white blood cells in patients, even with low doses of the compound AMD3100 (40 to 80 μg per kg). This led to an investigation into the particular type of white blood cells involved and it was revealed that AMD3100 showed a synergistic relationship with peg-filgrastim in mobilising stem cells from the bone marrow into the blood stream.[1] In 2006 the product was acquired by Genzyme and has since been relaunched commercially under the name of *Mozobil*, recently completing its second set of Phase III clinical trials as a stem cell mobiliser. Both studies successfully met the primary and secondary endpoints and marketing applications have been submitted in the United States with expected approval by the end of the year. European approval is expected in 2009 with subsequent global applications in up to 60 countries.[3] Approximately 55,000 stem cell transplants are performed each year for multiple myeloma, Hodgkin's and non-Hodgkin's lymphoma.[1]

The structure of xylyl-bicyclam is shown in Figure 4.1.

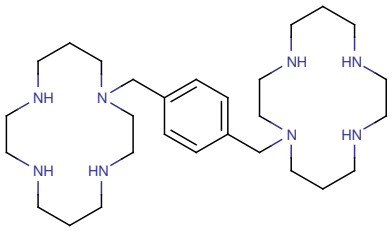

Figure 4.1 Xylyl-bicyclam, 16

4.1. Experimental

4.1.1. Materials

Starting materials were purchased from Sigma-Aldrich as detailed in Chapter 2. The solvents used for all synthetic work were anhydrous quality

from Sigma-Aldrich. HPLC Grade methanol and reagent grade diethyl ether were used for crystallisations. Reagent grade ethyl acetate and hexane were used as eluents for flash column chromatography. HPLC Grade methanol was used as the eluent for Sephadex column chromatography.

4.1.2 Synthesis of Xylyl-bicyclam, 16

Xylyl-bicyclam **16**, was synthesised from cyclam **17** using the route shown in Scheme 4.2.[4] Trifluoroacetate was used as protecting groups for three of the four amines and deprotection was carried out using 10% sodium hydroxide.

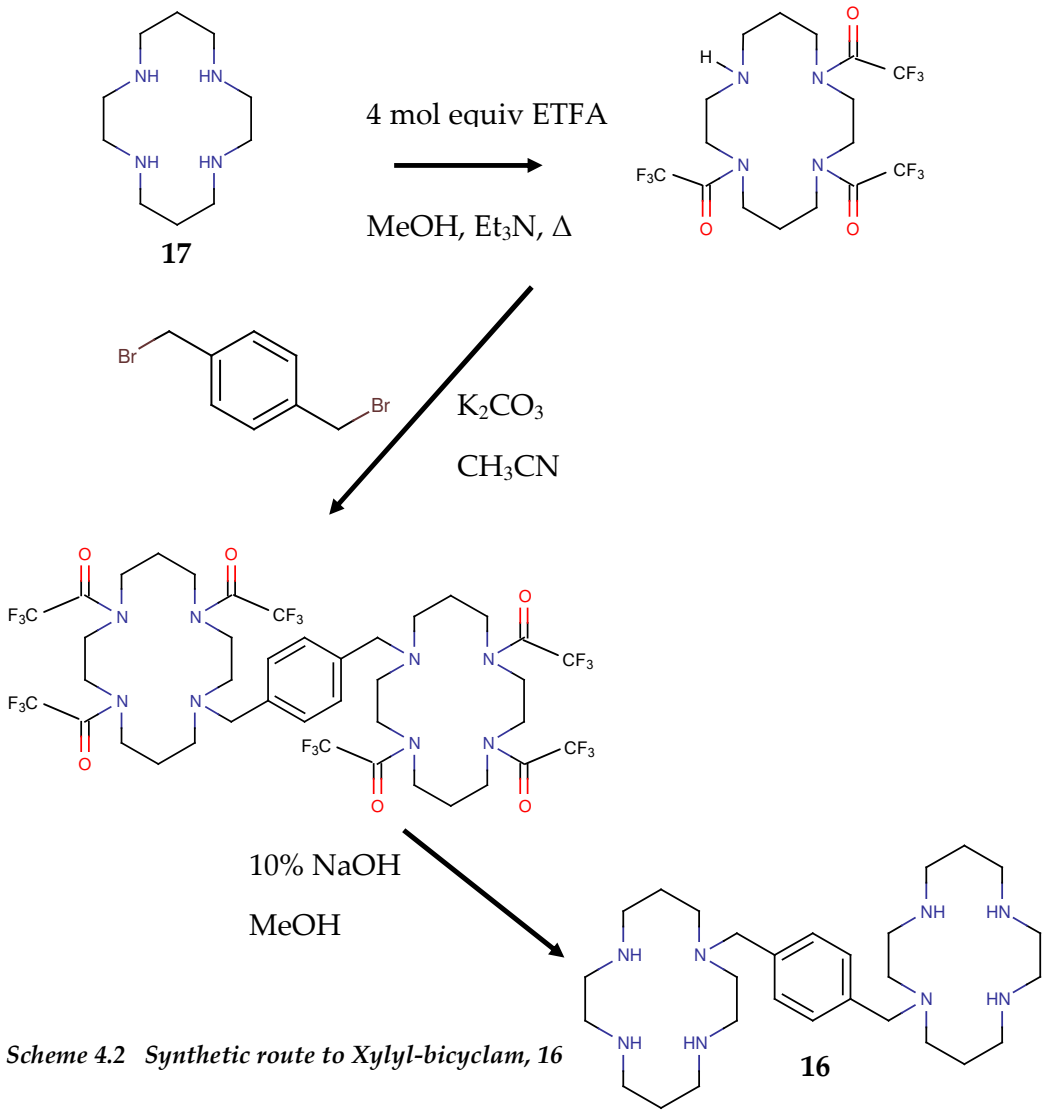

Scheme 4.2 Synthetic route to Xylyl-bicyclam, 16

4.1.3 Syntheses of oxovanadium(IV) cyclam complexes with aromatic pendant arm substituents

Compounds **30** and **31** were synthesised from xylyl-bicyclam **16,** shown in Scheme 4.3. Compound **34** was synthesised from the naphthyl-substituted cyclam **33** by Dr S J Paisey, University of Edinburgh and is shown in Scheme 4.4.

4.1.3.1 Synthesis of oxovanadium(IV) bicyclam complexes

Two complexes were prepared using the method outlined in Scheme 4.3.

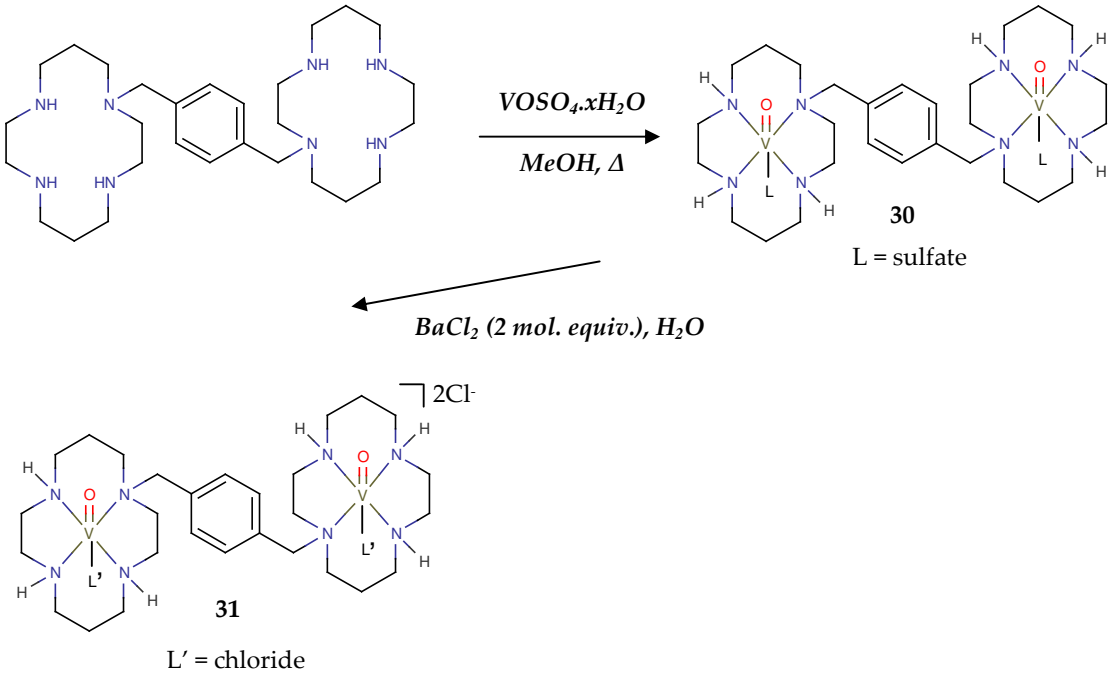

Scheme 4.3 General method used to prepare oxovanadium(IV) bicyclam sulfate 30 (L = sulfate) and chloride 31 (L′ = chloride).

The preparation of the bicyclam complexes was difficult and synthesis of only two products, **30** and **31**, were achieved in sufficient purity for characterisation and analysis. These two complexes were used as a direct

comparison with the oxovanadium(IV) cyclam analogues **21** (sulfate) and **22** (chloride) to investigate the chemistry of the oxovanadium(IV) group in macrocycles. Methanol was used as the reaction solvent and formation of these oxovanadium(IV) complexes appeared to be in competition with either a polymerisation of the oxovanadium(IV) groups or, alternatively, the formation of a bridged species. This by-product was insoluble in any of the organic solvents tested. On recrystallisation of the complexes after purification using Sephadex column chromatography, the products then tended to react with the recrystallisation solvent system resulting in precipitation of insoluble solids. This resulted in low yields of pure compound. Scaling up the synthetic process resulted in a higher percentage of the by-product and several small syntheses were required to provide suitable amounts of the intended product. Crystallisation of complexes **30** and **31** suitable for X-ray purposes was unsuccessful. Due to the paramagnetic nature of the oxovanadium(IV) metal centre, X-ray crystal structures would seem to be the best means of determining the configuration of the rings in the solid state.

Many syntheses were attempted in order to produce sufficient amounts of the complexes in this chapter necessary for analytical investigation, but not all gave good yields and in many cases the target compound was not achieved. Two alternative vanadium bicyclam complexes were attempted by exchanging the chloride ligands from complex **31**. The same methods and procedures used for ligand exchange syntheses of the cyclam complexes in Chapter 3 for thiocyanate (**26**) and cyclic GMP (**29**) were adopted. These two ligands were chosen due to their biological significance and the syntheses proceeded without any obvious problems. Unfortunately, mass spectrometry did not confirm the intended products

and the decision was taken to investigate a different macrocycle also bearing an aromatic pendant arm.

4.1.3.2 Synthesis of oxovanadium(IV) naphthyl cyclam complexes

A cyclam with a naphthyl pendant arm (**33**) was used to complex vanadium. Using the method adopted in Scheme 4.4, complexation was achieved using vanadium acetylacetonate as the vanadium salt.

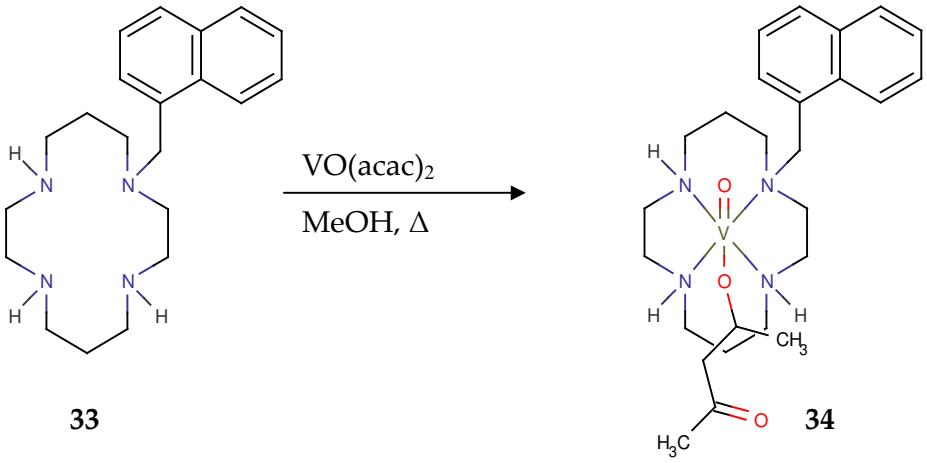

Scheme 4.4 Synthetic route for complexing naphthylated cyclam

On addition of $VO(acac)_2$ to a solution of cyclam, it was observed that the initial green solution did not change colour during the reaction time of 16 h. No insoluble by-product was formed using this salt and mass spectrometry confirmed the presence of two major fragments and the molecular ion. It was hoped that formation of single crystals for X-ray purposes would prove easier than for the bicyclam complexes, in an attempt to uncover information regarding ring configurations for oxovanadium(IV) complexes with aromatic linker arms. Information on this ligand might be

extrapolated to the bicyclam complexes **30** and **31** to help to explain the antiviral activity/inactivity of oxovanadium(IV) complexes associated with CXCR4 binding. Several crystallisations were attempted using the same method that afforded crystals of the cyclam complexes *i.e.* diffusion of ether into a methanolic solution of the compound but no crystals had formed at the time of writing.

4.1.4 FTIR and resonance Raman spectroscopy

Infrared absorptions for the V=O group were recorded for each complex and details are found in Table 4.5. A Raman signal is seen at 450 cm^{-1} for all complexes investigated in this chapter and is assigned to the V-N bond. Signals found in the frequency range 350-250 cm^{-1} are assigned to V-L bonds, where L = 6th axial ligand *trans*- to the V=O group. Selected spectra are shown in Figure 4.6.

Table 4.5 Infrared V=O and NH vibrations with Raman signals for V-N bonds

Complex	**V=O (cm^{-1})**	**NH (cm^{-1})**	**V-N (cm^{-1})**
30 (sulfate)	945	3278 (br), 3125 (br)	450
31 (chloride)	964	3230 (w), 3107 (br)	450
34 (acac)	995	3220 (br)	450

Raman spectra for complex **31** are shown for both 10% and 100% laser filter apertures. Signals for the V=O group were not seen for the bicyclam complexes but a strong signal was present at 995 cm^{-1} for the

naphthyl-cyclam complex **34** in both the infrared and Raman spectra. There was no variation in frequency for V-N in any of the complexes studied as expected.

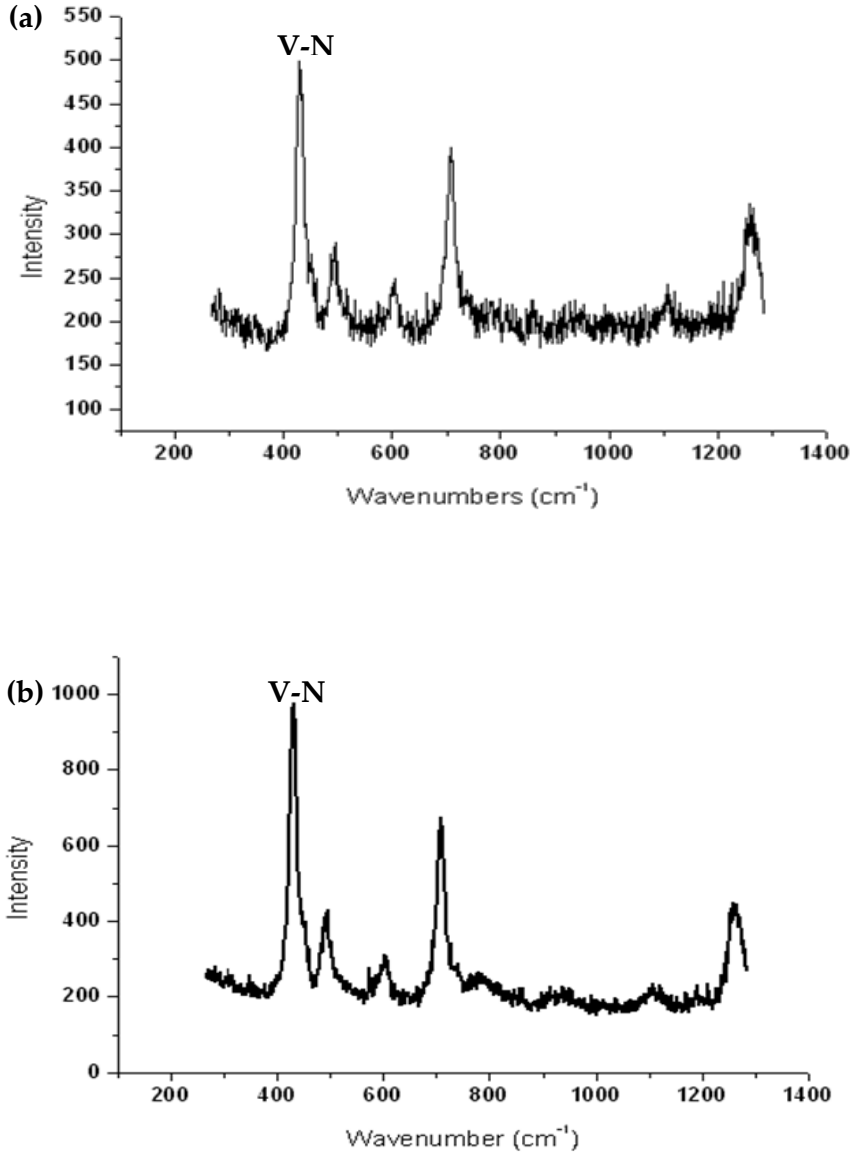

Figure 4.6 (a) Fingerprint region of Raman spectrum with 10% laser filter aperture of (a) oxovanadium(IV) bicyclam sulfate 30 and (b) oxovanadium(IV) bicyclam chloride, 31.

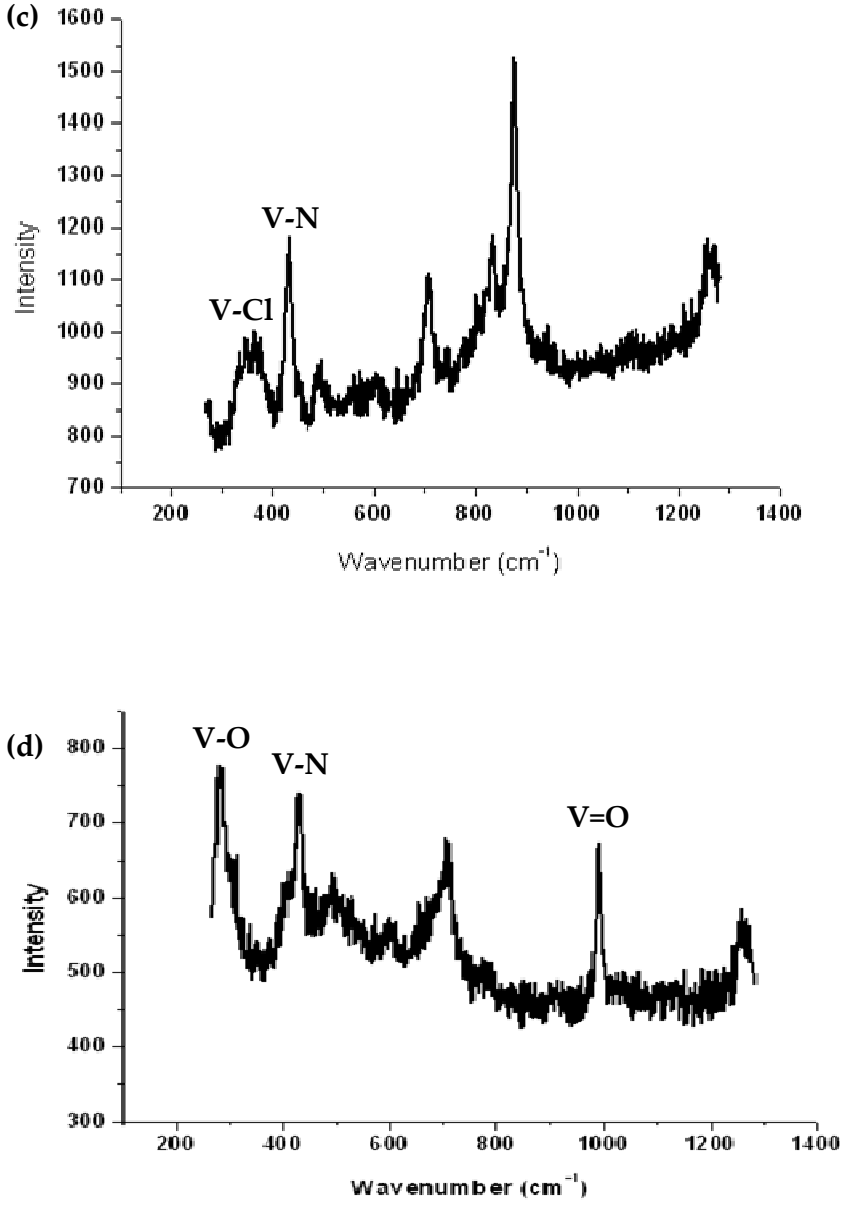

Figure 4.6 Raman spectra with 100% laser filter aperture of (c) oxovanadium(IV) bicyclam chloride 31 and (d)oxovanadium(IV) naphthyl cyclam, 34.

4.1.5 UV-Vis spectroscopy

The reaction of **30** with an excess of acetate was monitored over time. A 10 mM solution of **30** was prepared and the absorbance detected at 690 nm and 450 nm. Unfortunately, the complex precipitated from solution so the true concentration is unknown and no binding constants or extinction coefficients were determined. An excess of ammonium acetate (3M) was added to the solution to mimic potential carboxylate binding in the CXCR4 receptor site and to induce any observable spectral change. An isosbestic point was seen at 350 nm shown in Figure 4.8, but from these data we can only tentatively suggest that binding to acetate occurs. As millimolar concentrations were required to study these complexes, it was not possible to investigate acetate binding for the chloride sample, or to use UV-Vis spectroscopy for further analyses of these compounds.

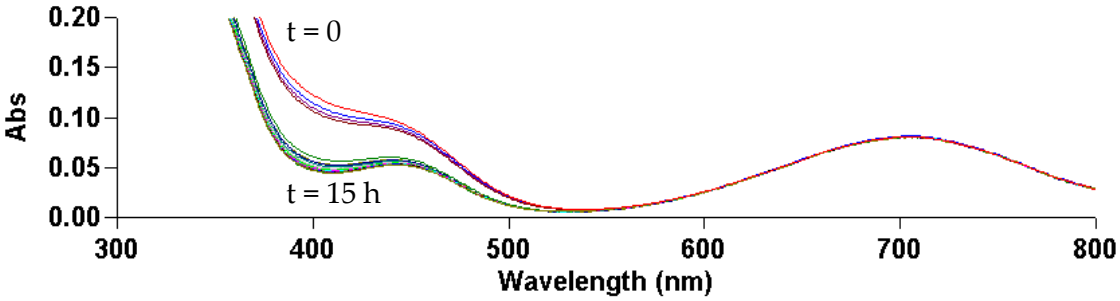

Figure 4.7 Aqueous solution of oxovanadium(IV) bicyclam, 30 at 298 K.

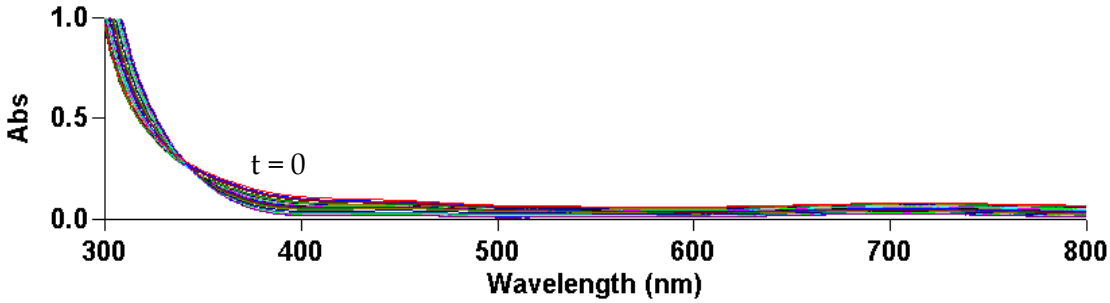

Figure 4.8 Addition of 3M ammonium acetate (0.5 mL) to an aqueous solution of oxovanadium(IV) bicyclam, 30 (0.5 mL) at 298 K.

4.1.6 EPR spectroscopy

EPR spectroscopy revealed 8-line spectra for the ^{51}V (I = $^{7}/_{2}$, 99.76% natural abundance) quadropolar nucleus, $3d^1$ complexes (no. lines = 2n*I*+1). All calculated A and *g*-values for 298 K and 77 K spectra are shown in Tables 4.9 and 4.11 respectively. Spectra for the bicyclam complexes **30** and **31** are shown in Figure 4.10 for room temperature analyses and in Figure 4.12 for frozen samples. Data were simulated using Bruker WINEPR Simphonia version 1.26 software by the National EPR Centre, University of Manchester and corrected as for the DPPH standard.[5] Room temperature spectra were obtained in water and methanol and compared to a reference complex **32**, synthesised by abstraction of the chloride from complex **31** using $AgPF_6$, where the 6th axial ligand *trans*- to the V=O group is expected to be a solvent molecule. Sufficient amounts were only available for analysis in water and composition of the reference compound (analogous to the cyclam complex, **23)** was confirmed by mass spectrometry as oxovanadium(IV) bicyclam, m/z 637.2 $[M\text{-}2H_2O]^+$.

Table 4.9 EPR parameters of oxovanadium(IV)-xylyl-bicyclam complexes

(a) water, 298 K ***(b) methanol, 298 K***

Ligand	**T (K)**	**A_{iso} (G)**	**g_{iso}**		**Ligand**	**T (K)**	**A_{iso} (G)**	**g_{iso}**
solvent (H_2O)	298	88	1.974		solvent (MeOH)	-	-	-
sulfate, **30**	298	84 95	1.974 1.972		sulfate, **30**	298	90	1.967
chloride, **31**	298 298	87 115	1.972 1.959		chloride, **31**	298	90	1.973

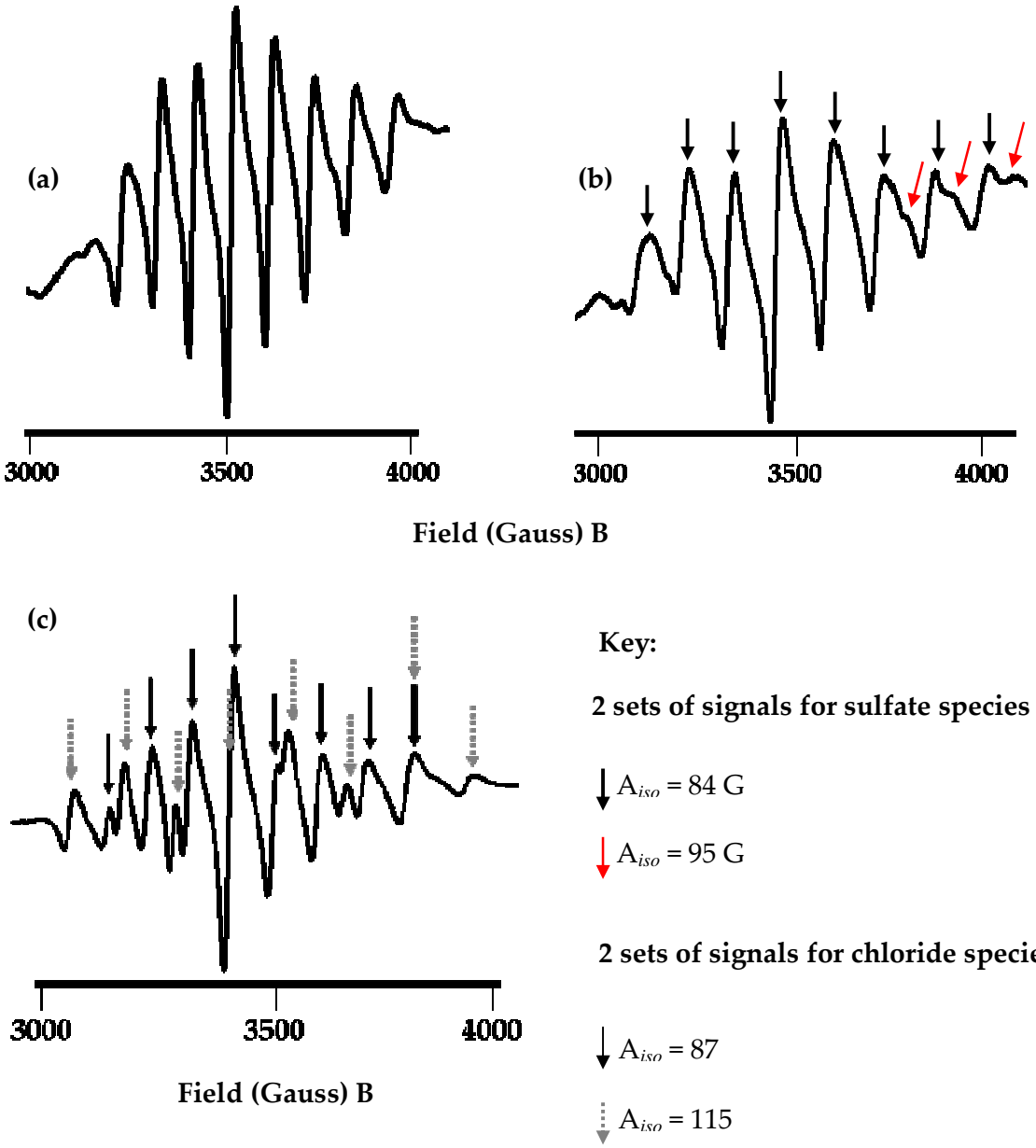

Figure 4.10 EPR spectra for oxovanadium xylyl-bicyclam complexes in water at room temperature. The axial ligand trans- to the V=O group is (a) H_2O 32, (b) sulfate 30 and (c) chloride 31.

Two sets of separate signals are clearly seen in the room temperature spectrum in water for the bicyclam chloride complex, **31**. Simulation of the data gave rise to the values shown in Table 4.9 and suggests there may be evidence of solvent exchange (A_{iso} = 87 G) and a different environment for the vanadium centre (A_{iso} = 115 G). Two sets of values were also found for the sulfate complex **30** and may suggest that each ring could be in a different configuration. No evidence of solvent exchange for the sulfate complex was apparent from the values obtained (A_{iso} = 84, 95 G).

Table 4.11 EPR parameters of frozen oxovanadium(IV) xylyl-bicyclam complexes in methanol

Ligand		**T (K)**	**A∥ (G)**	**A⊥ (G)**	*g*∥	*g*⊥
(a) sulfate, 30	**(A1)**	77	167 zz	53 xx 53 yy	1.957 zz	1.972 xx 1.972 yy
(b) chloride, 31	**(A1)**	77	167 zz	53 xx 53 yy	1.957 zz	1.971 xx 1.971 yy
	(A2)	77	174 zz	53 xx 53 yy	1.950 zz	1.971 xx 1.971 yy

Spectra for frozen solutions of complexes **30** and **31** show differences between the two. Only a single set of A∥ values can be extracted for the sulfate complex **30** with a corresponding A⊥ value and simulated values are in good agreement with manual calculations. The values are shown as **(A1)** on Table 4.11. The chloride complex **31** shows two separate sets of peaks for A∥ values and this is confirmed by the simulated data. Values for this second set of peaks listed as **(A2)** in Table 4.11 may relate to either a different configuration for one of the rings of the macrocycle, or an exchange of the chloride ligand by solvent. Due to the agreement in g-values, A∥ and A⊥

(A1) with the sulfate complex **30,** the nature of the bound ligands that give rise to these values may be similar.

An additivity relationship allows for the hyperfine coupling constant $A_{\parallel}$ to be correlated to the number and types of ligands present in the equatorial plane, with the most donating ligands contributing least to the hyperfine coupling.[6, 7] The formula, devised by Wüthrich[8] and refined later by Chasteen[6] unfortunately cannot be applied to the complexes in this work as all 4 equatorial ligands are identical, thereby making the same contribution.

Simulated spectra are listed in Appendix 1 for the data from frozen and room temperature samples. Simulation graphs for the bicyclam sulfate **30** and chloride **31** represent all sets of signals in the aqueous experiment overlaid in one averaged spectrum. This is also repeated for data for the frozen samples.

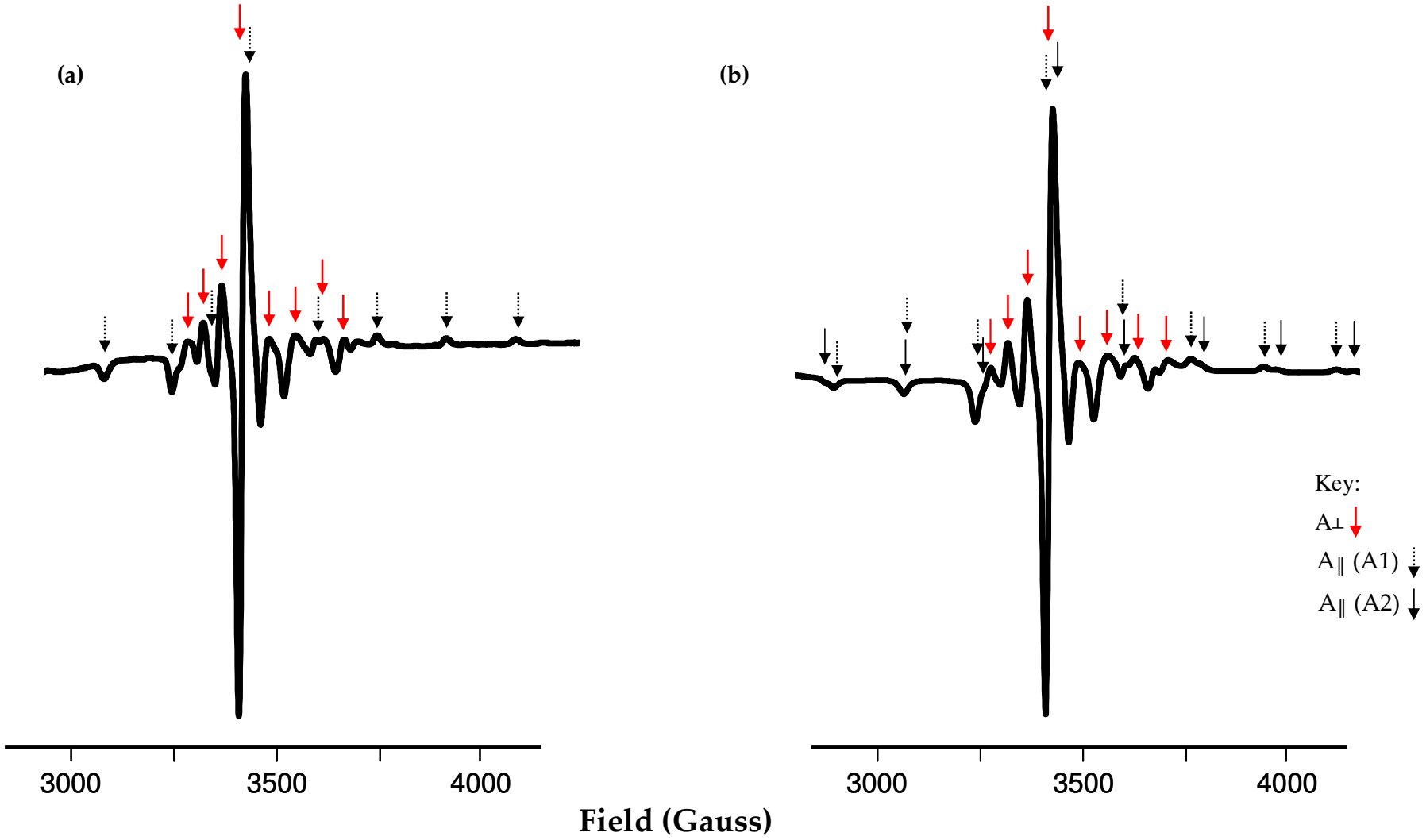

Figure 4.12 EPR frozen spectra for oxovanadium xylyl-bicyclam complexes in methanol. The axial ligand trans- to the V=O group is (a) sulfate 30 and (b) chloride 31. Two separate sets of peaks for A∥ are visible for the chloride structure, (b).

4.1.7 EXAFS/XANES

Spectra were obtained by Danielle Covelli, University of British Columbia at the Stanford Synchrotron Radiation Laboratory, for oxovanadium(IV) bicyclam complexes **30** (sulfate) and **31** (chloride) and compared with the cyclam analogues **21** (sulfate) and **22** (chloride) having identical axial ligands *trans*- to the V=O group. The data for **21** and **22** are also shown in Chapter 3.

Vanadium K-edge EXAFS data for bicyclam complexes **30** and **31** are shown in Figure 4.12. EXAFS parameters obtained from R-space fits for **21** (k^3, Δk = 2-13 $Å^{-1}$, Δr = 0.7-2.5 Å), **22** (k^3, Δk = 1.6-12.5 $Å^{-1}$, Δr = 0.5-2.6 Å), **30** (k^3, Δk = 1.7-12.5 $Å^{-1}$, Δr = 0.7-2.5 Å) and for **31** (k^3, Δk = 2-13 $Å^{-1}$, Δr = 0.7-2.5 Å) are listed in Table 4.13 and statistical parameters from best R-space fits for all four complexes are given in Table 4.14. All k-space data for the four complexes are given in Appendix 2. The XANES spectrum is shown in Figure 4.15 and includes data for all four complexes.

These spectra will be used to discuss the comparison between bicyclam and cyclam sulfate and chloride complexes.

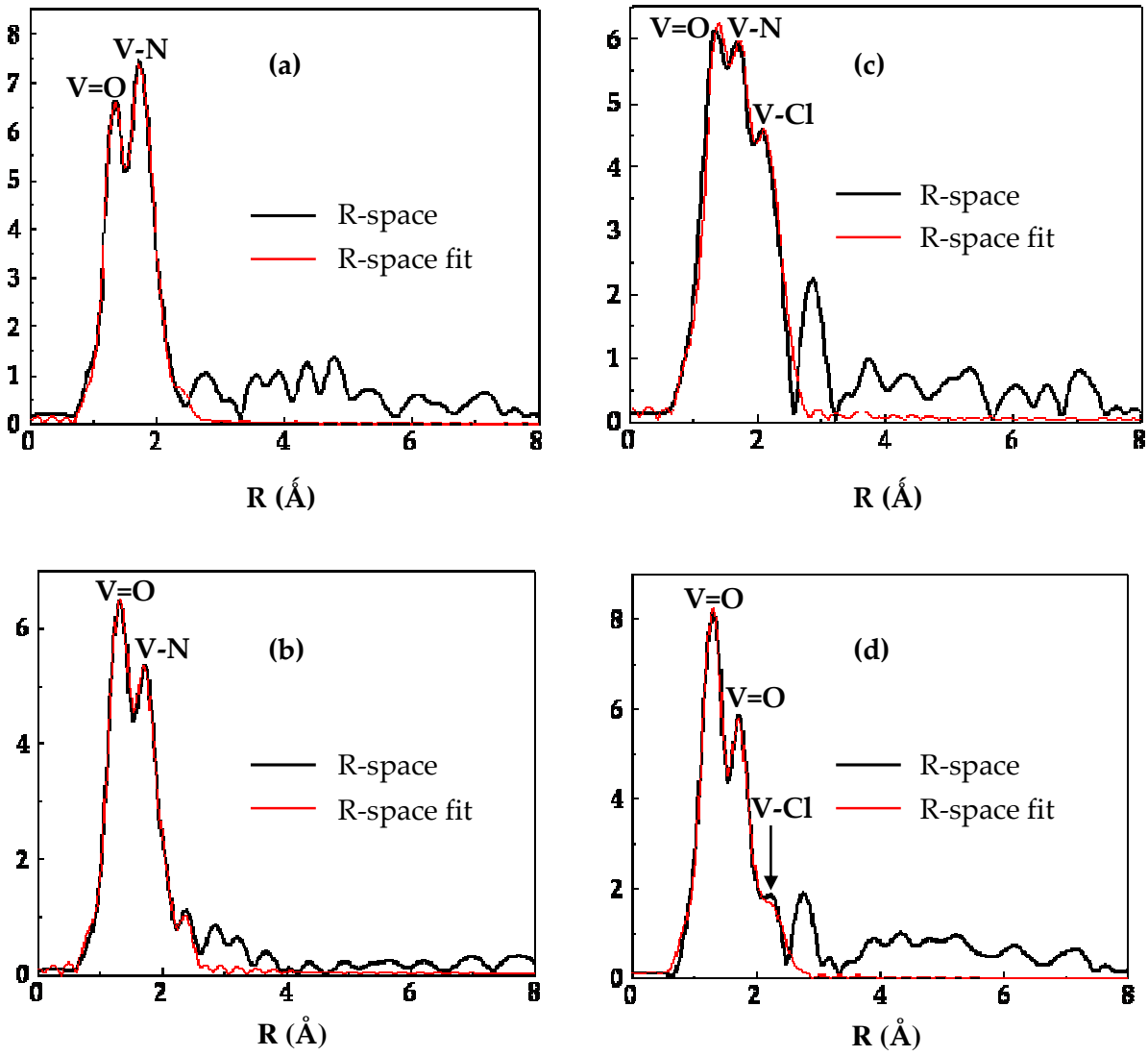

Figure 4.12 R-space (non-phase shift corrected) with calculated fits EXAFS data for (a) VO(cyclam)sulfate 21, (b) VO(bicyclam)sulfate 30, (c) VO(cyclam)chloride 22 and (d) VO(bicyclam)chloride 31

Table 4.13 EXAFS parameters for oxovanadium(IV) cyclam complexes 21 (sulfate) and 22 (chloride) and bicyclam complexes 30 (sulfate) and 31 (chloride)

Complex	Scattering Pair	N[a]	R (Å)[a]	σ^{2a}	SO_2^a	ΔE_o^a	CN[c]	Global SO_2^d
21	V-O	1[b]	1.63	0.00096	0.88	0.88	0.88	1.0
	V-N	4[b]	2.11	0.0016	0.96	0.19	3.84	
	V-O(sulfate)	1[b]	2.46	0.0023	0.84	1.37	0.84	
22	V-O	1[b]	1.63	0.0034	1.23	6.94	1.23	1.0
	V-N	4[b]	2.11	0.0017	0.81	5.69	3.24	
	V-Cl	1[b]	2.58	0.0044	1.43	-3.38	1.43	
30	V-O	1[b]	1.62	0.00083	1.03	-2.07	1.03	1.0
	V-N	4[b]	2.12	0.0020	0.80[b]	1.99	3.20	
	V-O(sulfate)	1[b]	2.59	0.0073	0.80[b]	19.81*	0.80	
31 Fit 1	V-O	1[b]	1.61	0.0011	1.31	-1.40	1.05	0.8
	V-N	4[b]	2.13	0.0054	1.26	1.33	4.03	
	V-Cl	1[b]	2.63	0.0052	0.59	-6.45	0.47	
31 Fit 2	V-O	1[b]	1.61	0.0011	1.31	-1.59	1.05	0.8
	V-N	4[b]	2.13	0.0059	1.36	1.68	4.35	
	V-Cl	1[b]	2.63	0.011	1.20[b]	-8.37	0.96	

Definitions from Table 4.13

[a] N = path degeneracy, R = distance in Å, σ^2 = bond variance (related to Debye-Waller factor), SO_2 = amplitude reduction parameter and ΔE_o = internal reference energy.

[b] These parameters were fixed during the fitting procedures.

[c] Estimated coordination number for each path, where $CN = N*SO_2*(GSO_2)$

[d] Global SO_2 (GSO_2) is defined as a global amplitude reduction factor (equivalent for all paths). GSO_2 was adjusted in cases where CN for V-O deviated significantly from 1.

* Note the ΔE_o is large for this sample; however, this provided the best possible fit.

Table 4.14 Statistical parameters obtained from the best R-space fits given in Table 4.13 for complexes 21, 22, 30 and 31

Sample	Number of Independent Variables	Chi Square	Reduced Chi Square	R-Factor
21	12	34.5	85.4	0.0027
22	12	49.2	22.4	0.0031
3	10	217.1	99.7	0.0011
4 (Fit 1)	12	23.9	59.1	0.0037
4 (Fit 2)	11	27.1	19.3	0.0042

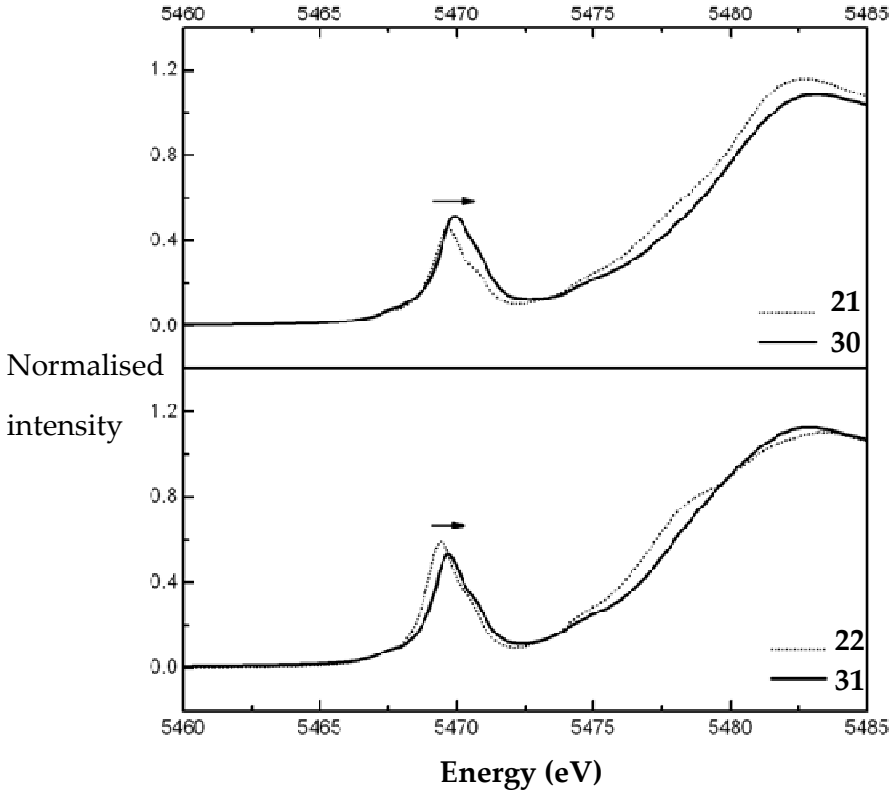

Figure 4.15 XANES spectra of the four complexes studied: (top) VO(cyclam)sulfate 21, VO(bicyclam)sulfate 30 and (bottom) VO(cyclam)chloride 22, VO(bicyclam)chloride 31.

The normalised XANES spectra of the four complexes are shown in Figure 4.15 with the emphasis on the pre-edge region. All four compounds show a very pronounced pre-edge feature. The pre-edge features result from a formally quadrupole-allowed dipole-forbidden 1s → 3d transition which is normally extremely weak. Due to the short V=O bond in these complexes a loss of centrosymmetry in the complex occurs and the pre-edge intensity increases.[9]

4.1.8 Anti-HIV activity

Complexes **30** and **31** were tested by Professor Dr Erik De Clercq, Rega Institute, Katholieke Universiteit Leuven, Minderbroedersstraat 10, B-3000 Leuven, Belgium for anti-HIV activity. Both xylyl-bicyclam complexes were found to be highly active against HIV. Information and results of the anti-HIV and cytotoxicity tests are detailed in Table 4.12 and a graphical representation of the data is set out in Figure 4.13. This bar chart compares levels of antiviral activity of the oxovanadium(IV) complexes with AMD3100 and the zinc form of AMD3100.

Table 4.12 Anti-HIV and cytotoxicity evaluation in III_B and ROD cell cultures

Complex	Strain	IC_{50} µM (µg/mL)	CC_{50} µM (µg/mL)	SI	Max Prot %	av. IC_{50} µM (µg/mL)	av. CC_{50} µM (µg/mL)	SI
30	III_B	**1.149 (0.951)**	> 151 (> 125)	> 131	101			
		1.57 (1.3)	> 151 (> 125)	> 96	95	**1.365 (1.13)**	**> 151 (> 125)**	> 111
	ROD	**4.457 (3.69)**	> 151 (> 125)	> 34	83			
		2.138 (1.77)	> 151 (> 125)	> 71	92	**3.297 (2.73)**	**> 151 (> 125)**	> 46
31	III_B	**0.119 (0.0925)**	> 161 (> 125)	> 1351	102			
		0.117 (0.0906)	> 161 (> 125)	> 1379	125	**0.116 (0.09)**	**> 161 (> 125)**	> 1365
	ROD	**0.236 (0.183)**	> 161 (> 125)	> 683	88			
		0.142 (0.11)	> 161 (> 125)	> 1139	96	**0.193 (0.15)**	**> 161 (> 125)**	> 853

** av. IC_{50} highlighted in red shows concentration of compound required to effect 50% inhibition of virus.*

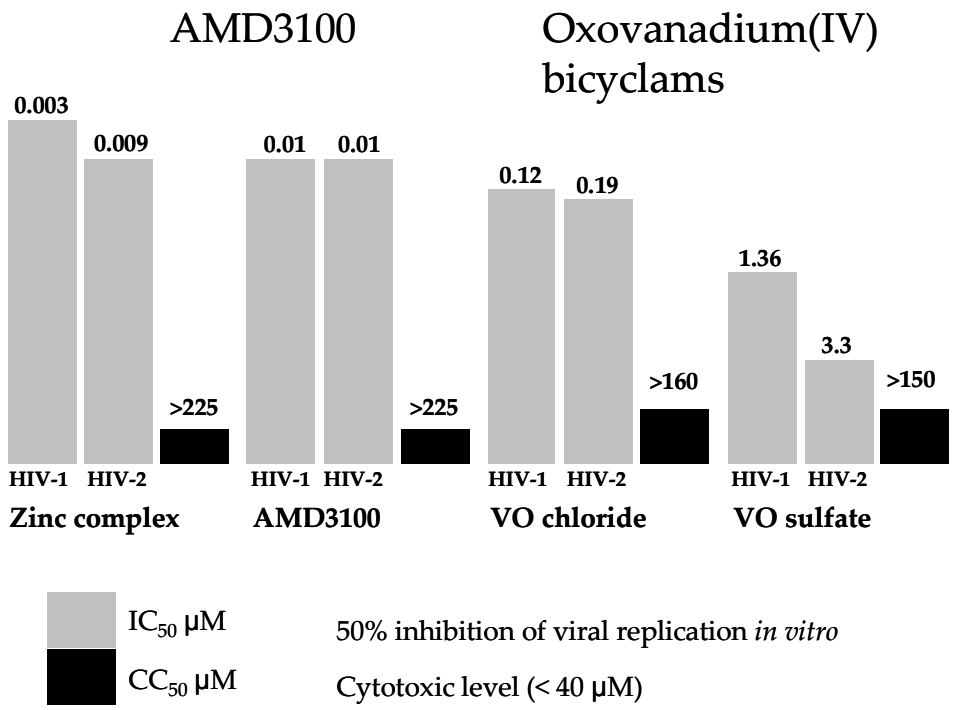

Figure 4.13 Bar chart representation of antiviral test results from Table 4.12. Higher bars for IC_{50} concentrations represent higher activity, higher bars for CC_{50} concentrations represent higher toxicity. As cytotoxic concentration is determined to be < 40 µM, all complexes show high activity and low levels of toxicity to cells. The y-axis is purely qualitative for comparison purposes and does not have any units assigned.

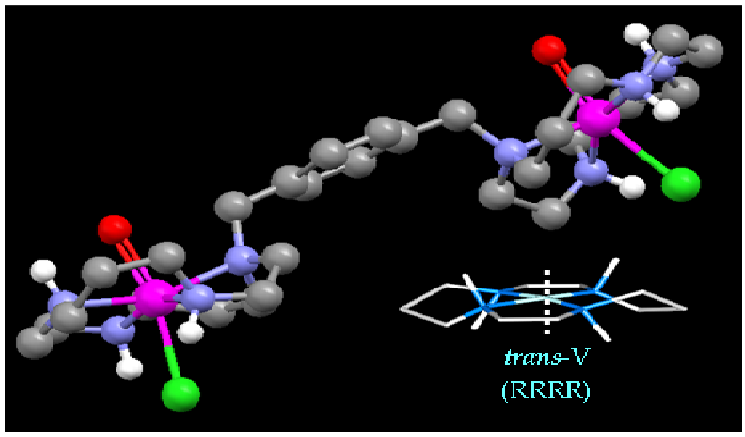

Figure 4.14 3D representation of a possible configuration for the bicyclam chloride complex, 31. The macrocycle should be able to adopt the cis-V configuration from this geometry.

In light of the results from the EPR investigation, a 3D representation of a possible configuration for the bicyclam complexes is shown in Figure 4.14 using the bicyclam chloride **31** structure as an example. The *trans*-V configuration shows how the chloride may be in a good position for hydrogen bonding with two NH protons of the ring and from this geometry it would be possible for the ring to adopt the more stable *cis*-V configuration, an important configuration for binding to carboxylates in the CXCR4 active site.

Due to the positive antiviral test results, it might be expected that at least one of the rings would be able to form the *cis*-V configuration based on previous results.[10]

4.2 Discussion

Strong vibrational stretches are seen in the infrared assigned to the V=O group for both complexes **30** (945 cm^{-1}) and **31** (964 cm^{-1}). No band for V=O is seen for either complex **30** or **31** in the Raman, but the naphthyl-cyclam **34** gave rise to both infrared and Raman signals for the V=O group. NH stretches were compared and found to be within expected values of 3000 – 3500 cm^{-1} with small variations between the complexes.[11] As reported for the cyclam complexes in Chapter 3, it would not be expected that the axial ligand trans- to the V=O group would affect the strength of the NH bonds nor the subsequent V-N bond as the electronic structure of the vanadium(IV) metal centre does not change with alternating axial ligand. Resonance Raman assignments were made for all three complexes for bonds between the oxovanadium(IV) metal centre with the nitrogen atoms of the macrocycle rings (V-N) at 450 cm^{-1}.[12] The V-N stretching frequency is documented for

V(0) and V(II) compounds and occurs between 385 – 370 cm^{-1}.[13] V(0) and V(II) compounds have d^5 and d^3 electronic structure respectively. An increase in oxidation state from 0 to II gives a slight increase in the V-N stretch from 371 cm^{-1} to 385 cm^{-1}. Further oxidation to V(IV), with a d^1 configuration, may be expected to show a more significant change in frequency due to the higher concentration of charge on the vanadium having a stronger electron-withdrawing effect on the nitrogen lone pair, resulting in a stronger bond. Raman signals were also seen in the range 350–250 cm^{-1} for two of the complexes and these have been assigned to the oxovanadium(IV)-axial ligand bond, *trans*- to the V=O group. They are evident for complexes **31** (V-Cl, 350 cm^{-1}) and **34** (V-O, 295 cm^{-1}). The assigned V-Cl signal became apparent on increasing the filter aperture of the laser from 10% to 100%, but the result of this was decomposition of the complex. This was confirmed by visual inspection which revealed charring in addition to a new signal *circa*. ~900 cm^{-1}, that cannot be assigned to the complex. This decomposition of the sample had already been seen for the cyclam complexes in Chapter 3, in particular complex **21** when a crystal was used for this type of analysis.

Analysis of room temperature data acquired by electron paramagnetic resonance spectroscopy revealed different behaviour in solution for bicyclam complexes **30** (sulfate) and **31** (chloride) from that of cyclam complexes with comparable axial ligands, **21** (sulfate) and **22** (chloride). The g-values are close to 2 in all cases as expected as the unpaired electron is in a non-degenerate orbital. In addition, there should also be negligible mixing in of an orbital component from excited states through spin-orbit coupling.[14, 15] The unpaired electron is in the *d*(xy) orbital and oriented between the N atoms in the cyclam plane.[16] As *d*(xy) is essentially non-bonding, any

interaction with the nitrogen orbitals is very small and no resolved coupling to nitrogen is seen. Any orbital angular momentum is subsequently quenched resulting in a "spin-only" system.[17]

In the sulfate **30** and chloride **31** complexes, significant differences are observed. Neither set of peaks for the bicyclam sulfate complex **30** show similar calculated values to the reference complex where the 6th axial ligand is H_2O and suggests there is no substitution of the 6th ligand by solvent, unlike that proposed for the cyclam complexes in Chapter 3. The low A_{iso} value of 84 (G) is at the lower end of that reported for other vanadium(IV) species with O-donor ligands (85 to 110 G), although not the lowest reported (71 G).[7, 18, 19] The values of g_{iso} (1.985, 1.983) fall within reported ranges. [7, 19] The separate set of signals observed and confirmed by simulation may also suggest that each vanadium centre is in a different environment, indicating that the macrocyclic rings could be in different configurations. The possibility of greater delocalisation onto the sulfate ligand may also result in the observed low A_{iso} value. Complex **31** (Figure 4.10c) clearly shows two sets of peaks for the room temperature spectrum. Some degree of partial substitution of the ligand by water is indicated by the g-value and A_{iso} = 87 (G) shown in Table 4.9. A larger A_{iso} value was calculated for the second set of peaks found for complex **31**, (A_{iso} = 115 G) and infers a stronger interaction exists between the unpaired electron and the vanadium centre. As the A-value is the hyperfine coupling constant and related to the unpaired electron density at the vanadium centre it may be that for this particular configuration the unpaired electron is more localised on the vanadium than for the other configuration where A_{iso} = 87 G. An interesting observation is that the average g and A values (energy units of cm^{-1}) used to describe the frozen solution spectra should approximate to the isotropic g and A values

(cm^{-1}) used to describe the fluid solution spectra. There are some differences between these values in the complexes described which may be explained by different solvent interactions of the complexes with water and methanol, or may indicate that certain configurations are being ' frozen out' in the frozen solution spectra. Large deviations from square-pyramidal geometry and also the nature of the 6th ligand can influence the A-value and *pi* bonding with electron donation to the *d*(xy) orbital can have a large effect. In light of these observations, it would appear that for the bicyclam complexes there is a 6th ligand affecting A.

EXAFS data for the two bicyclam complexes **30** and **31** were compared with that of the cyclam analogues, **21** and **22**. A comparison of the R-space EXAFS for the four complexes with both data and calculated fits is shown in Figure 4.12 and data were Fourier-transformed over a k-range varying from 1.6-13 $Å^{-1}$ depending on the compound. For the sulfate complexes **21** and **30**, two main first-coordination shells are clearly observed and are assigned as V=O and V-N. It is suspected that the signal for V-O is hidden under the large peak for V-N. For the chloride complexes **22** and **31**, three main first-coordination shells are clearly observed in the data, assigned as the V=O, V-N and V-Cl scattering pathways, respectively. A drastic change in the intensity of the V-Cl feature from the cyclam **22** to the bicyclam **31** is seen with an increase in the V-Cl bond distance from 2.58Å to 2.63Å, respectively. Such a large drop in intensity suggests that there may be loss of a chloride ligand in the solid state structure of **31**, or a large increase in disorder of the chloride ligand. To explore these two possibilities, different fits to the EXAFS data were attempted. The best fit to the first coordination sphere yields a coordination environment consistent with $VON_4Cl_{0.5}$ relating to the loss of one of the two axial chloride ligands in the bicyclam complex.

Enforcing the anticipated VON_4Cl coordination environment for each ring yields a significantly poorer fit with a concomitant doubling of σ^2 for the V-Cl pathway (Table 4.13). Although disorder of a chloride site cannot be discounted, the data does appear to support the $VON_4Cl_{0.5}$ fit. This could indicate either partial occupancy or, more probably, the presence of bridging chloride ligands creating oligomeric species in the solid state. This assumption is supported when considering how difficult the bicyclam complexes were to recrystallise. Problems were experienced during the synthetic work-up and recrystallisation process with precipitation of insoluble products, thought to be due to the formation of polymeric or bridged species.

Antiviral test results reveal that both bicyclam complexes are active against HIV, although less active than the zinc form of xylyl-bicyclam. The sulfate complex is active at a concentration of 1.36 μM and the chloride complex shows the highest activity of the two at a concentration of 0.12 μM. The result for the chloride complex is comparable with the anti-HIV activity of AMD3100, *i.e.* nanomolar concentrations are found to initiate an effect in the inhibitory process of blocking the virus via the CXCR4 receptor. It is difficult to postulate the factors involved in the mechanism of antiviral activity of these oxovanadium(IV) bicyclams. The EPR data suggests partial exchange of the axial chloride ligand may occur with H_2O and if so, may result in one ring adopting an unfavourable geometry as suggested for the oxovanadium(IV) cyclams in Chapter 3. Molecular modelling showed that on removing the 6th axial ligand it was possible for the macrocycle to be bound in such a way that the distance required for coordination bond formation between the metal and carboxylates in the binding site was not

possible. As the bicyclams are highly active, it is likely that the aromatic linker plays a very important part.

4.3 Conclusion

The starting material xylyl-bicyclam (**16**) was synthesised successfully and characterised by mass spectrometry and ^{1}H NMR spectroscopy, with assignments listed in the Experimental Section, Chapter 7. Two oxovanadium(IV) xylyl-bicyclam complexes were synthesised and have shown high activity against HIV as potential entry inhibitor drugs. In terms of determining the configuration of the rings, the mode of action of the antiviral activity is difficult to investigate due to the paramagnetic nature of the vanadium centre. Successful formation of single crystals may provide the only means of identifying the configurations of the macrocyclic rings, and potential binding interactions between the complexes and the CXCR4 receptor using techniques such as molecular modelling could then be applied.

Infrared and Raman spectroscopies in conjunction with electron paramagnetic resonance spectroscopy provided a useful insight into the electronic character of oxovanadium(IV) bicyclam complexes. The vibrational stretch of the V=O group is characteristic of vanadium in the 4^{+} oxidation state and ligands *trans*- to the V=O group may influence the resonant frequency in accordance with bond strength to the vanadium centre and possible geometry of the ring. Information gained through EPR revealed different behaviour in water for the bicyclam chloride complex **31** than for the bicyclam sulfate complex **30** and the data suggest that the axial ligand in both cases remains bound to vanadium. This may be crucial for directing the configuration of the rings in terms of binding with the CXCR4 receptor.

UV-visible spectroscopy provided only qualitative data due to problems with precipitation in solution but it was seen that binding to acetate occurs with time and induces a change in the complex. This could be indicative of a change in configuration to one with a preferred geometry for binding to carboxylates in the CXCR4 binding site. It is unknown which configuration this induced change represents and in light of the positive antiviral results it may be possible that the *cis*-V configuration could form in solution. There are of course other configurations such as *trans*-II that are thought to show activity against HIV, although these tend to be more predominant in constrained systems where the bicyclam rings are held rigid by a bridging tether.[20]

4.4 Bibliography

[1] E. De Clercq, *Nat. Rev. Drug Discov.,* **2003**, *2*, 581.

[2] S. M. Devine, N. Flomenberg, D. H. Vesole, J. Liesveld, D. Weisdorf, K. Badel, G. Calandra, J. F. DiPersio, *J. Clinic. Oncol.,* **2004**, *22*, 1095.

[3] www.webwire.com/ViewPressRel.asp, **2008**.

[4] W. Yang, C. M. Giandomenico, M. Sartori, D. A. Moore, *Tetrahedron Lett.,* **2003**, *44*, 2481.

[5] S. A. Al'tshuler, B. M. Kozyrev, *Electron Paramagnetic Resonance*, C P Joole, Jr., ed., Academic Press, New York, **1964**.

[6] N. D. Chasteen, *Biol. Mag. Res.,* **1981**, *3*, 53.

[7] T. S. Smith, R. LoBrutto, V. L. Pecoraro, *Coord. Chem. Rev.,* **2002**, *228*, 1.

[8] K. Wüthrich, *Helv. Chim. Acta* **1965**, *48*, 1012.

[9] M. Giorgetti, S. Passerini, W. H. Sneyrl, S. Mukerjee, X.Q. Yang, J. McBreen, *J. Electrochem. Soc.,* **1999**, *146*, 2387.

[10] X. Liang, J. A. Parkinson, M. Weishaupl, R. O. Gould, S. J. Paisey, H.-s. Park, T. M. Hunter, C. A. Blindauer, S. Parsons, P. J. Sadler, *J. Am. Chem. Soc.,* **2002**, *124*, 9105.

[11] J. B. Lambert, H. F. Shurvell, D. A. Lightner, R. G. Cooks, *Organic Structural Spectroscopy*, Prentice-Hall, New Jersey, **1998**.

[12] E. J. Baran, A. H. Juberta, E. G. Ferrer, *J. Raman Spectrosc.,* **1992**, *23*, 489.

[13] K. Nakamoto, *Infrared and Raman Spectra of Inorganic and Coordination Compounds*, 4 ed., Wiley - interscience, Canada, **1986**.

[14] F. E. Mabbs, *Chem. Soc. Rev.,* **1993**, *22*, 313.

[15] P. Basu, *J. Chem. Ed.,* **2001**, *78*, 666.

[16] C. Slebodnick, B. J. Hamstra, V. L. Pecoraro, *Modelling the biological chemistry of vanadium: Structural and reactivity studies elucidating biological function, Vol. 89*, Springer Verlag, Berlin, **1997**.

[17] Shriver, Atkins, *Inorganic Chemistry*, 3 ed., Oxford University Press, **1999**.

[18] G. G. Nunes, G. R. Friedermann, P. B. Hitchcock, E. L. de Sa, J. F. Soares, *Inorg. Chim. Acta* **2006**, *359*, 1435.

[19] B. Gahan, F. E. Mabbs, *J. Chem. Soc. Dalton Trans.,* **1983**, 1695.

[20] G. McRobbie, G. C. Valks, C. J. Empson, A. Khan, J. D. Silversides, C. Pannecouque, E. De Clercq, S. G. Fiddy, A. J. Bridgeman, N. A. Young, S. J. Archibald, *Dalton Trans.,* **2007**, 5008.

5. ZINC(II) CONSTRAINED CYCLAMS

This chapter describes the synthesis and characterisation of zinc(II) complexes of constrained cyclams. Numbers in bold after compound names refer to experimental data in Chapter 7.

The cyclam (1,4,8,11-tetra*aza*cyclotetradecane) ligand with *C*- and/or *N*-alkyl groups and the resulting complexes have received considerable attention because their structural and chemical properties may be quite different from those of the unsubstituted parent cyclam (1,4,8,11-tetra*aza*cyclotetradecane) macrocycle.[1] In this chapter, two constrained cyclams (**35** and **39**) and their zinc complexes (**36**-**38**, **40**-**42**) are characterised and compared (Scheme 5.3). The constrained ligand, HMC (5,16-dimethyl-2,6,13,17-tetraazatricyclo-(14,4,$0^{1.18}$,$0^{7.12}$)docosane) **35**, bearing an additional two cyclohexane rings and two methyl groups on the macrocycle has often shown different coordination behaviour from transition metal complexes with cyclam.[2-4] The macrocyclic 14-membered cyclam derivatives are moderately flexible structures and can adopt any of six configurations shown in Figure 5.1 as both *trans*- and *cis*- isomers.[2]

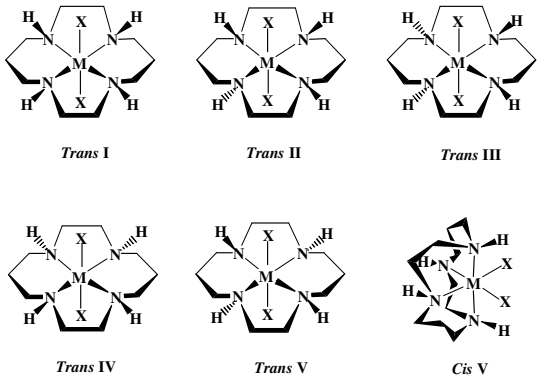

Figure 5.1 Configurations of metal cyclam complexes

There are several examples in the literature on the effect of ligand constraints of macrocyclic complexes.[5-11] For example, complexes of copper polythiaethers such as [14]aneS_4 are difficult to synthesise due to the unfavourable enthalpic contributions from the uncomplexed ligand. The *exo* conformation of the ligand results in the lone pairs of the sulfur donor atoms being oriented away from the ligand cavity. On addition of ring substituents such as benzene or cyclohexane rings, the sulfur donor atoms are expected to show a preference toward an *endo* conformation, placing the lone pairs toward the ligand cavity.[5] N-functionalised derivatives of cyclam that exhibit a novel cross-bridge linking symmetrical nitrogens of the ring show increased *in-vivo* stability in radiolabelled complexes when compared with an analogue with no cross-bridge.[12, 13] Similarly, a side-bridged macrocycle incorporating a coordinating acetate pendant arm displays only *trans*-II or *trans*-IV configurations showing how constraining substituents affect the preferred geometry of the ring.[6] It is of paramount importance to understand the metabolic fate of radio-metal labelled complexes in their application in areas of diagnostic imaging and targeted radiotherapy. Copper radioisotopes used in conjunction with current bifunctional chelators show successful inhibition of tumour growth, but retention of activity is also seen in organs such as the blood, liver and bone marrow. This observation suggests that the radio-isotope (e.g. ^{64}Cu) may dissociate from the complex and further bind to proteins such as superoxide dismutase in the liver.[14] Reducing the flexibility of the ring through the addition of constraining substituents may result in a potential increase in kinetic stability, an important advance when addressing the problem of increased kinetic lability *in vivo* of existing bifunctional radiopharmaceutical chelators.

An investigation into the effect on stability constants in complexes with comparable constraining substituents was made. Using the [14]aneS_4 macrocycle, cyclohexanediyl and cyclopentanediyl ring substituents showed that although stability constants for Cu(II)L increased upon the introduction of *cis*-cycloalkyl groups, a decrease in stability of approximately 10-fold is seen on the introduction of the *trans*-cyclopentanediyl substituent. The *trans*-cyclohexanediyl showed the same effect as the *cis*-cyclohexanediyl derivative. The cyclopentane substituent is less flexible than the cyclohexane rings and the *trans*-cyclopentane rings appear to orient the donor atoms of the macrocycle causing internal strain on attempted coordination with Cu(II).[7]

The effect of constraining substituents continues to be investigated in this work, in particular the effect of adding substituents that may result in a single isomer in solution.

Acetate is a ligand that can coordinate with a metal ion *via* one or two *O* atoms (unidentate, chelating bidentate and bridging bidentate). Acetate can also adopt two different bridging conformations, the *syn-syn* mode and the *syn-anti* mode allowing coordination to a metal in one of the various modes (Figure 5.2).[15]

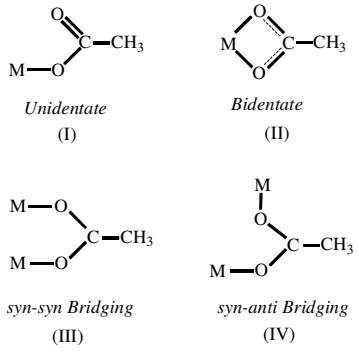

Figure 5.2 Possible types of metal-acetate coordination

Zinc(II) complexes of both cyclam and xylyl-bicyclam greatly enhance the anti-HIV activity in comparison to the macrocycles alone[17] and it is suggested that the carboxylate groups of aspartate residues Asp171 and Asp262 of the CXCR4 chemokine receptor play key roles in the recognition of cyclams.[18, 19] The understanding of binding affinity and configuration between carboxylate groups and zinc(II)-constrained cyclams has become extremely important in the improved design and development of new highly effective anti-HIV drugs that specifically target alternative events in the HIV replicative cycle.

5.1. Experimental

Zinc(II) complexes of constrained cyclams were synthesised as shown in Scheme 5.3.

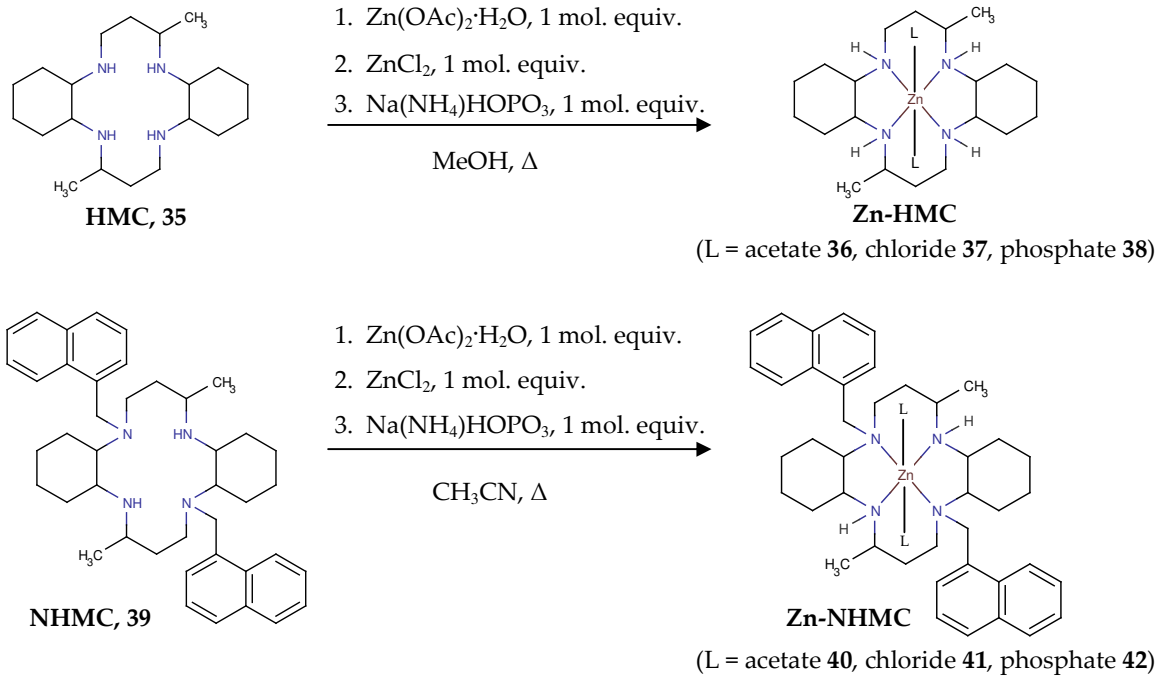

Scheme 5.3 General preparative route to zinc(II) macrocycle complexes where L = acetate, chloride or phosphate assuming octahedral geometry (experimental details are in Chapter 7)

5.1.1. Materials

Cyclam ligands, HMC (Hexyl-Me_2-cyclam) **35** and NHMC (Naphthyl-hexyl-Me_2-cyclam) **39**, were synthesised adopting a previously published method,[2, 20] by Professor Jong-Ha Choi, Department of Chemistry, Andong National University, Andong 760-749, South Korea and were very kindly donated. All other starting materials were purchased from Sigma-Aldrich as detailed in Chapter 2. Solvents used for synthetic work were HPLC grade methanol and ultra-dry acetonitrile from Sigma-Aldrich. HPLC grade methanol and reagent grade diethyl ether were used for recrystallisations.

5.2. Results

5.2.1. Infrared spectroscopy

The infrared spectrum of Zn(II)-hexyl-Me_2-cyclam(diacetate) **36**, was recorded at room temperature as a KBr disc and shows three weak absorption bands (546, 526, 488 cm^{-1}) in the 400-600 cm^{-1} region, indicating a *trans-* arrangement of the unidentate ligand.[15] The *cis-* complex would be expected to show more bands and more splitting in this region due to lower symmetry. The infrared spectral data of this complex appear to be consistent with the *trans-* configuration. The spectrum obtained for the chloride complex **37** also shows three bands in this region, although the second band at 528 cm^{-1} is very weak. These bands are not seen for the phosphate complex **38** as the ν_4 strong O-P-O stretch found in this region splits into two bands at 482 cm^{-1} and 559 cm^{-1} and masks any weak signals. The splitting of the band indicates a reduction in symmetry from the free phosphate ion and suggests the phosphate is coordinated. Absorption bands for all three complexes are listed in Table 5.4. Spectra obtained for the

Zn(II)-naphthyl-hexyl-Me_2-cyclam(diacetate) complex **40** also shows three weak absorption bands in the 400-600 cm^{-1} region that may infer *trans*- geometry of the acetate ligands. The chloride species gives similar results and the phosphate analogue revealed a strong O-P-O vibrational stretch that may overlap weak signals found in this region. Absorption bands for each complex are listed in Table 5.5.

Table 5.4 Infrared absorption bands in 400-600 cm^{-1} region for Zn(II)-hexyl-Me_2-cyclams

Complex	Band 1 (cm^{-1})	Band 2 (cm^{-1})	Band 3 (cm^{-1})
36	546	526	488
37	546	528	490
38 (O-P-O)	559	-	482

Table 5.5 Infrared absorption bands in 400-600 cm^{-1} region for Zn(II)-naphthyl-hexyl-Me_2-cyclams

Complex	Band 1 (cm^{-1})	Band 2 (cm^{-1})	Band 3 (cm^{-1})
40	479	508	561
41	486	507	559
42 (O-P-O)	557	-	480

5.2.2. X-ray crystallography

Three X-ray crystal structures of zinc(II) constrained cyclam complexes were achieved in this work. All three structures were determined at 150 K (Figures 5.8, 5.10 and 5.12). Selected bond lengths and angles are detailed in Table 5.6 with supporting crystallographic data in Table 5.7. Complex **36** crystallised in the *trans*-III configuration with axial acetate ligands. Complex **38** crystallised as 2 separate 5-coordinate zinc macrocycles, bound to a shared phosphate through zinc-oxygen bonds. Complex **41**

crystallised in a *trans*-I configuration containing a 4-coordinate tetrahedral zinc centre to three of the ring nitrogen atoms. For complex **38**, only cell dimensions are available and these are listed in Table 5.7.

Table 5.6 Selected bond lengths (Å) and angles (°) for zinc(II) constrained cyclam complexes

Axial ligand and complex identification		**Acetate (36) 150 K**	**Chloride (41) 150 K**
Zn-N bond lengths			
Zn(1)-N(1) #1	HMC	2.1368(8)	-
Zn(1)-N(8) #1		2.0660(8)	-
Zn(1)-N(3)	NHMC	-	2.053(4)
Zn(1)-N(7)		-	2.070(4)
Zn-L* bond lengths			
Zn(1)-O(1) #1	HMC	2.2940(7)	-
Zn(1)-Cl(2)	NHMC	-	2.1949(14)
L* bond lengths (acetate)			
C(102)-O(1)	HMC	1.2715(12)	-
C(102)-O(2)		1.2459(13)	-
L*-Zn-N bond angles			
O(1)-Zn(1)-N(1)	HMC	81.64(3)	-
O(1)-Zn(1)-N(8)		88.49(3)	-
Cl(2)-Zn(1)-N(3)	NHMC	-	118.95(12)
Cl(2)-Zn(1)-N(7)		-	120.14(12)
N-Zn-N bond angles			
N(1)-Zn(1)-N(1)	HMC	179.995	-
N(8)-Zn(1)-N(8)		179.994	-
N(1)-Zn(1)-N(8)		83.36(3)	-
N(3)-Zn(1)-N(7)	NHMC	-	99.51(17)
N(3)-Zn(1)-N(10)		-	104.30(17)
N(7)-Zn(1)-N(10)		-	87.28(18)

**** L = bonding atom of axial ligands***

HMC = Hexyl-Me_2-cyclam complexes

NHMC = Naphthyl-hexyl-Me_2-cyclam complexes

Table 5.7 X-ray crystallographic data for zinc(II) constrained cyclam complexes

Axial ligands and complex identification	**Acetate (36)**	**Phosphate (38)**	**Chloride (41)**
Formula	$C_{24}H_{46}N_4O_4Zn_1$	$C_{48}H_{92}N_8O_4P_1Zn_2$	$C_{42}H_{54}Cl_1N_4Zn_1$
Formula weight	520.03	-	715.75
Crystal system	Monoclinic	-	Monoclinic
Space group	*P* 1 2_1/*n* 1	-	*C* 1 2/*c* 1
a / Å	9.2392(3)	21.2436(14)	24.5797(11)
b / Å	10.5922(3)	16.3400(11)	29.3304(12)
c / Å	13.2643(4)	17.2105(12)	13.1572(6)
α / °	90	90	90
β / °	105.727(2)	108.902(4)	95.597(3)
γ / °	90	90	90
Cell vol. / Å^3	1249.50(7) A^3	5652.0(8)	9440.2(7)
Z	2	-	8
Density (Calc) mg/m^3	1.382	-	1.007
Abs. coeff. mm^{-1}	1.020	-	0.604
Reflections collected	22930	-	33746
Independent reflections	3647 [R(int) = 0.037]	-	9733 [R(int) = 0.088]
R1 (obs/all refl)	0.0254 [2932 data]	-	0.0819 [6280 data]
wR2 (obs/all refl)	0.0685	-	0.1922

Zn(II)-hexyl-Me$_2$-cyclam, 36

The molecular structure of complex **36** was determined by single-crystal X-ray diffraction and structure determination was carried out at 150 K. The structure with atomic numbering scheme is shown in Figure 5.8. The complex adopts the thermodynamically stable *trans*-III configuration. The constrained cyclam ring is *trans*-III and the acetate is axially coordinated forming hydrogen bonds to one of two NH groups resulting in additional stabilisation. The bond angles of five- and six-membered chelate rings around the zinc(II) are 83.36(3)° and 96.64(3)° respectively. The crystals are held together by hydrogen bonds between secondary NH groups of the constrained cyclam and acetate groups. The proton bonded to N8 forms a strong intramolecular hydrogen bond with the non-coordinating oxygen atom O2 of acetate (1.985 Å). This value is comparable with typical hydrogen bonds found in H_2O (1.97 Å) and these hydrogen-bonded networks help to stabilise the crystal structure.

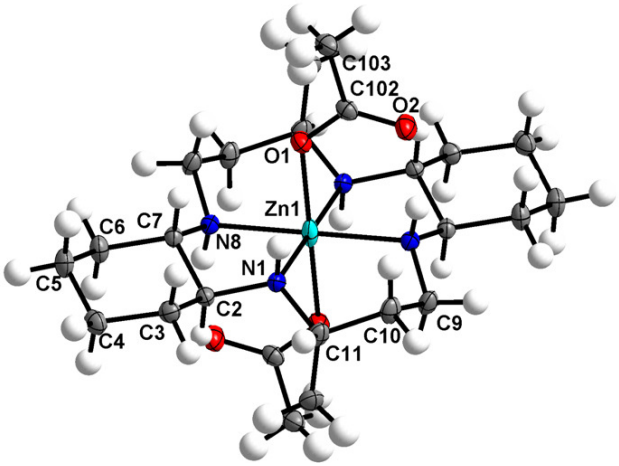

Figure 5.8 Zn(II)-hexyl-Me$_2$-cyclam, 36

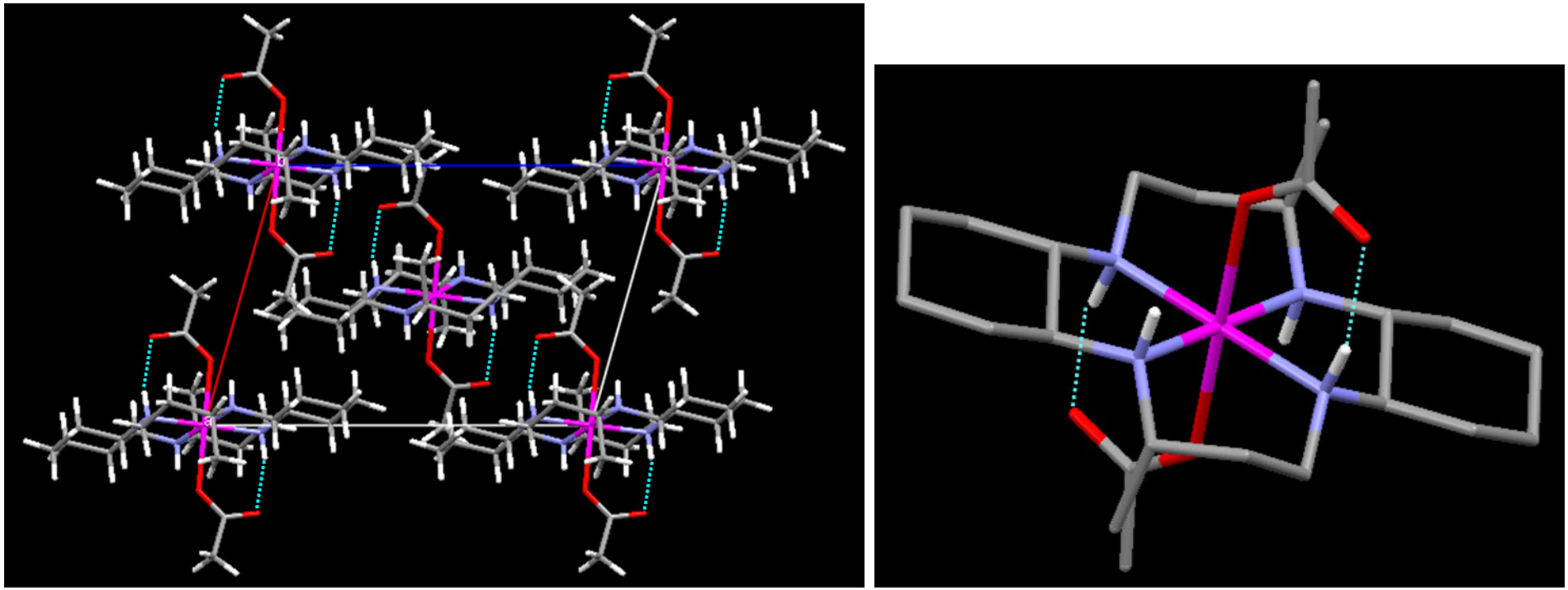

Figure 5.9 Crystal packing of Zn(II) hexyl-Me_2-cyclam(diacetate), 38. Hydrogen bonding is seen between NH protons and oxygen atoms of axial acetates. The macrocycle is in the trans-III configuration.

Zn(II)-hexyl-Me$_2$-cyclam(diphosphate), 38

The molecular structure of complex **38** was determined by single-crystal X-ray diffraction and structure determination was carried out at 150 K. Complex **38** did not crystallise in the expected structure and is shown in Figure 5.10. Mass spectrometry identified the molecular ion as the diphosphate structure **38**, (*m*/*z*: 497.2, $[M]^+$), but crystals formed of the dimer (labelled as **38a**) with a shared phosphate group between two zinc 5-coordinate centres. Problems were encountered with refinement of the structure thought to be due to the presence of a disordered zinc atom. The structure exhibits a peak close to one of the Zn atoms which suggests that the Zn is positionally disordered over two sites, one (the major occupancy) where it is coordinated to the phosphate, and the other (minor occupancy) when it is coordinated to a chloride. The chloride site is similarly disordered. The chloride must be acting as either a 6th ligand or counter ion for charge balance. As complex **38** was synthesised from complex **37**, the presence of chloride suggests that not all chloride was removed prior to addition of phosphate.

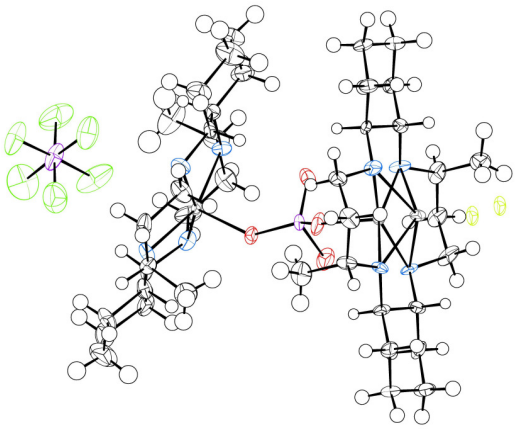

Figure 5.10 Zn(II)-hexyl-Me$_2$-cyclam(diphosphate), 38a

Zn(II)-naphthyl-hexyl-Me_2-cyclam(dichloride), 41

The molecular structure of complex **41** was determined by single-crystal X-ray diffraction and structure determination was carried out at 150 K (Figure 5.11). Initially, problems were encountered with data collection as the crystal cracked before all data was accumulated. A second set of data revealed a different unit cell and the possibility of polymorphism was suspected.

Differential Scanning Calorimetry (DSC) analysis was used to find the temperature at which any phase transition occurred, but results showed none was present. Data collection was eventually successful at 150 K using different crystals. It is noted that the chloride counter ion is not seen in the data and is suspected to be moving rapidly in the large solvent channels that exist between molecules. These channels can be seen in the packing diagram shown as Figure 5.12.

Complex **41** crystallised as a 4-coordinate zinc centre, bound to three nitrogens of the macrocycle with a fourth bond to a chloride ligand. The zinc centre is tetrahedral and the NH protons of the ring align in the same direction across the diagonal indicating that the ring is in the *trans*-I configuration.

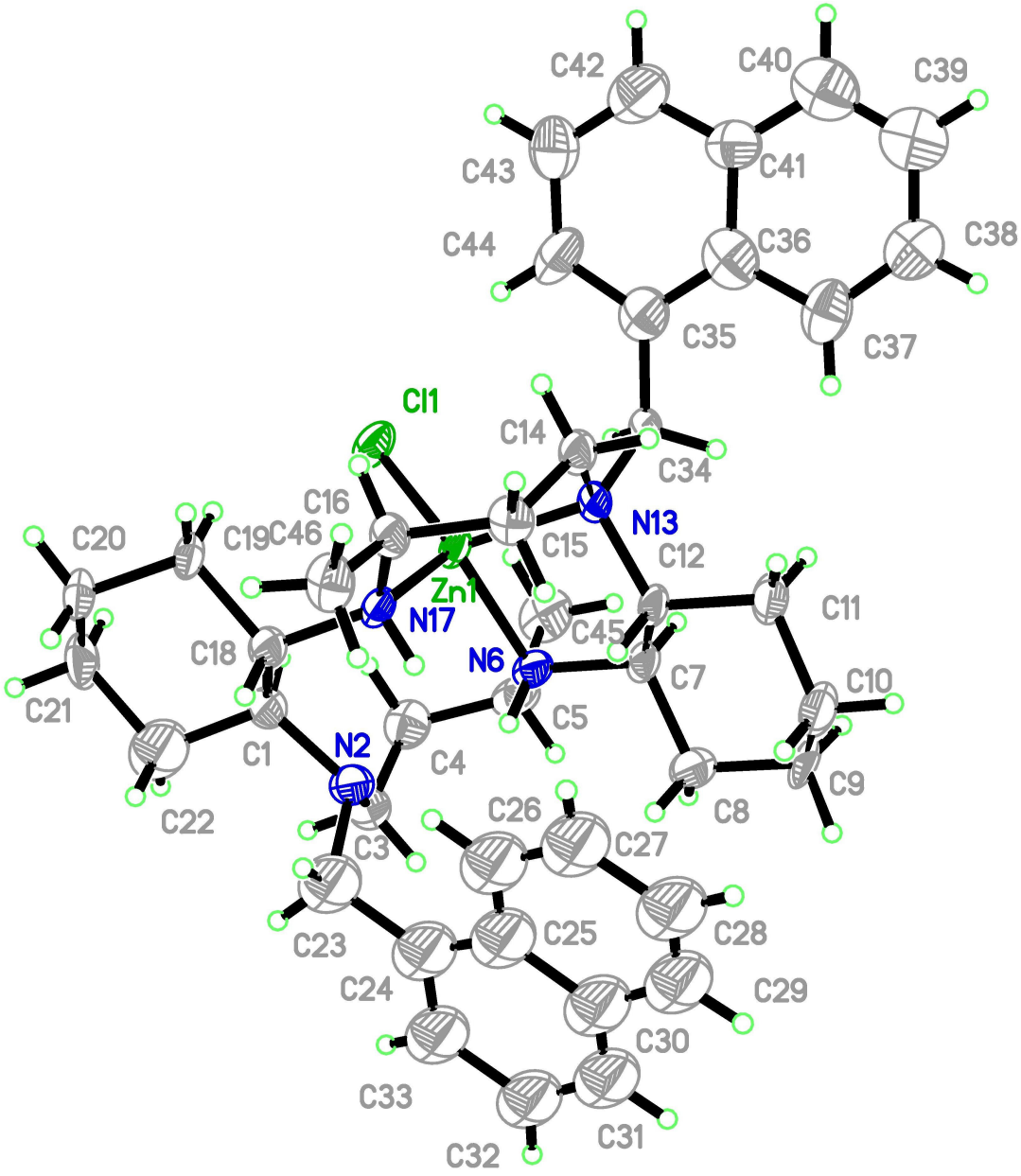

Figure 5.11 Zn(II)-naphthyl-hexyl-Me_2-cyclam, 41(a)
Complex 41 is the dichloride, but no chloride counter ion is seen in the crystal structure.

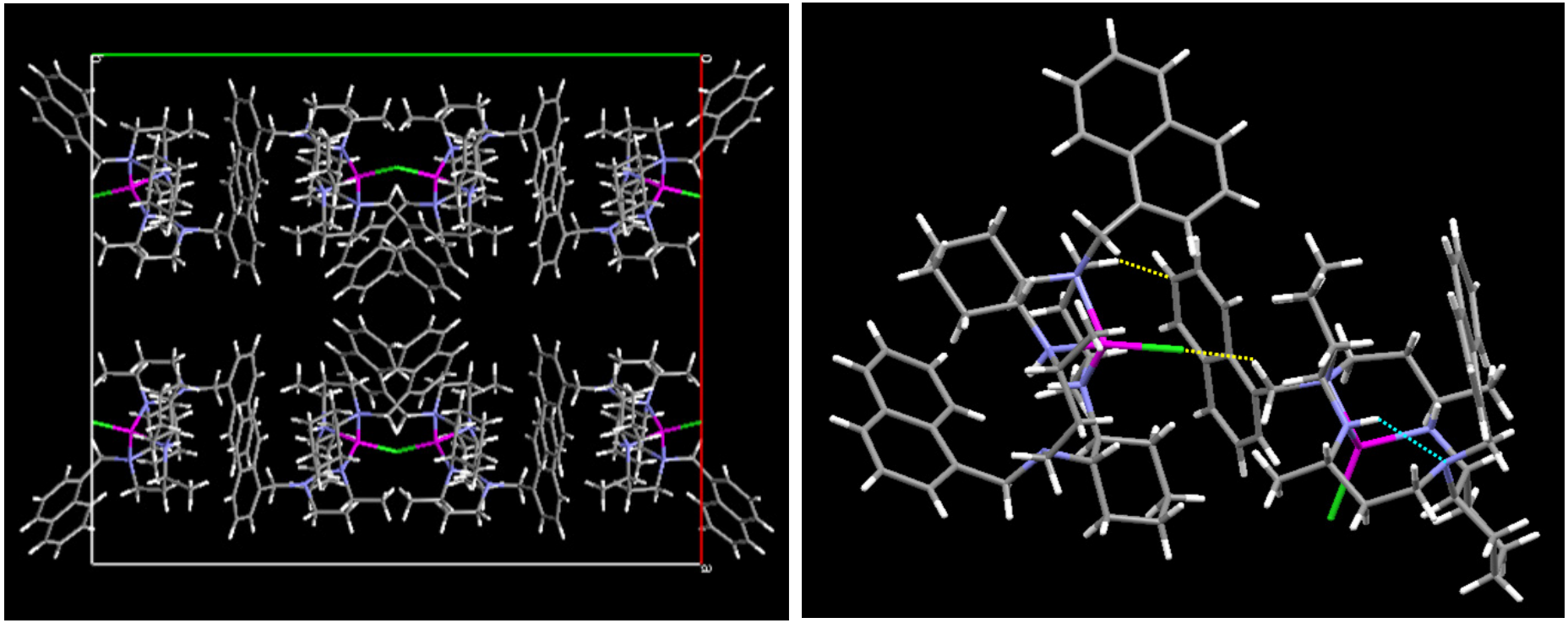

Figure 5.12 Crystal packing of Zn(II)-naphthyl-Me_2-cyclam, 41(a) projected along the c axis of the unit cell and rotated by 90°. Hydrogen bonds are shown (cyan) between an unbound nitrogen and a protonated nitrogen of the macrocycle. Short contacts (yellow) are seen between chloride ligands of one macrocycle and methylene protons of the naphthyl of a neighbouring macrocycle. Short contacts also form between protons of the hexyl rings with carbon atoms of the aryl rings.

5.2.3. Comparison of bond lengths and angles of constrained metallomacrocycles

5.2.3.1. Zinc-oxygen bond length comparison (Zn(II)-HMC, 36)

Zn-O bond lengths of Zn(II)-hexyl-Me_2-cyclam(diacetate) (Zn(II)-HMC), **36** were compared with those of three zinc(II) cyclams reported in the literature, labelled as $[Zn(II)(cyclam)(H_2O)_2](OAc)_2$, **A**[21], $[Zn(II)(cyclam)(OClO_3)_2]$, **B**[22] and a zinc(II) constrained cyclam [Zn(II)-hexyl-Me_2-cyclam$(H_2O)_2]Cl_2$, **C.**[23] Details are listed in Table 5.13. Comparing the two cyclam structures **A** and **B,** the perchlorate ligand of **B** has a significantly longer Zn-O bond length than **A** (bound water). The two constrained cyclams (**36**, **C**) also show a significant difference in Zn-O bond lengths with the bound water ligand of **C** longer than the acetate ligand of **36**. Bond lengths of Zn-O between **B** (cyclam-perchlorate ligand) and **C** (constrained cyclam-bound water ligand) are comparable. Comparing the two complexes with bound water ligands **A, C** reveals the Zn-O bond length of **C** (constrained cyclam) is significantly longer than in **A** (cyclam).

5.2.3.2. Zinc-nitrogen bond length comparison (Zn(II)-HMC, 36)

Zn-N bond lengths of complex **36** were also compared with compounds **A**, **B** and **C**. The bond length for the longer of the two Zn-N bonds (Zn-N*a*) in complex **36** is significantly longer than in any of the other three comparison compounds. The bond length for the shorter of the two Zn-N bonds (Zn-N*b*) in complex **36** is significantly shorter than in any of the comparison compounds. Data are listed in Table 5.13.

Table 5.13 Comparison of Zn-N and Zn-O bond lengths (Å) and bond angles (deg) in zinc cyclam and constrained cyclams (italics refer to actual numbering scheme used in literature for identical bonds/angles being compared).

Axial ligand and complex identification	**H_2O (A)**[21]	**$OClO_3^-$ (B)**[22]	**H_2O (C)**[23]	**CH_3COO^- (36)**
Bond lengths, Å				
Zn-O	2.2719(14)	2.380(2)	2.388(3)	2.2940(7)
Zn-N*a*	2.1198(15)*(N1)*	2.086(2)*(N1)*	2.084(2) *(N1)*	2.1368(8)*(N1)*
Zn-N*b*	2.0809(15)*(N4)*	2.090(2)*(N4)*	2.113(2) *(N2)*	2.0660(8)*(N8)*
Bond angles, °				
O-Zn-N*a*	-	86.0(1) *(N1)*	90.70(1) *(N1)*	81.64(3) *(N1)*
O-Zn-N*b*	-	89.0(1) *(N4)*	85.80(1) *(N2)*	88.49(3) *(N8)*

Bond angles between the oxygen of the axial bound ligand, zinc and the shortest Zn-N bond (O-Zn-N*b*) were compared between complex **36** and comparison compounds **B** and **C**. Data for **A** are not available in the literature. For complex **36**, this angle is intermediate between values for compounds **B** and **C**, being significantly larger than **C** but smaller than **B**. Bond angles were also compared between the oxygen of the axial bound ligand and the zinc centre with the longest Zn-N bond (O-Zn-N*a*). For complex **36**, this angle is significantly smaller than either **B** or **C** and **C** is significantly larger than for **B**.

5.2.3.3. Zinc-chloride bond length comparison (Zn(II)-NHMC, 41)

The Zn-Cl bond length of complex **41** (Zn(II)-NHMC), was compared with 3 crystal structures found in the Cambridge Structural Database for tetrahedral zinc bound to 3 nitrogens and one chloride. Complex **D** is an aliphatic, tripodal ligand. Complex **E** is a [12]aneN_3 ligand and compound **F** is a constrained cyclam. The complexes are named as below.

D [(N,N-bis(3-aminopropyl)-N-3-hydroxypropylamine)ZnCl]Cl [24]

E [ZnCl($C1_2H_{27}N_3$)]PF_6 [25]

F [Zn-hexyl-Me_2-cyclam(dihydroxypropyl)Cl]$ClO_4.H_2O$ [26]

Bond lengths are compared between the zinc and the chloride ligand, and between zinc and nitrogen atoms of the rings. Details are listed in Table 5.14. For complex **41**, the zinc chloride bond length is significantly shorter than the corresponding bond in complex **D**, also with a chloride counter ion. It is marginally shorter than the Zn-Cl bond in **E** and comparable with the constrained cyclam, **F**.

5.2.3.4. Zinc-nitrogen bond length comparison (Zn(II)-NHMC, 41)

All Zn-N bond lengths for complex **41** are comparable, but complex **D** (chloride counter ion) has one Zn-N bond length which is significantly longer than the other two, and longer than those for complex **41**. Complexes **E** and **F** show comparable bond lengths with complex **41**. Bond angles were

compared and are comparable between complexes **41**, **E** and **F**. In particular, bond angles are in good agreement between complex **41** and complex **F**.

Table 5.14 Comparison of Zn-Cl and Zn-N bond lengths (Å) and bond angles (deg) in Zn-3N bound complexes. Italics refers to actual numbering scheme used in literature for identical bonds being compared.

Counter ion and complex identification	**Cl^- (D)**	**PF_6^- (E)**	**ClO_4^- (F)**	**Cl^- (41)**
Bond lengths, Å				
Zn-Cl	2.2318(3)	2.2009(4)	2.196(2)	2.1949(14)
Zn-N*a*	2.0864(10) *(N1)*	2.0429(13) *(N1)*	2.042(4) *(N1)*	2.053(4) *(N3)*
Zn-N*b*	1.9939(11) *(N2)*	2.0484(13) *(N10)*	2.058(4) *(N3)*	2.070(4) *(N7)*
Zn-N*c*	1.9965(11) *(N3)*	2.0363(13) *(N11)*	2.042(4) *(N4)*	2.053(4) *(N10)*
Bond angles, °				
Cl-Zn-N*a*	109.01(3) *(N1)*	113.21(4) *(N1)*	116.2(1) *(N1)*	118.95(12) *(N3)*
Cl-Zn-N*b*	111.71(4) *(N2)*	113.13(4) *(N6)*	124.4(1) *(N3)*	120.14(12) *(N7)*
Cl-Zn-N*c*	111.55(3) *(N3)*	117.37(4) *(N11)*	117.4(1) *(N4)*	120.69(13)*(N10)*
N*a*-Zn-N*b*	101.60(4)*(N1,N2)*	104.45(5)*(N6,N11)*	105.1(2)*(N1,N3)*	99.51(17)*(N3,N7)*
N*a*-Zn-N*c*	98.83(4) *(N1,N3)*	104.76(5)*(N1,N11)*	101.6(2)*(N1,N4)*	104.30(17)*(N3,N10)*
N*b*-Zn-N*c*	122.01(5)*(N2,N3)*	102.41(5)*(N1,N6)*	86.8(2) *(N3,N4)*	87.28(18) *(N7,N10)*

5.2.4. NMR spectroscopy

^{1}H, ^{13}C and ^{15}N NMR spectra were acquired from 2D experiments as detailed in Chapter 2. Chemical shifts and coupling constants for proton and carbon data are listed for each complex in the experimental section found in Chapter 7. Ligands **35** and **39** were also characterised as part of this work. 2D NMR was used to identify the configurations present in solution for four of the six structures in this chapter. Analysis of the two phosphate complexes was problematic and details of the syntheses are given.

Zn-hexyl-Me$_2$-cyclam(diacetate), 36: NH protons from the 1D spectrum were identified using 2D [^{1}H, ^{13}C] HSQC, identified from the lack of crosspeak seen and [^{1}H, ^{1}H] COSY and TOCSY were recorded (Figure 5.15). Figure 5.16 highlights the assignments for all protons. Chemical shifts are listed in the experimental section in Chapter 7 and assignments identified in Table 5.17 for the ligand **35** and complex **36**. Key signals for complex **36** are summarised in Table 5.18.

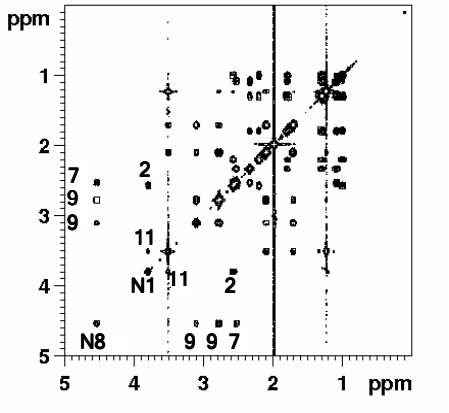

Figure 5.15 [^{1}H, ^{1}H] COSY spectrum of Zn(II)-hexyl-Me$_2$-cyclam(diacetate), 36

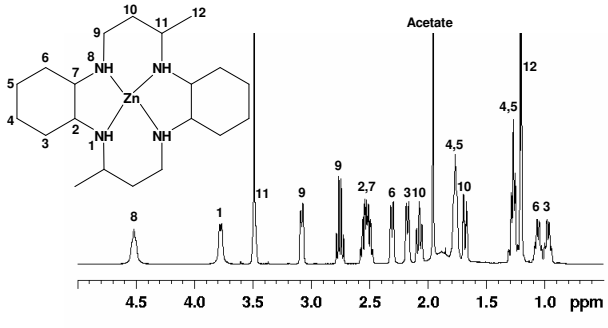

Figure 5.16 ^{1}H spectrum of Zn(II)-hexyl-Me$_2$-cyclam(diacetate), 36

Table 5.17 [^{1}H, ^{13}C] NMR chemical shifts (δppm) of Hexyl-Me_2-cyclam 35 (HMC), and Zn(II)-hexyl-Me_2-cyclam(diacetate)] (Zn(HMC)), 36 recorded in $CDCl_3$, 298 K

Signal	HMC, 35	Zn-HMC, 36	Δδ ppm
N1H	1.67	3.78	2.11
N8H	3.65	4.51	0.86
C2	2.28	2.55	0.27
C3a	0.73	0.97	0.24
C3b	2.19	2.17	-0.02
C4a	1.19	1.27	0.08
C4b	1.69	1.77	0.08
C5a	1.19	1.27	0.08
C5b	1.69	1.77	0.08
C6a	0.92	1.05	0.13
C6b	2.12	2.31	0.19
C7	2.05	2.51	0.46
C9a	2.50	2.75	0.25
C9b	2.85	3.08	0.23
C10a	1.71	2.07	0.36
C10b	1.71	1.68	-0.03
C11	3.34	3.49	0.15
C12	0.96	1.20	0.24

$\Delta\delta$ = [δ [Zn(II)-HMC(diacetate], 36 – δ HMC, 35]

^{13}C data for **36**: δ 17.0, 27.2, 28.1, 31.8, 32.3, 37.0, 43.0, 49.8, 53.5, 58.9, 62.6

Table 5.18 ^{1}H NMR chemical shifts of Zn(II)-hexyl-Me_2-cyclam(diacetate), 36

δ ^{1}H / ppm				
N**CHCH**N	NCH_2**CH_2**CHN	CHN**CH_2**	CHN**CH**	**NH**
C2, *2.55*	C10a, *2.07*	C9a, *2.75*	C11, *3.49*	N(1), *3.78*
C7, *2.51*	C10b, *1.68*	C9b, *3.08*		N(8), *4.51*

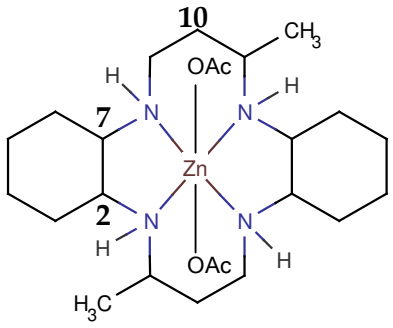

On identification of one of the NH protons, assignment of all peaks in the ^{1}H NMR spectrum was aided by 2D [^{1}H, ^{13}C] HSQC and [^{1}H, ^{1}H] COSY NMR spectroscopy (Figure 5.15). Protons N1H and N8H of complex **36** are in different environments and the 2D [^{1}H, ^{13}C] HSQC spectrum shows no coupling correlation for the signal at 3.65 ppm. An assignment is made at 3.65 ppm for the nitrogen proton (N8H) coupling to three protons from the 2D [^{1}H, ^{1}H] COSY data. The N1H proton is not clearly visible from the 1D or 2D spectra but integration shows it is hidden under the large peak centred at 1.70 ppm, and most likely between 1.60-1.65 ppm. On complexing with zinc acetate, a downfield shift of around 2 ppm is seen and the N1H proton appears clearly in the spectrum at 3.75 ppm. The N8H proton is hydrogen bonded to an acetate ligand that acts to deshield the proton and the signal is found shifted downfield to 4.50 ppm. Signals for protons 3b and 10b move to a slightly lower chemical shift upon complexation.

Zn-hexyl-Me$_2$-cyclam(dichloride), 37: 2D [^{1}H, ^{13}C] data showed more than one species is present in solution. 2D [^{1}H, ^{1}H] TOCSY analysis showed that the free ligand was present giving rise to signals at 0.68, 0.75, 0.95, 1.20, 1.70, 2.05, 2.12, 2.20, 2.29, 2.50, 2.85 and 3.35 ppm. This made the interpretation of 2D [^{1}H, ^{1}H] COSY very difficult as many overlapping signals were evident. 2D [^{1}H, ^{15}N] gives rise to six signals. If the structure of complex **37** is a 6-coordinate zinc centre with axial chloride ligands, then the *trans*-III configuration would be expected to show two signals. These are assigned as 63.3 and 54.1 ppm. If the structure of complex **37** is a 4-coordinate zinc centre bound to only three nitrogens of the macrocycle with a fourth bond to a chloride, three signals are expected for NH protons in the *trans*-I configuration. Of the three bound NH protons, two are equivalent (diagonal protons across the cavity) and the fourth remains unbound. A 4-coordinate

zinc centre in the *trans*-III configuration would give rise to four signals as each proton is in a different environment. Signals observed in the [^{1}H, ^{15}N] HSQC spectrum for complex **37** are assigned as 63.1, 54.1 and 54.0 ppm for a 4-coordinate 3N-bound zinc centre. 2D [^{1}H, ^{13}C] data also show that signals for the free ligand **35** overlap with at least one of the Zn-3N or Zn-4N bound species present. The weak signal at 1.75 ppm in the [^{1}H, ^{15}N] HSQC spectrum is assigned to the free ligand, **35**. Integration of the signals indicates that the ratios of species present are in agreement with these assignments for the six signals. Figure 5.20 shows the spectrum for the [^{1}H, ^{15}N] HSQC with labelled assignments.

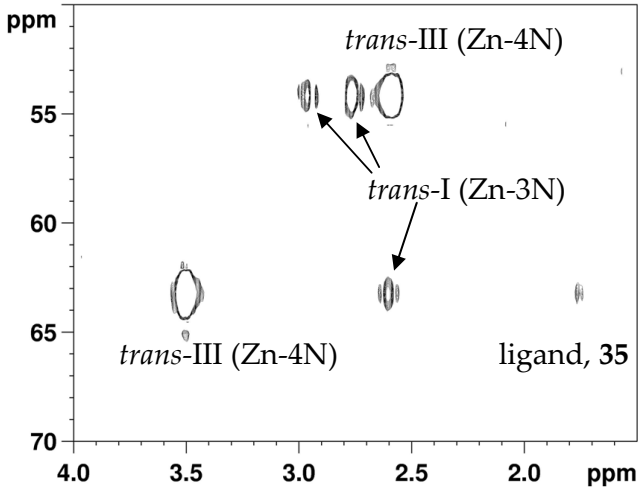

Figure 5.20 2D [^{1}H, ^{15}N] HSQC NMR spectrum of Zn(II)-hexyl-Me$_2$-cyclam(dichloride), 37

Zn-hexyl-Me$_2$-cyclam(diphosphate), 38: On acquiring a ^{1}H spectrum of complex **38** before and after all 2D data was collected, there was evidence of new signals. It is believed some decomposition of the product in the solution has occurred and may indicate that the phosphate complex is less stable than

the acetate **36** and chloride **37** species. Details of the synthesis are discussed more fully in Section 5.6.2.

Zn-naphthyl-hexyl-Me$_2$-cyclam(diacetate), 40: ^{1}H NMR chemical shifts are assigned for the free ligand **39** and listed in the experimental section in Chapter 7 and [^{1}H, ^{13}C] data for the acetate complex **40** showed very convoluted data. Analysis by 2D [^{1}H, ^{15}N] HSQC was used to investigate configurations of the macrocycle using NH protons as probes for the identification of isomers in solution.

The 2D [^{1}H, ^{15}N] spectrum for ligand **39** is shown in Figure 5.22. One signal is present due to the equivalence of both nitrogen protons on the macrocycle. Figure 5.23 shows the 1D spectrum with the signal for the equivalent NH protons highlighted.

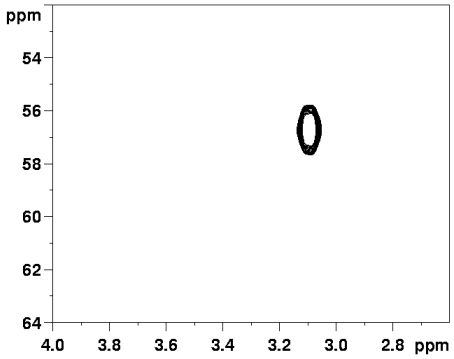

Figure 5.22 [^{1}H, ^{15}N] HSQC NMR spectrum of constrained cyclam NHMC 39, in $CDCl_3$, 298 K

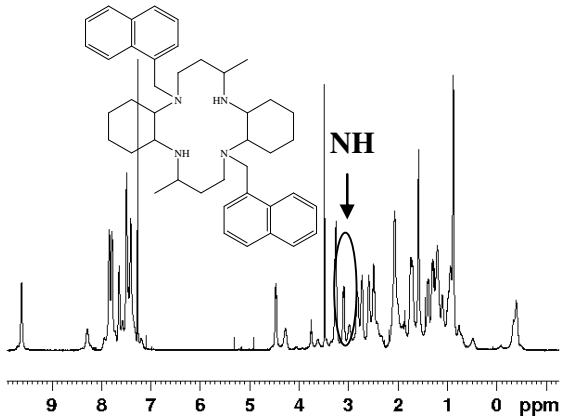

Figure 5.23 ^{1}H NMR spectrum of NHMC 39, in $CDCl_3$, 298 K

2D [^{1}H, ^{15}N] data were acquired for complex **40** and compared with ligand **39**. Two signals were observed (Figure 5.24) and the *trans*-III configuration is assigned to **40**. No other NH signals were seen and only one isomer appears to exist in solution.

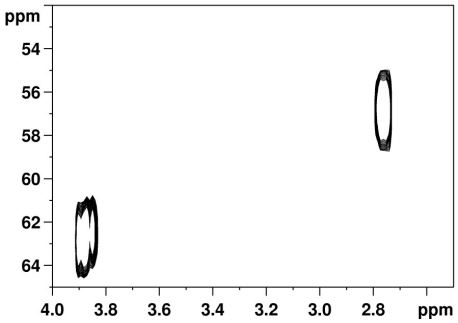

Figure 5.24 [^{1}H, ^{15}N] HSQC NMR spectrum of Zn-NHMC 40, in $CDCl_3$, 298 K

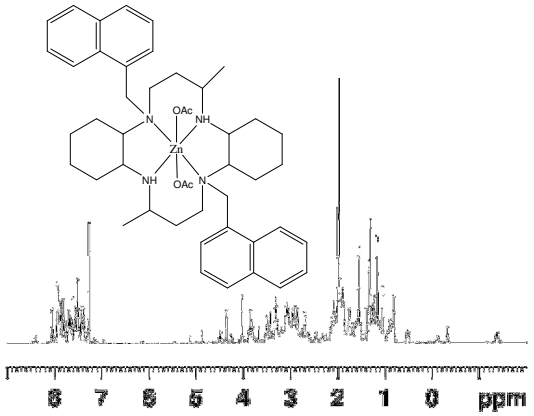

Figure 5.25 ^{1}H NMR spectrum of Zn-NHMC 40, in $CDCl_3$, 298 K

In the absence of a crystal structure for complex **40**, the NH proton at 3.84 ppm is tentatively assigned as hydrogen bonded to the acetate ligand based on the downfield shift from the 2D [^{1}H, ^{15}N] HSQC data for ligand **39**. The appearance of two signals indicates a *trans*-III configuration exists for complex **40** with each NH proton in different chemical environments. Exchange of NH protons with D_2O was observed for ligand **39**, but no exchange was seen for complex **40**. The NH protons are therefore not acidic indicating a strong Zn-N bond exists with high stability of the complex in solution. Sodium hydroxide and hydrochloric acid were used to achieve pH10, pH7 and pH3 solutions of the complex. D_2O was added in 100 μL additions until the volume in the NMR tube contained 50% D_2O. No evidence of NH exchange was seen in the ^{1}H spectra after 24 h.

Zn(II)-naphthyl-hexyl-Me$_2$-cyclam(dichloride), 41: 2D [^{1}H, ^{15}N] HSQC data were acquired for complex **41** to investigate configurations of the macrocycle using NH protons as probes for the identification of isomers in solution. The data gave rise to five separate signals and upon integration the signals were assigned ratios relating to the probability of configurations present. X-ray crystal data show that the structure is a 4-coordinate zinc centre bound to three nitrogens. In solution, it appears there may be a mixture of 4-coordinate zinc with Zn-3N binding (species **A**) and either a 5- or 6-coordinate zinc with Zn-4N binding (species **B**). Species **A** has a *trans*-III (two cross peaks) configuration and appears to interconvert with species **B**. It is unknown whether species **B** is a 5- or 6-coordinate zinc structure. Signals are assigned to *trans*-I and *trans*-III configurations for species **B**. Figure 5.26 shows spectra obtained at different time intervals and assigned signals for both species are labelled. An additional [^{1}H, ^{15}N] signal is seen at 61.3 ppm in the spectrum after one week but does not relate to the free ligand, **39**. This may be another *trans*-I isomer but it is unknown which of the *trans*-I isomers belong to each species.

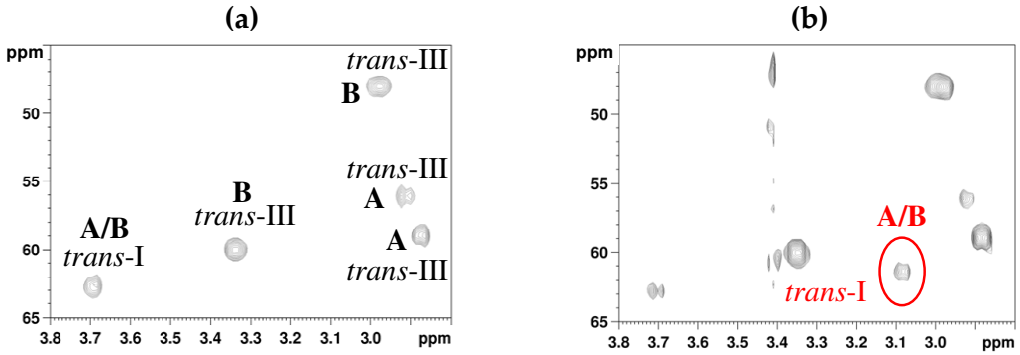

Figure 5.26 2D [^{1}H, ^{15}N] HSQC NMR of Zn(II)-naphthyl-hexyl-Me$_2$-cyclam, 41 at (a) t = zero and (b) t = 1 week with additional signal highlighted in red.

After two weeks the spectrum shows no change and no additional signals appear. The same spectrum at a later point showed a new signal, further upfield from the existing signals at 2.53 (56.9) ppm. This has not been assigned to any configuration and may be due to decomposition products although a signal for the free ligand **39** is not seen. It may be possible the signal relates to an unbound NH proton if loss of a naphthyl ligand resulted in protonation of the free nitrogen.

5.3. Antiviral Testing

5.3.1. Anti-HIV

The ligand **35** and complex **36** were tested by Professor Dr Erik De Clercq, Rega Institute, Katholieke Universiteit Leuven, Minderbroedersstraat 10, B-3000 Leuven, Belgium for anti-HIV activity. Tests were carried out against a range of cell lines and both ligand and complex were found to be highly active against HIV. Information and results of the anti-HIV and cytotoxicity tests are detailed in Table 5.27 and a graphical representation of the data is set out in Figure 5.28. This bar chart compares levels of antiviral activity of the constrained cyclams with the oxovanadium(IV) complexes from Chapter 4, AMD3100 and the zinc form of AMD3100.

Table 5.27 Anti-HIV and cytotoxicity evaluation in IIIB and ROD cell cultures

Ligand / complex	Strain	IC_{50} µM (µg/mL)	CC_{50} µM (µg/mL)	SI	Max Prot %	av. IC_{50} µM (µg/mL)	av. CC_{50} µM (µg/mL)	SI
HMC, 35	IIIB	**10.33 (3.47)**	> 372 (> 125)	> 36	102			
		10.69 (3.59)	> 372 (> 125)	> 35	145	**10.51 (3.53)**	**> 372 (> 125)**	> 35
	ROD	**> 100 (41.6)**	> 372 (> 125)	> 3	71			
		> 100 (48.3)	> 372 (> 125)	> 3	74	**> 130 (44.95)**	**> 372 (> 125)**	> 3
Zn(II)-HMC, 36	IIIB	**3.73 (1.94)**	> 100 (53.7)	= 28	99			
		3.27 (1.7)	> 129 (67.4)	= 40	114	**3.50 (1.82)**	**> 110 (57.55)**	32
	ROD	**> 100 (> 54.2)**	> 100 (54.2)	< 1	42			
		> 100 (> 54.9)	> 105 (54.9)	< 1	46	**> 104 (> 54.55)**	**> 110 (57.55)**	< 1

** av. IC_{50} highlighted in red shows concentration of compound required to effect 50% inhibition of virus.*

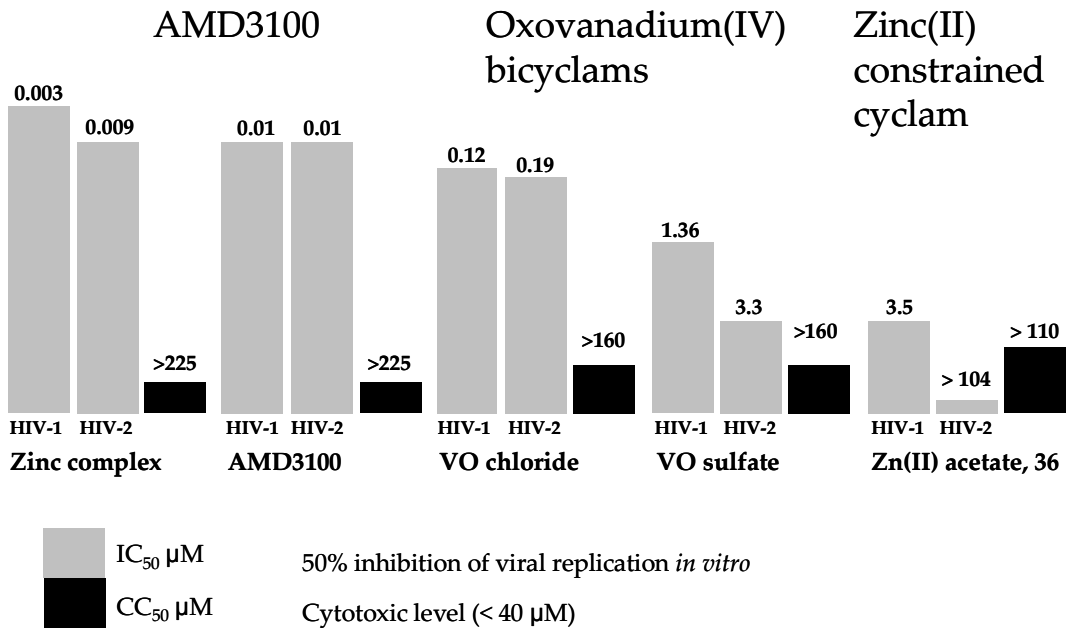

Figure 5.28 Bar chart representation of antiviral test results from Table 5.26. The y-axis is purely qualitative for comparison purposes and does not have any units assigned.

The bar chart representation of antiviral test results from Table 5.27 shows higher bars for IC_{50} concentrations that represent higher activity, and higher bars for CC_{50} concentrations represent higher toxicity. As cytotoxic concentration is determined to be < 40 μM, all complexes show high activity and low levels of toxicity to cells.

It is difficult to see how these constrained macrocycles could adopt a *cis*-V configuration, previously shown to be important in the binding of antagonist molecules with CXCR4.[27] The activity must arise from a different interaction and hydrophobic contributions may be more important for the constrained macrocycles.

5.3.2. Antibody Binding Competition Tests

Investigations were carried out for the naphthylated constrained cyclam complexes (**39**-**41**) for anti-HIV activity by investigating antibody competition binding, but no antiviral activity was detected. The antagonist molecules may be binding to CXCR4, but are easily displaced by the antibody. These experiments were carried out by Dr Steve Archibald, Departments of Chemistry and Biological Sciences, University of Hull, Hull, U.K.

Figure 5.29 shows the plot obtained for complex **40** which is representative of all complexes tested. The plot shows the fluorescence lies in the region of the positive control meaning that none of the complex was found to be strongly bound to CXCR4. The natural antibody was largely favoured and may have displaced the antagonist molecule.

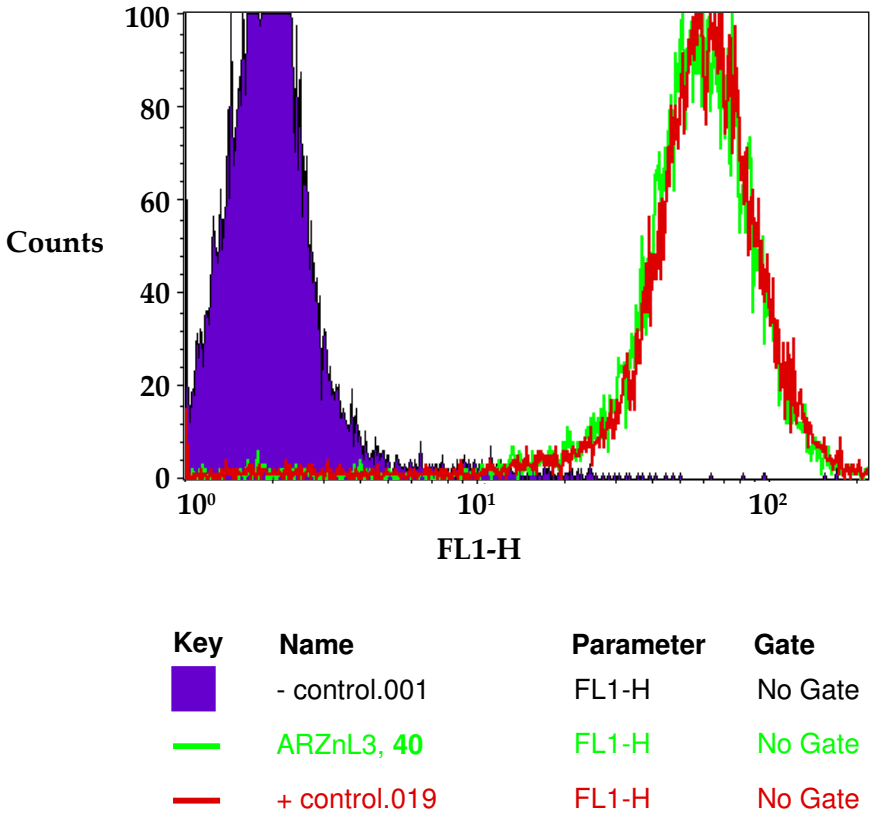

Figure 5.29 Fluorescence plot from antibody competition binding studies

5.4. Discussion

Zinc complexes of two different constrained cyclams were synthesised and characterised using infrared spectroscopy and X-ray crystallography. The effect on configurational change for different axial ligands was investigated using 2D [^{1}H, ^{13}C] and [^{1}H, ^{15}N] solution NMR spectroscopy.

5.4.1. Infrared spectroscopy

Infrared spectroscopy is frequently useful in determining structures and numbers of functional groups involved in coordination. The relative

position of a peak in a certain absorption band has shown to be dependent on the structure of the complex, and binding of acetate groups is compared between complexes **36** and **40**.[15]

The infrared spectrum of Zn(II)-hexyl-Me_2-cyclam(diacetate) **36** recorded at room temperature shows three weak absorption bands (546, 526, 488 cm^{-1}) in the 400-600 cm^{-1} region, indicative of a *trans-* arrangement of the unidentate ligand.[15] The *cis-* complex would be expected to show more bands and more splitting in this region because of lower symmetry. These data appear to be consistent with the *trans-* configuration. The spectrum for Zn(II)-naphthyl-hexyl-Me_2-cyclam(diacetate) **40,** shows similar weak absorbances in the 400-600 cm^{-1} region. In complex **36**, the asymmetric stretching vibration ν_{as}(COO) of the acetate ligand is observed at 1567 cm^{-1}, while the symmetric stretching vibration ν_s(COO) appears at 1412 cm^{-1}. The difference between ν_{as} and ν_s of approximately 155 cm^{-1} is not consistent with a monodentate coordination mode for the acetato group.[15] The lower value may be due to the presence of an intramolecular hydrogen bond formed by the carboxylate oxygen to an NH group of the constrained cyclam ligand. In complex **40**, the asymmetric stretching vibration ν_{as}(COO) is observed at 1596 cm^{-1}, while the symmetric stretching vibration ν_s(COO) appears at 1395 cm^{-1}. The difference of approximately 201 cm^{-1} is higher than that of acetato ionic complexes but the lack of a strong band at 540 cm^{-1} [$\pi(CO_2)$] would indicate that the acetato group is not monodentate.

Data acquired for complex **36** show an absorption near 3405 cm^{-1} and the broadness of the band indicates there are hydrogen bonds in this complex. The bands in the 3240-2850 cm^{-1} regions are due to symmetric and asymmetric NH and CH stretching modes, respectively. The two bands of

ν(NH) observed at 3243 and 3180 cm^{-1} are responsible for the intramolecular hydrogen bond. It is reported[28] that the *cis-* isomers of cyclam complexes exhibit at least three bands in the 890-830 cm^{-1} region due to the NH wagging modes, while the methylene vibration splits into two peaks in the 830-790 cm^{-1} region. The *trans-* isomers show two groups of bands, a doublet near 890 cm^{-1} arising from the secondary amine vibration, and only one band near 800 cm^{-1} due to the methylene vibration.[22, 28-31] Complex **36** exhibits a strong band at 898 cm^{-1} and a much weaker band at 837 cm^{-1} in the NH wagging frequency region. These vibrational modes are not significantly affected by differing counter anions or metal ions. Metal-ligand stretching bands occur in the far infrared range. Complex **40** exhibits two bands in the 890-830 cm^{-1} region due to the NH wagging modes of the secondary amines; a doublet at 891 cm^{-1} suggests a *trans-* arrangement and an additional peak at 851 cm^{-1} is seen. Surprisingly, the methylene vibration splits into two peaks seen at 807 cm^{-1} and 785 cm^{-1} thought to be indicative of a *cis-* arrangement.[28]

For the chloride analogues, complex **37** shows two NH stretching bands at 3292 cm^{-1} (sharp) and 3367 cm^{-1} (broad), the latter indicative of hydrogen-bonding in the complex. Weak signals below 400 cm^{-1} suggest a *trans-* geometry for axial ligands. Complex **41** shows two NH stretching bands at 3244 cm^{-1} (sharp) and 3467 cm^{-1} (broad). Again, evidence of hydrogen bonding is apparent by the broadness of the band at 3467 cm^{-1}.

For the phosphate analogues, complex **38** shows very broad NH bands at 3450 cm^{-1} masked by water absorption as this complex is very hygroscopic. A strong band at 739 cm^{-1} is due to NH deformation and any weak signals below 400 cm^{-1} are masked by a strong O-P-O stretch. For complex **42**, NH stretching bands are also broad at 3440 cm^{-1} and 3224 cm^{-1}

and O-P-O and P=O stretches are evident at 557 cm^{-1} and 1400 cm^{-1} respectively.

5.4.2. NMR spectroscopy of Zn(II)-hexyl-Me_2-cyclams

For complexes **36** and **40**, the coupling constant between protons on carbons C2 and C7 could not be readily determined as the signals appear as a multiplet in the spectrum. This made it difficult to assign a geometry for the protons although it is expected that a *trans*- arrangement exists with the cyclohexyl rings in the more energy favourable chair configuration due to the constraints provided by these rings. A *cis*- arrangement of the two protons is unlikely as this would result in the higher energy twist-boat configuration for the cyclohexyl rings. Assignment of all signals reveals that only one configuration is present in solution for both acetate complexes and is likely to be the *trans*-III configuration.

For the chloride complexes **37** and **41**, different isomers exist in solution. In complex **37** carbon data show two sets of signals and there may be a third isomer hidden. 2D [^{1}H, ^{15}N] data show signals assigned to a Zn-3N bound complex in the *trans*-I configuration (species A) and a Zn-4N bound complex in the *trans*-III configuration (species B) (Figure 5.25). The zinc centre in the 3N-bound complex (species A) is tetrahedral and no evidence of a *trans*-III configuration is seen. The zinc centre in the 4N-bound complex (species B) may not be octahedral and the difference in chemical shifts of the NH protons for species B suggest it may be square pyramidal with a chloride acting as counter ion. If the zinc centre is 6-coordinate, it might be expected that the signals for species B would have a more similar chemical shift as the axial chloride has an equal effect on both NH protons. The difference observed in the chemical shift between the two signals may

imply that the zinc is in fact 5-coordinate and the chloride ligand is hydrogen bonding with only one NH proton shifting one further downfield than the other.

The phosphate complexes **38** and **42** were difficult to synthesise. Complex **38** was very hygroscopic and complex **42** could only be synthesised with very low yield. The most problematic part of the synthesis was the removal of solvent from the phosphate complexes. The solution foamed considerably under reduced pressure and much of the compound was lost at this stage. Drying under vacuum resulted in a very thin layer of product that was difficult to retrieve. The product was redissolved at this stage, transferred into a narrow sample vial used for recrystallisations and again dried under vacuum. The yield for complexes **38** and **42** was not sufficient for NMR analysis due to the concentration required for [^{1}H, ^{15}N] HSQC. The ^{1}H spectra cannot be assigned without 2D data and in the case of complex **38**, decomposition products appeared before all of the 2D data could be collected. It was decided to try and synthesise the phosphate complexes by a more direct method using zinc-phosphate. This was not successful as it was discovered after the first attempt that zinc phosphate has extremely low solubility. The compound is not a 1:1 salt as initially expected, but a 3:2 compound of zinc and phosphate.

5.5. Conclusion

Zinc complexes of constrained macrocycles were synthesised and characterised. The identification of different isomers in solution was investigated and NMR analysis showed evidence of both single and multiple configurations in solution for different axial ligands. A possible intermediate

in the mechanism for uptake and release of metals by cyclams was isolated and complexes with both three and four nitrogens from the macrocyclic ring bound to zinc centres were observed. It may be that the Zn-3N and Zn-4N species interconvert in solution. The zinc centre in the 4N-bound species appears to be 5-coordinate and most likely adopts a square-pyramidal geometry. In theory, this would allow the zinc centre to interact with carboxylate oxygens in the CXCR4 binding site through a vacant 6th axial ligand position. From EPR studies for the oxovanadium(IV) bicyclams in Chapter 4, it is suggested that the axial ligand, and in particular chloride, is important for directing the macrocycle into a favourable configuration for binding to CXCR4.

Binding to CXCR4 was investigated through antibody competition binding studies and this showed that no binding occurred that could be sustained. The chloride complexes **37** and **41** have not yet been tested for antiviral activity against the cell lines used for complex **36**. Complex **36** showed activity at a concentration of 3 μM, but also failed to give a positive result using the antibody binding tests. The mode of action relating to the activity seen for the constrained cyclams needs to be investigated.

5.6. Bibliography

[1] M. Zimmer, *Coord. Chem. Rev.,* **2001**, *212*, 133.

[2] S. G. Kang, J. K. Kweon, S. K. Jung, *Bull. Korean Chem. Soc.,* **1991**, *12*, 483.

[3] K. Cho, J. C. Kim, A. J. Lough, *Inorg. Chem. Commun.,* **2003**, *6*, 284.

[4] S.-G. Kang, S.-J. Kim, *Bull. Korean Chem. Soc.,* **2003**, *24*, 269.

[5] L. Aronne, B. C. Dunn, J. R. Vyvyan, C. W. Souvignier, M. J. Mayer, T. A. Howard, C. A. ASalhi, S. N. Goldie, L. A. Ochrymowycz, D. B. Rorabacher, *Inorg. Chem.,* **1995**, *34*, 357.

[6] J. D. Silversides, C. C. Allan, S. J. Archibald, *Dalton Trans.,* **2007**, 971.

[7] S. H. Kakos, L. T. Dressel, J. D. Bushendorf, C. P. Kotarba, P. Wijetunge, C. P. Kulatilleke, M. P. McGillivary, G. Chaka, M. J. Heeg, L. A. Ochrymowycz, D. B. Rorabacher, *Inorg. Chem.,* **2006**, *45*, 923.

[8] N. M. Villeneuve, R. R. Schroeder, L. A. Ochrymowycz, D. B. Rorabacher, *Inorg. Chem.,* **1997**, *36*, 4475.

[9] R. C. Reid, M. J. Kelso, M. J. Scanlon, D. P. Fairlie, *J. Am. Chem. Soc.,***2002**, *124*, 5673.

[10] M. P. Glenn, L. K. Pattenden, R. C. Reid, D. P. Tyssen, T. J. D. A, C. J. Birch, D. P. Fairlie, *J. Med. Chem.,* **2002**, *45*, 371.

[11] P. V. Bernhardt, T. E. Dyahningtyas, S. C. Han, J. M. Harrowfield, I. C. Kim, Y. Kim, G. A. Koutsantonis, E. Rukmini, P. Thuery, *Polyhedron* **2004**, *23*, 869.

[12] X. K. Sun, M. Wuest, G. R. Weisman, E. H. Wong, D. P. Reed, C. A. Boswell, R. Motekaitis, A. Martell, M. J. Welch, C. J. Anderson, *J. Med. Chem.,* **2002**, *45*, 469.

[13] C. A. Boswell, X. K. Sun, W. J. Niu, G. R. Weisman, E. H. Wong, A. L. Rheingold, C. J. Anderson, *J. Med. Chem.,* **2004**, *47*, 1465.

[14] L. A. Bass, M. Wang, M. J. Welch, C. J. Anderson, *Bioconjugate Chem.,* **2000**, *11*, 527.

[15] K. Nakamoto, *Infrared and Raman Spectra of Inorganic and Coordination Compounds*, 4 ed., Wiley - interscience, Canada, **1986**.

[16] S. Hatse, K. Princen, E. De Clercq, M. M. Rosenkilde, T. W. Schwartz, P. E. Hernandez-Abad, R. T. Skerlj, G. Bridger, D. Schols, *Biochem. Pharmacol.,* **2005**, *70*, 752.

[17] L. O. Gerlach, J. S. Jakobsen, K. P. Jensen, M. M. Rosenkilde, R. T. Skerlj, U. Ryde, G. Bridger, T. W. Schwartz, *Biochemistry* **2003**, *42*, 710.

[18] X. Liang, P. J. Sadler, *Chem. Soc. Rev.,* **2004**, *33*, 246.

[19] S. Paisey, P. J. Sadler, *Chem. Commun.,* **2004**, 306.

[20] R. W. Hay, G. A. Lawrence, *J. Chem. Soc. Dalton Trans.,* **1975**, 1466.

[21] X. Liang, M. Weishaupl, J. A. Parkinson, S. Parsons, P. A. McGregor, P. J. Sadler, *Chem. Eur. J.,* **2003**, *9*, 4709.

[22] T. A. Tyson, K. O. Hodgson, B. Hedman, G. R. Clark, *Acta Cryst. C* **1990**, *C46*, 1638.

[23] K.-Y. Choi, I.-H. Suh, C. J. Kim, *Polyhedron* **1997**, *16*, 1783.

[24] F. E. Hahn, C. Jocher, T. Lugger, T. Pape, *Z. Anorg. Allg. Chem.,* **2003**, *629*, 2341.

[25] N. W. Alcock, H. J. Clase, S. Siltchenko, E. Rybak-Akimova, D. H. Busch, *Acta Cryst. C* **1998**, *54*, 338.

[26] K.-Y. Choi, Y.-M. Jeon, C. P. Hong, H. Ryu, I.-H. Suh, *J. Chem. Cryst.,* **2001**, *31*, 197.

[27] X. Liang, J. A. Parkinson, M. Weishaupl, R. O. Gould, S. J. Paisey, H.-s. Park, T. M. Hunter, C. A. Blindauer, S. Parsons, P. J. Sadler, *J. Am. Chem. Soc.,* **2002**, *124*, 9105.

[28] C. K. Poon, K. C. Pun, *Inorg. Chem.,* **1980**, *19*, 568.

[29] J. H. Choi, *Spectrochim. Acta* **2000**, *56A*, 1653.

[30] J. H. Choi, *Chem. Phys.,* **2000**, *256*, 29.

[31] J. H. Choi, I. G. Oh, R. Linder, T. Schonherr, *Chem. Phys.,* **2004**, *297*, 7.

6. Conclusions and future work

6.1. Conclusions

The work contained in this thesis covers the synthesis and characterisation of potential oxovanadium(IV) bicyclam and zinc(II) constrained cyclam anti-HIV agents, with the synthesis and characterisation of oxovanadium(IV) cyclam complexes, shown in Chapter 3 to be inactive against HIV. The complete inactivity of the cyclam complexes is intriguing and may be due to a combination of factors. A facile exchange of the axial ligand *trans*- to the V=O group in solution is suggested and may result in a subsequent weak interaction between the V=O group and the protein backbone, forcing the macrocycle into an unfavourable position for binding to CXCR4 - an important receptor for HIV-1. EPR measurements show identical spectra for all oxovanadium(IV) cyclam complexes in solution and results from conductivity tests and solution IR spectroscopy indicate that the axial ligand undergoes exchange in water.

In contrast to this, the bicyclams give markedly different EPR spectra and measurements suggest there may be more than one environment for vanadium in these complexes. Retention of the axial ligand may be crucial in determining how the macrocycle binds to CXCR4 and could be an important component in directing optimum ring configurations for binding to the receptor. The oxovanadium(IV) bicyclam chloride complex in particular showed high activity against HIV and is comparable with AMD3100. Slight geometric differences were seen between the bicyclam and cyclam complexes on analysis by EXAFS/XANES and these differences may contribute to retention of the axial ligand in the bicyclams. Alternatively, the bicyclams

may be displaying a much slower rate of exchange than the cyclams. EXAFS data also showed that the bicyclam chloride complex may in fact be an oligomeric species, a possibility previously considered during synthesis as problems encountered with recrystallisation suggested either a polymer or bridged species had formed. There may be different ring configurations present in solution for the bicyclams but no conclusive evidence could be obtained from the analyses carried out. As both cyclam and bicyclam complexes contain identical chemical groups, it is likely that the aromatic linker plays an important role in the activity seen for the bicyclams.

X-ray crystallography showed interesting differences between the cyclam complexes, in particular where two complexes have the same chloride axial ligand but different counter ions. By increasing the size of the counter ion, networks of hydrogen bonding between axial ligands, NH protons of the ring and solvent molecules were removed. This in turn affected the angle sizes across the diagonal of the ring cavity. Oxovanadium(IV) cyclam also showed a high preference for hard ligands in accordance with Pearson's Classification.[1]

A constrained cyclam and its zinc(II)-diacetate complex showed high activity against HIV when tested against the III_B cell line, but antibody competition binding tests did not reveal any sustained binding to CXCR4. This may indicate that a different mechanism is involved for the constrained cyclams and needs to be investigated. 2D [^{1}H, ^{13}C] COSY NMR analysis revealed the complex adopted only one configuration in solution (*trans*-III) and is stable with no exchange of NH protons seen on deuteration of the solution. On addition of naphthyl substituents to the constrained cyclam, no

change is seen for 2D NMR analysis of the zinc(II)-diacetate complex and this structure is also thought to be in the *trans*-III configuration in solution.

2D [^{1}H, ^{15}N] HSQC NMR analysis of a zinc(II)-dichloride constrained cyclam showed that an equilibrium mixture may exist between a 4-coordinate tetrahedral zinc bound to only three nitrogens of the ring with a fourth bond to chloride, and a 5-coordinate square-pyramidal zinc bound to all four nitrogens of the ring with a fifth bond to chloride. The number of signals in the spectrum increased with time and a new signal for the uncomplexed ligand suggests demetallation occurred. On addition of naphthyl substituents to the constrained cyclam, the same analysis revealed no additional signals over the same period of time and no signal was seen for the demetallated complex. It would appear that the presence of the naphthyl substituents may serve to stabilise the structure.

6.2. Future Work

6.2.1. Oxovanadium(IV) complexes

A promising result from this work was the high antiviral activity seen for the bicyclam sulfate and chloride complexes, with emphasis on the chloride structure warranting further investigation. Solution chemistry of this particular structure may be complex, as possible demetallation and hydrolysis (or partial hydrolysis) of one or both rings may lead to several different species in solution. The need for structural information on ring configurations in solution requires paramagnetic NMR analysis, and this presents its own challenges. Recently, 2D IR spectroscopy has been used to demonstrate how the nitrile functional groups of an existing NNRTI are in different protein environments[2] and ion-mobility mass spectrometry in

conjunction with theoretical modelling has been used to evaluate the three-dimensional structure of possible E- and Z- isomers of a copper(II)-anthracenyl cyclam.[3] Application of these techniques may provide further information on the structure of the oxovanadium(IV) bicyclam sulfate and chloride complexes.

It would also be useful to know whether zinc can displace vanadium in these complexes and kinetic studies may reveal important information in terms of uptake rates of vanadium in the presence of zinc. Previous studies have shown how copper has a higher affinity for cyclam than zinc, but the uptake rate is slowed in the presence of zinc.[4] These types of investigation would first require an improved synthesis and purification method for the bicyclam complexes to avoid precipitation in solution of possible oligomeric species. Alternatively, synthesis could be concentrated on obtaining a different oxidation state for vanadium in these complexes, making analysis by NMR more accessible.

Molecular modelling could also be applied further to investigate amino acid residues near the aromatic linker of the bicyclam complexes to look at hydrophobic interactions that may play a part in directing the bicyclams into a favourable configuration within the CXCR4 binding site. It would also be interesting to investigate whether the complexes synthesised in this thesis might bind with a different 7-helix transmembrane receptor, such as the D6 protein. The promiscuous receptor D6 (or CCBP2) is now thought to be important for HIV pathogenesis in the brain and is shown to be a functional coreceptor for HIV-1 and HIV-2 on astrocytes which are glial cells found in the central nervous system.[5]

The literature states that only two receptors are used by the HIV virus, CCR5 and CXCR4, and that the antagonist molecule AMD3100 is highly specific for CXCR4[6], but no published work appears to exist on attempts to test the viability of D6 as a target for zinc(II) xylyl-bicyclam and other metallo-macrocycles. The receptor CXCR4 has 33% sequence identity agreement with bovine rhodopsin. A 17% sequence identity agreement is found between D6 and bovine rhodopsin with 46% alignment agreement overall. This is sufficient for homology modelling purposes confirmed in a critical assessment.[7] The overlap is significant as the folding matches well in terms of topology. More recently, a crystal structure for another GPCR, the human B_2-adrenergic receptor has been reported[8, 9] and may provide an alternative template for the engineering of new models.

Preliminary work has produced a model for D6 (Figure 6.1) using bovine rhodopsin as a template and the same programs used to construct the CXCR4 model in order to compare both location and distances between binding site residues. It is hoped this model might be used to look at possible binding interactions with the complexes synthesised in this thesis, to see if and how they might bind with this receptor. This investigation would be useful in conjunction with biological testing for uptake of the complexes by cell lines known to express the D6 receptor and may be the first step toward investigating a possible different mode of action for anti-HIV activity.

The D6 receptor displays a similar binding site to CXCR4 with the exception of one aspartate residue substituted by glycine. This would remove what is thought to be an important acidic residue necessary for metal-carboxylate binding, but substitution by glycine may provide a

suitable environment for hydrogen bonding between the carbonyl and macrocycle backbone, seen previously in studies of metal cyclams with binding to lysozyme.[10]

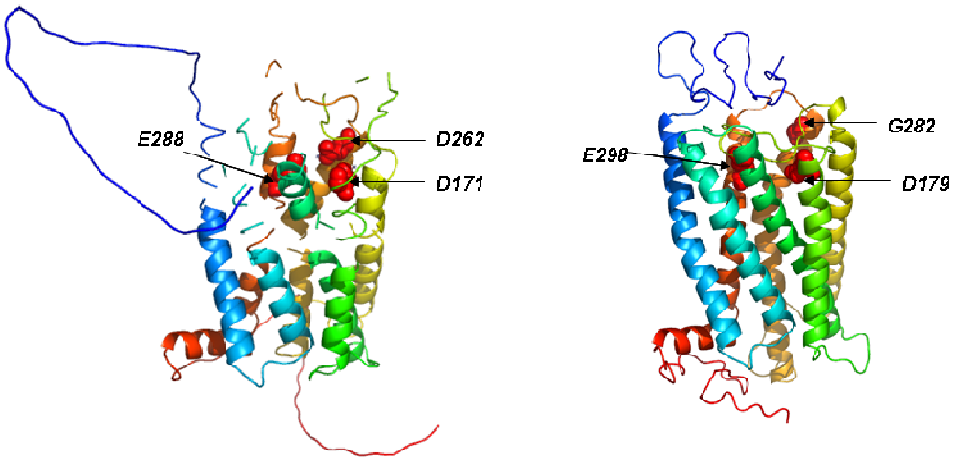

Figure 6.1 Location of residues involved in $Zn(II)_2$-xylyl-bicyclam binding is shown on the model of CXCR4 in the left-hand side panel. The location of equivalent residues in D6 is shown in the right-hand side panel. Residues are depicted as spheres and coloured red.

From the homology model of D6, a histidine residue (His 186) is found in the binding site and this may be a possible candidate for metal binding. Investigation into whether tryptophan residues W195 and W283 (present in the CXCR4 binding site) are conserved may lead to the further possibility of D6 being a viable target for antagonist molecules with anti-HIV or other antiviral activity.

6.2.2. Zinc(II) constrained cyclam complexes

The most interesting discovery from this thesis was the identification of possible intermediates in the uptake and release of metals by cyclams and

the ability to retain a single configuration in solution. This work requires more analytical investigation to look at how different steric substituents can improve stabilisation and possibly lead to the isolation of a particular species through the retention of one configuration in solution. If significant energy differences exist between the Zn-3N and Zn-4N bound complexes, further [^{1}H, ^{15}N] NMR work at low temperatures may reveal the lowest energy configuration.

6.3. Conferences Attended

8th course: Biophysics and the Challenges of Emerging Threats

Ettore Majorana Foundation and Centre for Scientific Culture,

Erice – Sicily, 19-30 June 2007

Oral & Poster Presentation

ICBIC XIII

13th International Conference on Biological Inorganic Chemistry

Vienna – Austria, 15-20 July 2007

*Poster Presentation – **Prize Winner***

USIC 2007

Universities of Scotland Inorganic Chemistry

Edinburgh – UK, 6-7 September 2007

Poster Presentation

RSC UK Macrocyclic & Supramolecular Chemistry Group Meeting

University of Manchester – UK, 17-19 December 2007

Oral & Poster Presentation

RSC IRM/CCDG

Reaction Mechanisms Coordination Chemistry Discussion Group Meeting

University of Edinburgh – UK, 18-20 June, 2008

Poster Presentation

V6

6th International Vanadium Symposium

Lisbon – Portugal, 17-19 July 2008

Poster Presentation

6.4. Bibliography

[1] R. G. Pearson, *J. Am. Chem. Soc.,* **1963**, *85*, 3533.

[2] C. Fang, J. D. Bauman, K. Das, A. Remorino, E. Arnold, R. M. Hochstrasser, *Proc. Natl. Acad. Sci., USA* **2008**, *105*, 1472.

[3] E. S. Baker, J. E. Bushnell, S. R. Wecksler, M. D. Lim, M. J. Manard, N. F. Dupuis, P. C. Ford, M. T. Bowers, *J. Am.. Chem. Soc.,* **2005**, *127*, 18222.

[4] S. Paisey, P. J. Sadler, *Chem. Commun.,* **2004**, 306.

[5] S. J. D. Neil, M. M. I. Aasa-Chapman, P. R. Clapham, R. J. Nibbs, A. McKnight, R. A. Weiss, *J. Virol.,* **2005**, *79*, 9618.

[6] J. A. Esté, C. Cabrera, E. De Clercq, S. Struyf, J. Van Damme, G. Bridger, R. T. Skerlj, M. J. Abrams, G. Henson, A. Gutierrez, B. Clotet, D. Schols, *Mol. Pharmacol.,* **1999**, *55*, 67.

[7] C. S. Reddy, K. Vijayasarathy, E. Srinivas, G. Madhavi Sastry, G. Narahari Sastry, *Comp. Biol. Chem.,* **2006**, *30*, 120.

[8] S. G. Rasmussen, H. J. Choi, D. M. Rosenbaum, T. S. Koblika, F. S. Thian, P. C. Edwards, M. Burghammer, V. R. Ratnala, R. Sanishvili, R. F. Fischetti, G. F. Schertler, W. I. Weis, B. K. Koblika, *Nature* **2007**, *450*, 383.

[9] V. Cherezov, D. M. Rosenbaum, M. A. Hanson, S. G. Rasmussen, T. F. S, K. T. S, H. J. Choi, P. Kuhn, W. I. Weis, B. K. Koblika, R. C. Stevens, *Science* **2007**, 1258.

[10] T. M. Hunter, I. W. McNae, X. Liang, J. Bella, S. Parsons, M. D. Walkinshaw, P. J. Sadler, *Proc. Natl. Acad. Sci., USA* **2004**, *102*, 2288.

7. Experimental

7.1. General Experimental

7.1.1. Materials

Cyclam (1,4,8,11-tetra*aza*cyclotetradecane), *α*-*α′*-dibromo-*p*-xylene, ethyl trifluoroacetate, triethylamine, zinc acetate dihydrate, zinc chloride, barium chloride, vanadyl sulfate hydrate, vanadyl acetylacetonate, sodium bromide, potassium iodide, sodium thiocyanate, sodium ammonium phosphate tetrahydrate, silver hexafluorophosphate, guanosine 5′-monophosphate disodium salt hydrate (from yeast) guanosine 3′,5-cyclic monophosphate sodium salt and NMR solvents, deuterium oxide (99.9%) and chloroform-*d* (99.9%) were purchased from Aldrich Chemical Co., and were reagent grade unless otherwise stated.

7.1.2. Infrared spectroscopy

Infrared spectra were recorded as detailed in Chapter 2 and data are listed as the wavenumber (ν_{max}) in units of cm^{-1}.

7.1.3. Thin layer chromatography

Analytical thin layer chromatography (TLC) was performed using aluminium backed plates with a coating of Merck Kieselgel 60 F254 silica. Chromatograms were inspected under ultraviolet light at 254 nm.

7.1.4. Flash column chromatography

Flash chromatography was performed[1] using Chromatography Grade Silica 60A Particle size 35-70 micron (Silica 60A) from Fisher Scientific and Sephadex LH-20 (Amsersham Biosciences) with methanol as the eluent.

7.1.5. Mass spectrometry

Mass spectral analyses were carried out by the service provided by University of St. Andrew's as described in Chapter 2.

7.1.6. Nuclear Magnetic Resonance Spectroscopy

All NMR spectroscopy was obtained in deuterated solvents and carried out as described in Chapter 2. Data listed contains the following abbreviations: *J* = coupling constant (Hz), s (singlet), d (doublet), t (triplet), q (quartet), m (multiplet).

7.1.7. Evaporation of solvents

All solvents are reagent grade or ultra-dry purchased from Sigma Aldrich. The term "removed under reduced pressure" means that the solvent or solvents were removed from solutes under reduced pressure using a Buchi Rotovapor R-200. The term "further dried under vacuum" refers to the situation where the former procedure was insufficient to remove all traces of solvent. A high vacuum (approximately 1 mm Hg) was used to

remove final traces of solvent. Organic extracts were dried with powdered, anhydrous magnesium sulfate unless otherwise stated.

7.1.8. Nomenclature

Compounds in the experimental section are named according to IUPAC rules. Numbers in bold in brackets refer to the number given to the compound name in Chapters 3-5.

7.1.9. Crystallographic data

All crystallographic data was acquired and processed as described in Chapter 2.

7.1.10. Glassware

All glassware was oven dried for at least 24 h prior to use.

7.2. Synthesis of oxovanadium(IV) and zinc(II) macrocycle complexes

Oxovanadium(IV)-1,4,8,11-tetra*aza*cyclotetradecane sulfate (21)

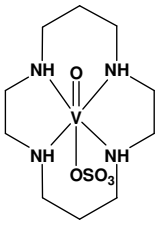

Cyclam, (1,4,8,11-tetra*aza*cyclotetradecane, 913.50 mg, 4.56 mmol) was dissolved in HPLC Grade methanol (35 mL) and refluxed under N_2 for 10 min. Vanadyl sulfate hydrate (1.072 g, 4.56 mmol, 1 mol. equiv.) was added and the reaction refluxed for 24 h. On stirring, a colour change was observed from blue to green after 1 min and to grey after 3 min. After 15 min the solution turned cloudy green and after 30 min was blue/grey in colour. After 2½ h this colour deepened to a dark blue/grey. The solution settled into two layers. The top layer was a vivid green solution and a blue precipitate settled out as the bottom layer. The top layer was separated using centrifuge then filtration and the solvent removed under reduced pressure to give a green powder (1.5 g, 4.13 mmol, 90.6% yield). The product was further dried under vacuum and crystals for X-ray were formed by slow diffusion of ether into a methanolic solution of the product at 4 °C. Anal. Calc. for $C_{10}H_{24}N_4VSO_5 \cdot MeOH \cdot 0.5H_2O$: %C, 32.70; %H, 6.23; %N, 13.86. Found %C, 32.43; %H 6.49; %N 14.46. ESI-MS: m/z = 363.90 $[M+H]^+$; ν_{max} (KBr)/cm^{-1} V=O, 974; SO_4, ν_3 1106, 1064, 1028; ν_4 619, 598.

Oxovanadium(IV)-1,4,8,11-tetra*aza*cyclotetradecane dichloride (22)

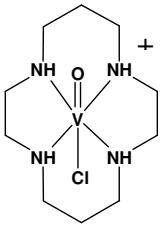

Oxovanadium(IV) cyclam **21** (72.66 mg, 0.21 mmol), was dissolved in distilled water (10 mL) and barium chloride (62.48 mg, 0.3 mmol, 3 mol. equiv. excess) added as an aqueous solution (4 mL). A white precipitate formed immediately and the mixture was stirred at room temperature in air for 16 h. The mixture was separated using centrifugal force (4000 rpm, 1 h) and the green

solution filtered. The solvent was removed under reduced pressure and further dried under vacuum to give a crystalline green powder. Crystals for X-ray were formed by slow diffusion of ether into a methanolic solution of the product at 4 °C (26 mg, 0.08 mmol, 36.6%). Anal. Calc. for $C_{10}H_{24}N_4VOCl_2 \cdot H_2O$ %C, 33.70; %H, 7.35; %N, 15.70. Found %C, 34.04; %H, 7.22; %N 16.05. ESI-MS: m/z = 302.10 (Cl^{35}), 304.00 (Cl^{37}) $[M]^+$; ν_{max} (KBr)/cm^{-1} V=O, 945.

Oxovanadium(IV)-1,4,8,11-tetra*aza*cyclotetradecane·2PF_6 (23)

Oxovanadium(IV) cyclam dichloride **22** (250 mg, 0.74 mmol) was dissolved in 15 mL distilled water and stirred at room temperature. Silver hexafluorophosphate (374.18 mg, 1.48 mmol, 2 mol. equiv.) was added and an instant precipitate formed in the solution. The mixture was stirred at room temperature for 1 h and separated using centrifugal force (4000 rpm, 30 min). The solvent was removed by freeze-drying to give a crystalline green powder (156.74 mg, 0.59 mmol, 80%). Anal. Calc. for $C_{10}H_{26}N_4VO_2 \cdot 2PF_6 \cdot AgPF_6 \cdot CH_3OH$ %C, 15.36; %H, 3.52; %N, 6.51. Found %C, 15.56; %H, 3.47; %N 6.49. ESI-MS: m/z = 265.9 $[M\text{-}H_2O]^+$; ν_{max} (KBr)/cm^{-1} V=O 949.

Oxovanadium(IV)-1,4,8,11-tetra*aza*cyclotetradecane dibromide (24)

Oxovanadium(IV) cyclam **23** (13.35 mg, 0.05 mmol), was dissolved in 10 mL distilled water. Sodium bromide (5.15 mg, 0.05 mmol, 1 mol. equiv.) was added and stirred at room temperature for 16 h. The mixture was separated using centrifugal force (4000 rpm, 30 min) and solvent was removed under reduced pressure to give a crystalline green powder (5 mg, 0.01 mmol, 11.8 %). Crystals for X-ray were formed by slow diffusion of ether into a methanolic

solution of the product at room temperature. Anal. Calc. for $C_{10}H_{24}N_4VOBr_2 \cdot AgPF_6 \cdot 2CH_3OH$ %C, 19.37; %H, 4.34; %N, 7.53. Found %C, 19.59; %H, 3.28; %N 7.40. ESI-MS: m/z = 346.1 (Br^{79}), 348.1 (Br^{81}) $[M]^+$; ν_{max} (KBr)/cm^{-1} V=O, 949.

Oxovanadium(IV)-1,4,8,11-tetra*aza*cyclotetradecane iodide·PF_6 (25)

Oxovanadium(IV) cyclam **23** (13.35 mg, 0.05 mmol) was dissolved in 10 mL

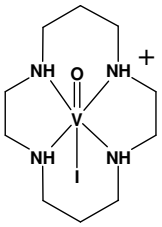

distilled water. Potassium iodide (8.30 mg, 0.05 mmol, 1 mol. equiv.) was added and stirred at room temperature for 16 h. The mixture was filtered and solvent was removed under reduced pressure with further drying under vacuum to give a crystalline green powder (12.75 mg, 0.03 mmol, 64.7%). Crystals for X-ray were formed by slow diffusion of ether into a methanolic solution of the product at room temperature. Anal. Calc. for $C_{10}H_{24}N_4VOI \cdot PF_6$ %C, 15.17; %H, 3.05; %N, 7.07. Found %C, 15.18; %H, 2.64; %N 6.75. ESI-MS: m/z = 394.1 $[M]^+$; ν_{max} (KBr)/cm^{-1} V=O 948.

Oxovanadium(IV)-1,4,8,11-tetra*aza*cyclotetradecane thiocyanate·PF_6 (26)

Oxovanadium(IV) cyclam **23** (20.02 mg, 0.075 mmol) was dissolved in 10 mL

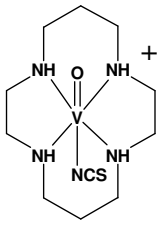

distilled water. Sodium thiocyanate (6.08 mg, 0.075 mmol, 1 mol. equiv.) was added and stirred at room temperature for 5 h. The mixture was filtered and the solvent removed under reduced pressure with further drying under vacuum to give a green powder (25 mg, 0.05 mmol, 70.9 %). Crystals for X-ray were formed by slow diffusion of ether into a methanolic solution of the product at room temperature. Anal. Calc. for $C_{11}H_{24}N_5VOS \cdot PF_6 \cdot 3AgPF_6$ %C, 10.75; %H, 1.97; %N, 5.70. Found %C, 11.53; %H, 2.21; %N 6.49. ESI-MS: m/z = 325.1 $[M]^+$; ν_{max} (KBr)/cm^{-1} V=O 964, N=C 2084.

Oxovanadium(IV)-1,4,8,11-tetra*aza*cyclotetradecane phosphate (27)

Oxovanadium(IV) cyclam **23** (13.35 mg, 0.05 mmol) was dissolved in 10 mL distilled water. Sodium ammonium phosphate tetrahydrate (10.45 mg, 0.05 mmol, 1 mol. equiv.) was added and stirred at room temperature for 16 h. The mixture was filtered and the solvent removed under reduced pressure with further drying under vacuum to give a pale green powder (10 mg, 0.03 mmol, 55%). Anal. Calc. for $C_{10}H_{24}N_4VO_5 \cdot NH_4PF_6 \cdot 2CH_3OH$ %C, 24.41; %H, 6.32; %N, 11.86. Found %C, 26.40; %H, 5.53; %N 11.97. ESI-MS: m/z = 364.0 $[M+H]^+$; ν_{max} (KBr)/cm^{-1} V=O, 933.

Oxovanadium(IV)-1,4,8,11-tetra*aza*cyclotetradecane guanosine monophosphate (GMP) (28)

Oxovanadium(IV) cyclam **23** (13.35 mg, 0.05 mmol) was dissolved in 10 mL distilled water. GMP (20.36 mg, 0.05 mmol, 1 mol. equiv.) was added and stirred at room temperature for 2.5 h. The mixture was filtered and the solvent removed under reduced pressure to give a green powder (20 mg, 0.03 mmol, 59%). Anal. Calc. for $C_{20}H_{36}N_9VO_8 \cdot PF_6 \cdot AgCl \cdot H_2O$ %C, 26.15; %H, 4.17; %N, 13.72. Found %C, 25.72; %H, 3.79; %N 13.60. ESI-MS: m/z = 651.0 $[M+Na]^+$; ν_{max} (KBr)/cm^{-1} V=O 985, C=O 1695.

Oxovanadium(IV)-1,4,8,11-tetra*aza*cyclotetradecane cyclic guanosine monophosphate (cGMP) (29)

Oxovanadium(IV) cyclam **23** (20.02 mg, 0.075 mmol) was dissolved in 10 mL distilled water. cGMP (27.54 mg, 0.075 mmol, 1 mol. equiv.) was added and stirred at room temperature for 5 h. The mixture was separated by centrifugal force and the solvent

removed by freeze-drying to give a green powder (17 mg, 0.03 mmol, 35.7%). Anal. Calc. for $C_{20}H_{35}N_9VO_8 \cdot PF_6 \cdot AgCl$ %C, 26.70; %H, 3.92; %N, 14.01. Found %C, 26.85; %H, 3.74; %N 13.61. ESI-MS: m/z = 611.2 $[M]^+$; ν_{max} (KBr)/cm^{-1} V=O 968, C=O 1698.

1-1'-[1,4-phenylenebis(methylene)]-bis(1,4,8,11-tetra*aza*cyclo-tetradecane) (16)

For the first step and protection of the NH groups, cyclam (2.02 g, 10.08 mmol) was dissolved in methanol (8 mL) and stirred under an argon atmosphere.[2] Triethylamine (1.4 mL, 1 mol. equiv.) was added resulting in a pale yellow solution. The solution was cooled in an ice bath and ethyl trifluoroacetate (4 mol. equiv., 40.32 mmol, 4.82 mL) was added dropwise over 10 min. After 1 h the ice bath was removed and the reaction was stirred at room temperature for a further 4 h. The solvent was removed under reduced pressure and further dried under vacuum. The resulting sticky residue was dissolved in ethyl acetate and passed through a silica plug (8 g) and the solvent removed under reduced pressure. Further drying under vacuum resulted in a white foam (2.2 g, 4.5 mmol, 44.6%). ESI-MS: m/z = 489.2 $[M+H]^+$. ^1H NMR (250 MHz, $CDCl_3$): 3.91-3.47 (m, 12H), 3.17-2.65 (m, 4H), 2.30-1.73 (m, 4H).

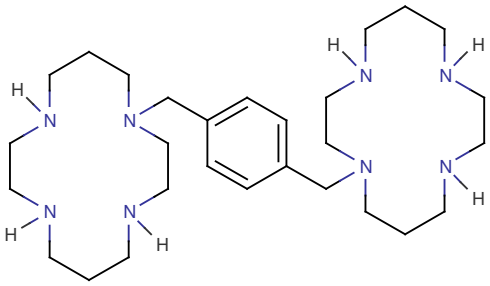

For the second step and dimerisation with an aromatic linker, tri-protected cyclam (2.2 g, 4.5 mmol) was dissolved in ultra-dry acetonitrile (100 mL) under an argon atmosphere and potassium carbonate (3 mol. equiv., 13.5 mmol, 1.86 g) was added. After addition of α,α'-dibromo-*p*-

xylene (0.594 g, 2.25 mmol, 0.5 mol. equiv.) the reaction was refluxed for 24 h. The resulting cloudy mixture was filtered and the solvent removed under reduced pressure. The product was paritioned with water (30 mL) and dichloromethane (100 mL) and the aqueous layer was washed with portions of dichloromethane (3 x 50 mL). The combined organic layers were dried over $MgSO_4$. The solution was filtered and the solvent removed under reduced pressure to give an off-white powder. The product was purified by column chromatography on silica gel using a 9:1 ratio of ethyl acetate:hexane. The solvent was removed under reduced pressure to give a white solid (2.80 g, 2.6 mmol, 57.7%). ESI-MS: m/z = 1079.8 $[M+H]^+$. ^1H NMR (250 MHz, $CDCl_3$): 7.23-7.10 (m, 4H), 3.83-3.25 (m, 24H), 2.85-1.54 (m, 20H).

For the final step, deprotection was achieved by dissolving the hexa-protected bicyclam (2.80 g, 2.6 mmol) in methanol (15 mL) and adding 10% NaOH (15 mL). A white precipitate formed immediately that disappeared on stirring. The solution was stirred for 6 h at room temperature to give a colourless solution. The aqueous layer was extracted with chloroform (3 x 50 mL) and the organic layer dried with sodium sulfate. After filtration, the solvent was removed under reduced pressure to give a white powder (1.90 g, 3.78 mmol, 68.8%). ESI-MS: m/z = 504.1 $[M+H]^+$. ^1H NMR (250 MHz, $CDCl_3$): 7.50-7.32 (m, 4H), 3.83 (s, 4H), 3.32-2.70 (m, 32H), 2.18-2.08 (m, 4H), 1.92-1.78 (m, 4H).

Oxovanadium(IV)-1-1'-[1,4-phenylenebis(methylene)]-bis(1,4,8,11-tetra*aza*cyclotetradecane) disulfate (30)

Xylyl-bicyclam **(16)** (50.2 mg, 0.1 mmol) was dissolved in 5 mL anhydrous methanol and refluxed gently under argon for 5 min. Vanadyl sulfate hydrate (47 mg, 0.2 mmol, 2 mol. equiv.) was added and a colour

change was observed, both in the solution and in the solid added. After 3 mins the initial clear solution began to turn green and the blue solid (vanadyl sulfate hydrate) turns grey. After 15 min, the reaction becomes more homogenous and the colour darkens to brown. On standing, the flask contents settled into two layers with a pale green solution forming on top of the dark solid. The reaction was refluxed for 16 h and the solution on standing was green in colour. The dark solid changed colour to light blue. The green solution was separated from the blue solid under centrifugal force, 4000 rpm, 1 h and the solvent removed under reduced pressure and further dried under vacuum. The product dried to give a dark green powder (51.3 mg, 0.06 mmol, 61.88%). Anal. calc. for $C_{28}H_{54}N_8V_2S_2O_{10}\cdot MeOH\cdot 3H_2O$, %C 38.07, %H 7.05, %N 12.25, Found %C 37.53, %H 7.29, %N 11.67. ESI-MS: *m*/*z* = 829.1 $[M+H]^+$; ν_{max} (K/Br)cm^{-1} V=O 945; SO_4^{2-} ν_3 1120, 1034; ν_4 615.

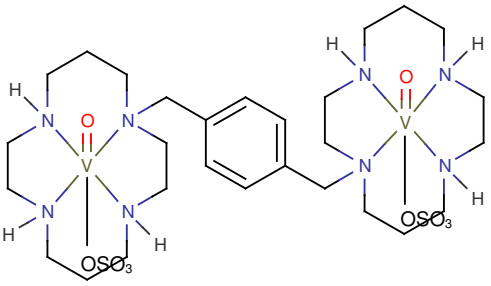

Oxovanadium(IV)-1-1'-[1,4-phenylenebis(methylene)]-bis(1,4,8,11-tetraazacyclotetradecane) tetrachloride (31)

Oxovanadium(IV)-(xylyl-bicyclam)-sulfate **16**, (51.3 mg, 0.06 mmol) was dissolved in water (3 mL) and heated until fully dissolved. Barium chloride (24.99 mg, 0.12 mmol, 2 mol. equiv.) was added as an aqueous solution (2 mL) and a cloudy solution was formed immediately. The mixture was stirred for 16 h at room

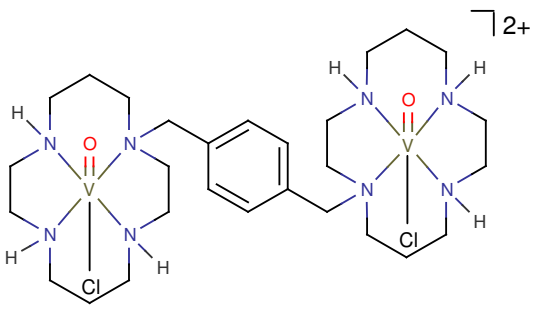

temperature then separated under centrifugal force to give a green solution and a blue solid. The green solution was decanted, filtered and the solvent was removed by freeze-drying. On drying, a colour change was noted from green to brown and on redissolving in water a green solution is obtained (35 mg, 4.5 mmol, 75%). CHN analysis cannot be quoted as product is suspected to be an oligomer of varying polymer units. ESI-MS: *m/z* = 705.4 $[M\text{-}2Cl]^{2+}$ (100%), 741.3 $[M\text{-}Cl]^{+}$; ν_{max} (K/Br)cm^{-1} V=O 964.

Oxovanadium(IV)-1-1'-[1,4-phenylenebis(methylene)]-bis(1,4,8,11-tetra*aza*cyclotetradecane)·4PF_6 (32)

Oxovanadium(IV)-bicyclam chloride **(31)** (30.25 mg, 0.04 mmol) was dissolved in 8 mL HPLC Grade methanol at room temperature. An aqueous solution (2 mL) of silver hexafluorophosphate (40.45 mg, 0.16 mmol, 4 mol. equiv.) was added and an instant white precipitate was observed. The reaction was stirred at room temperature for 16 h. The solution was separated under centrifugal force (4000 rpm, 30 min) resulting in a green solution and white solid. The green solution was filtered and the solvent removed under reduced pressure. The product was further dried under vacuum and dried to a green powder (10 mg, 0.02 mmol, 40%). Anal. Calc. for $C_{28}H_{58}N_4V_2O_4{\cdot}4PF_6{\cdot}CH_3OH$ %C, 27.11; %H, 4.86; %N, 8.72. Found %C, 27.95; %H, 5.20; %N 8.12. ESI-MS: *m/z* = 637.2 $[M\text{-}2H_2O]^{+}$; ν_{max} (K/Br)cm^{-1} V=O 966.

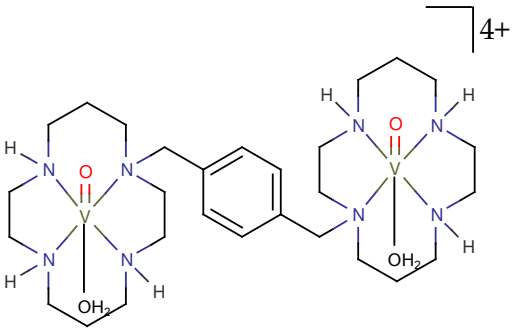

Naphthyl-1,4,8,11-tetraazacyclotetradecane (33)

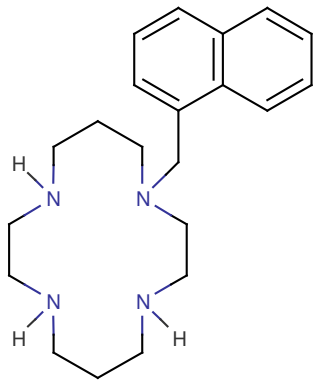

This ligand was prepared and kindly donated by Dr S J Paisey, University of Edinburgh. ν_{max} (K/Br)cm^{-1} NH 3423 (br); ^{1}H NMR (250 MHz): 1.90 (4H, m, 2 x CH_2), 3.15 (16H, m, 8 x CH_2), 4.20 (2H, s, CH_2), 7.40 (3H, m, 3 x CH), 7.83 (4H, m, 4 x CH).

Oxovanadium(IV)-naphthyl-1,4,8,11-tetraazacyclotetradecane (34)

Naphthyl-cyclam **33** (48.55 mg, 0.1 mmol) was dissolved in HPLC Grade MeOH (20 mL) and refluxed under argon until dissolution was complete. Vanadium acetylacetonate (26.52 mg, 0.1 mmol, 1 mol. equiv.) was added and the colourless solution turned green. The mixture was refluxed for 16 h with no other colour changes observed. The green solution was filtered and the solvent removed under reduced pressure with further drying under vacuum. This resulted in a green, crystalline material (20 mg, 0.03 mmol, 33.7%). ESI-MS: *m/z* = 481.54 [M-C_2H_6O]$^+$; ν_{max} (K/Br)cm^{-1}: V=O 995.

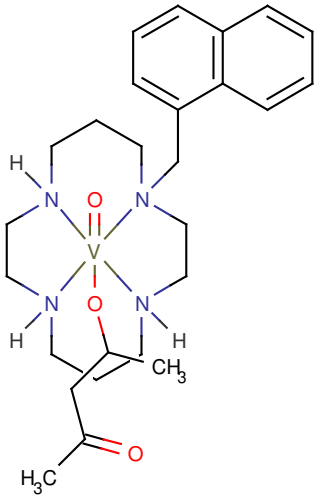

(5,16-dimethyl-2,6,13,17-tetra*aza*tricyclo [14,4,$0^{1.18}$,$0^{7.12}$]docosane (35)

Hexyl-Me_2-cyclam **35**, was synthesised as described in the literature [3, 4] and

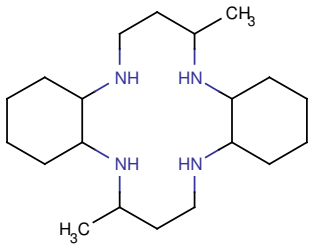

kindly donated by Professor Jong-Ha Choi, Department of Chemistry, Andong National University, Andong 760-749, South Korea. Anal. Calc. for $C_{20}H_{40}N_4$ %C 71.37, %H 11.98, %N 16.65. Found %C 71.54, %H 12.04, %N 17.07. ^{1}H NMR (600 MHz): 0.68 (2H, m, 2 x CH), 0.75 (2H, m, 2 x NH), 0.90 (2H, m, 2 x CH), 0.95 (6H, s, 2 x CH_3), 1.20 (4H, m, 2 x CH_2), 1.65 (4H, m, 2 x CH_2), 1.70 (4H, m, 2 x CH_2), 2.05 (2H, m, 2 x CH), 2.12 (2H, d, *J* 13.22, 2 x CH), 2.20 (2H, d, *J* 13.60, 2 x CH), 2.29 (2H, m, 2 x CH), 2.50 (2H, t, *J* 12.09, 2 x CH), 2.85 (2H, t, *J* 12.09, 2 x CH), 3.35 (2H, s, 2 x CH), 3.65 (2H, bd, *J* 11.33, 2 x NH).

Zinc(II)-(5,16-dimethyl-2,6,13,17-tetra*aza*tricyclo [14,4,$0^{1.18}$,$0^{7.12}$]- docosane diacetate (36)

Hexyl-Me_2-cyclam **35** (33.76 mg, 0.1 mmol) was dissolved in HPLC Grade

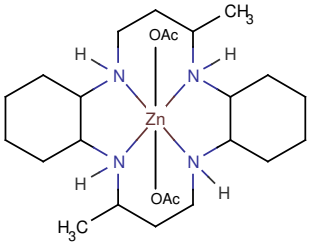

MeOH (20 mL) and stirred at room temperature. Zinc acetate dihydrate (30.73 mg, 0.1 mmol, 1 mol. equiv.) was added and the resulting colourless mixture refluxed for 2 h. The solution was filtered and the solvent removed under reduced pressure with further drying under vacuum. The product was a white powder (16 mg, 0.03 mmol, 30.8%) and crystals formed from the slow evaporation of $CHCl_3$ at room temperature. Anal. Calc. for $C_{22}H_{46}N_4O_4Zn{\cdot}0.5H_2O$ %C 54.48, %H 8.90, %N 10.59. Found %C 54.45, %H 8.53, %N 10.18. ESI-MS: *m*/*z* = 520.6 $[M+H]^+$, 445.2 $[M\text{-}OAc]^+$

(100%); ν_{max} (K/Br)cm^{-1}: H-bonding 3405 (br); NH 3243, 3180; COO_{as} 1567, COO_s 1412. ^{1}H NMR (600 MHz): 0.95 (2H, m, 2 x CH), 1.05 (2H, m, 2 x CH), 1.20 (6H, d, *J* 6.80, 2 x CH_3), 1.28 (4H, m, 4 x CH), 1.67 (2H, dt, *J* 4.53, 2 x CH), 1.75 (4H, m, 4 x CH), 1.95 (6H, s, 2 x CH_3), 2.08 (2H, t, *J* 14.35, 2 x CH), 2.18 (2H, d, *J* 13.22, 2 x CH), 2.30 (2H, d, *J* 13.22, 2 x CH), 2.50 (2H, m, 2 x CH), 2.55 (2H, m, 2 x CH), 2.75 (2H, q, *J* 12.09, 2 x CH), 3.10 (2H, d, J 11.71, 2 x CH), 3.49 (2H, s, 2 x CH), 3.79 (2H, bd, *J* 10.58, 2 x NH), 4.51 (2H, bs, 2 x NH). ^{13}C NMR (600 MHz): 17.0, 27.2, 28.1, 31.8, 32.3, 37.0, 43.0, 49.8, 53.5, 58.9, 62.6.

Zinc(II)-(5,16-dimethyl-2,6,13,17-tetra*aza*tricyclo [14,4,0$^{1.18}$,0$^{7.12}$]- docosane dichloride (37)

Hexyl-Me_2-cyclam **35** (33.66 mg, 0.1 mmol) was dissolved in HPLC Grade MeOH (20 mL) and refluxed under argon until dissolution complete. Zinc chloride (13.63 mg, 0.1 mmol, 1 mol. equiv.) was added and the mixture refluxed for 6 h. The resulting clear solution was filtered and the solvent removed under reduced pressure with further drying under vacuum. The product was a white powder (37.10 mg, 0.08 mmol, 78.7%). Anal. Calc. for $C_{22}H_{46}N_4O_4ZnCl_2 \cdot 2H_2O$ %C 47.20, %H 8.72, %N 11.01. Found %C 47.03, %H 8.56, %N 10.32. ESI-MS: *m*/*z* = 435.2 [M-Cl]$^+$; ν_{max} (K/Br)cm^{-1}: H-bonding (br) 3367; NH 3292, 3172. ^{13}C NMR (600 MHz): 17.7, 19.5, 27.1, 27.4, 27.9, 31.8, 32.4, 32.8, 33.3, 37.0, 38.4, 43.2, 45.3, 49.2, 50.2, 53.1, 59.2, 59.8, 62.5, 65.6. ^{15}N NMR (600 MHz): 54.1 (x2), 63.3.

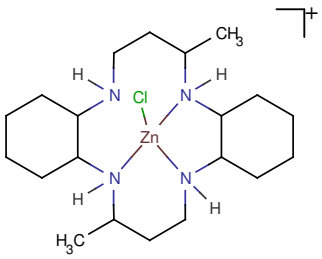

Zinc(II)-(5,16-dimethyl-2,6,13,17-tetra*aza*tricyclo [14,4,$0^{1.18}$,$0^{7.12}$]- docosane diphosphate (38)

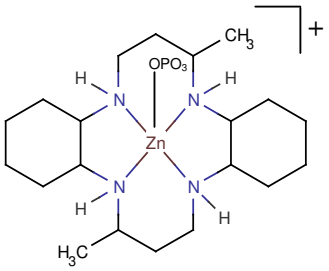

Zinc(II)-hexyl-Me_2-cyclam dichloride **37** (37.10 mg, 0.08 mmol) was dissolved in distilled water (10 mL) and stirred at room temperature. Silver hexafluorophosphate (20.23 mg, 0.08 mmol, 1 mol. equiv.) was added and an immediate white precipitate was formed. The mixture was stirred at room temperature for 1 h and the solution filtered to remove the precipitate. Sodium ammonium phosphate tetrahydrate was added (33.45 mg, 0.16 mmol, mol. equiv.) and stirred at room temperature for 16 h. The solution was filtered and the solvent removed under reduced pressure with further drying under vacuum. The product was a white powder (40.6 mg, 0.07 mmol, 68.5%) and crystals formed from a methanolic solution with diffusion of diethyl ether. No CHN available due to decomposition. ESI-MS: m/z = 497.2 $[M]^+$; ν_{max} (K/Br)cm^{-1}: H-bonding (br) 3421; NH 3224; P=O 1400; P-O 1084; P-F 841, 742; O-P-O 482.

[2,13-N,N'-dinaphthyl 5,16-dimethyl-2,6,13,17-tetra*aza*tricyclo-[14,4,$0^{1.18}$,$0^{7.12}$] docosane (39)

Naphthyl-hexyl-Me_2-cyclam **39**, was synthesised according to a published procedure [5] and with addition of 1-chloromethyl naphthalene. The ligand was kindly donated by Professor Jong-Ha Choi, Department of Chemistry, Andong National University, Andong 760-749, South Korea. Anal. calc. for $C_{42}H_{56}N_4$ %C 81.77, %H 9.15, %N 9.08. Found %C 82.12, %H 9.41, %N 9.37.

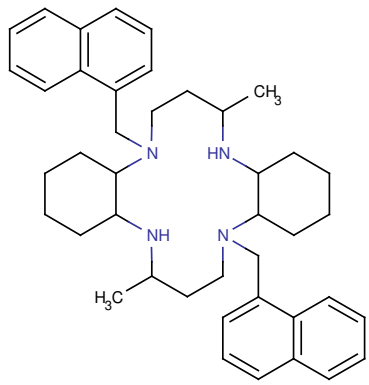

^{1}H NMR (600 MHz): 0.9 (6H, s, 2 x 3H), 0.95 (2H, m, 2 x CH), 1.3 (6H, m, 6 x 6H), 1.39 (2H, bd, *J* 11.71, 2 x CH), 1.72 (6H, m, 6 x CH), 2.06 (4H, m, 4 x CH), 2.49 (2H, m, 2 x CH), 2.59 (2H, s, 2 x CH), 2.73 (2H, d, *J* 11.71, 2 x CH), 2.82 (2H, d, *J* 9.06, 2 x CH), 3.1 (2H, d, *J* 11.33, 2 x NH), 3.27 (4H, d, *J* 10.58, 4 x CH), 4.48 (4H, d, *J* 11.33, 4 x CH), 7.4 (2H, m, 2 x CH), 7.49 (2H, s, 2 x CH), 7.64 (2H, bs, 2 x CH), 7.81 (4H, m, 4 x CH), 9.60 (2H, m, 2 x CH). ^{13}C NMR (600 MHz): (aliph) 22.3, 22.9, 27.2, 28.1, 32.1, 36.0, 52.1, 52.7, 53.6, 55.5, 62.3, (arom) 127.7, 128.1, 129.0, 130.2, 130.4, 130.6, 132.0. ^{15}N NMR (600 MHz): 56.6.

Zinc(II)-[2,13-N,N'-dinaphthyl 5,16-dimethyl-2,6,13,17-tetra*aza*tricyclo-[14,4,0$^{1.18}$,0$^{7.12}$] docosane diacetate (40)

Naphthyl-hexyl-Me$_2$-cyclam **39** (123.38 mg, 0.2 mmol) was dissolved in ultra-dry acetonitrile (35 mL) and refluxed under argon until dissolution complete. The compound is not fully soluble at this stage. Zinc acetate dihydrate (43.90 mg, 0.2 mmol, 1 mol. equiv.) was added to the flask and the mixture refluxed for 16 h. The solution was filtered and the solvent removed under reduced pressure with further drying under vacuum (65 mg, 0.08 mmol, 40.67%). Anal. calc. for $C_{44}H_{62}N_4O_4Zn{\cdot}2ZnOAc{\cdot}CH_3OH$ %C 56.65, %H 6.71, %N 5.18. Found %C 56.14, %H 6.01, %N 5.27. ESI-MS: *m*/*z* = 739.2 $[M\text{-}OAc]^+$; ν_{max} (K/Br)cm^{-1}: H-bonding 3425 (br); NH 3251, 3141; COO_{as} 1596, COO_s 1395. ^{15}N (600 MHz): 56.8, 62.9.

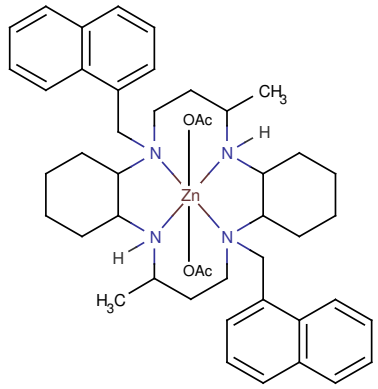

Zinc(II)-[2,13-N,N'-dinaphthyl 5,16-dimethyl-2,6,13,17-tetra*aza*-tricyclo[14,4,$0^{1.18}$,$0^{7.12}$] docosane dichloride (41)

Naphthyl-hexyl-Me_2-cyclam **39** (61.69 mg, 0.1 mmol) was dissolved in ultra-dry CH_3CN (30 mL) and refluxed under argon until dissolution was complete. Zinc chloride (13.63 mg, 0.1 mmol, 1 mol. equiv.) was added and the mixture refluxed for 3 h. The resulting clear solution was filtered and the solvent removed under reduced pressure with further drying under vacuum. The product was a pale pink/white powder (60 mg, 0.08 mmol, 79.9%) and colourless block crystals formed from a methanolic solution diffused with diethyl ether. Anal. calc. for $C_{42}H_{56}N_4ZnCl{\cdot}PF_6$ %C 58.47, %H 6.54, %N 6.49. Found %C 58.48, %H 6.63, %N 6.54. ESI-MS: *m*/*z* = 717.4 $[M+H]^+$. ν_{max} (K/Br)cm^{-1}: H-bonding (br) 3467; NH 3244, 3157, 3057. ^{15}N (600 MHz): 47.9, 55.9, 56.9, 58.8, 62.6.

Zinc(II)-[2,13-N,N'-dinaphthyl 5,16-dimethyl-2,6,13,17-tetra*aza*-tricyclo-[14,4,$0^{1.18}$,$0^{7.12}$] docosane diphosphate (42)

Zinc(II)-naphthyl-hexyl-Me_2-cyclam dichloride **41** (30 mg, 0.04 mmol) was dissolved in HPLC Grade MeOH (5 mL) and stirred at room temperature. Silver hexafluoro-phosphate (10.12 mg, 0.04 mmol, 1 mol. equiv.) was added and an immediate white precipitate was formed. The mixture was stirred for 1 h and the resulting pink solution was separated under centrifugal force, 4000 rpm, 30 min. Sodium ammonium

phosphate tetrahydrate was added (7.0 mg, 0.04 mmol, 1 mol. equiv.) and refluxed under argon for 16 h. The solution was separated under centrifugal force, 4000 rpm, 10 min, then decanted and filtered. The solvent was removed under reduced pressure with further drying under vacuum. The product was a white powder (11 mg, 0.01 mmol, 31.5%) that quickly decomposed in air, so no CHN analysis is available. ESI-MS: m/z = 763.2 $[M+2H]^+$; ν_{max} (K/Br)cm^{-1}: H-bonding (br) 3440; NH 3224; P=O 1400; P-O 1205, 1142, 1082; P-F 839; O-P-O 557.

7.3. Antibody Competition Binding Tests

These experiments were carried out by Dr Steve Archibald, Departments of Chemistry and Medical Biology, University of Hull, Hull, UK. Cell cultures, assays and flow cytometry were carried out by Mr Abid Khan, a PhD student of Dr Steve Archibald.

7.3.1. Cell cultures

Human leukaemia T cell lymphoblasts (Jurkat) were obtained from the MRL (University of Hull, Hull, UK). These cells were cultured in RPMI 1640 medium (Invitro technologies, UK) containing 10% (v/v) heat inactivated fetal bovine serum (FBS)(Biowest, France), 1% glutamate (2mM), 1% (v/v) penicillin and streptomycin (100 units/mL) antibiotics. The cell cultures were maintained at 37°C in a humidified, CO_2 (5%) controlled atmosphere with subculturing done every 2-3 days as appropriate.

7.3.2. Antibodies, chemokines and fluorescent dyes

Unconjugated mouse anti-human CXCR4 mAb clones 44708.111, 44716.111, 44717.111 and 12G5 were purchased from R & D systems Europe, Abingdon, UK. Negative control mouse IgG and the secondary fluorescein isothiocyanate conjugated anti-mouse antibody (IgG-FITC) were purchased from Serotec, UK. Dilutions of mAbs were prepared using PBS supplemented with 0.25% (v/v) BSA and 0.01 M NaN_3. All reagents, antibodies, chemokines and fluorescent dyes were reconstituted and stored according to the manufacturer's instructions unless otherwise stated.

7.3.3. Assay to measure displacement of antagonist with anti-CXCR4 antibodies by flow cytometry

Cell cultures were centrifuged (180 x g for 3 min), re-suspended in 10 mL PBS and centrifuged (180 x g, 3 m). The cell pellet was re-suspended in 1.0 mL PBS and counted using the Trypan-blue test. Cells at a density of 2.0 – 2.5 x 10^5 cells were aliquoted into polypropylene FACS tubes (Falcon 2054 tubes), the cell solution was then incubated with 10 μL of the antagonist compound (20 μM) (or PBS for the controls) for 30 min at 4°C. The cells were washed with 1.0 mL PBS (centrifuged at 180 x g, 3 m) to remove excess compound. They were then incubated with 10 μL of the appropriate concentration of antibody (10 & 1 μg/mL) for 1 hr at 4°C. Cells were again washed (centrifuged at 180 x g, 3 m) with 1.0 mL PBS/0.25% BSA/0.01 M NaN_3 and incubated with the secondary fluorescein isothiocyanate conjugated anti-mouse antibody (IgG-FITC) (diluted 1:100 in PBS/0.25% BSA/0.01 M NaN_3), 30 m, 4°C. After further washing (centrifuged at 180 x g, 3 m) with 1.0 mL PBS/0.25% BSA/0.01 M NaN_3, cell samples were fixed in 300 μL of PBS/0.25% BSA/0.01 M NaN_3 and analysed on a FACScan flow cytometer (BD Biosciences Europe, Erembodegem, Belguim). Data were

acquired and analysed with CellQuest software (Becton Dickinson) on an Apple Macintosh computer. As a negative control for non specific background staining, the cells were stained in parallel with the negative control mouse IgG (diluted 1:100 in PBS/0.25% BSA/0.01 M NaN_3).

7.4. Bibliography

[1] W. C. Still, M. Kahn, A. Mitra, *J. Org. Chem.,* **1978**, *43*, 2923.

[2] W. Yang, C. M. Giandomenico, M. Sartori, D. A. Moore, *Tetrahedron Lett.,* **2003**, *44*, 2481.

[3] R. W. Hay, G. A. Lawrence, *J. Chem. Soc. Dalton Trans.,* **1975**, 1466.

[4] S. G. Kang, J. K. Kweon, S. K. Jung, *Bull. Korean Chem. Soc.,* **1991**, *12*, 483.

[5] S.-G. Kang, S.-J. Kim, *Bull. Korean Chem. Soc.,* **2003**, *24*, 269.